

SPECIATION & SEPARATIONS STUDIES OF TETRAETHYL DIGLYCOLAMIDE

by

Andrew Fletcher

A thesis submitted to the Faculty and the Board of Trustees of the Colorado School of Mines in partial fulfillment of the requirements for the degree of Master of Science (Nuclear Engineering).

Golden, Colorado

Date _____

Signed: _____
Andrew Fletcher

Signed: _____
Dr. Jenifer Shafer
Thesis Advisor

Golden, Colorado

Date _____

Signed: _____
Dr. Mark Jensen
Professor and Director
Nuclear Science and Engineering Program

ABSTRACT

The aqueous-soluble diglycolamide TEDGA has recently been of interest as a selective trivalent f-element complexant. While initial studies show that TEDGA can improve $\text{Am}^{3+}/\text{Cm}^{3+}$ separations, solution behavior of lanthanide- and actinide-TEDGA complexes are not well-studied. This research evaluates TEDGA chemistry during complexation with trivalent lanthanides and actinides to gain an understanding of driving forces for selectivity.

Using spectrophotometric, calorimetric, and chromatographic methods, TEDGA was shown to have thermodynamic selectivity for trivalent f-elements. Specifically, stability constants, formation enthalpies, and formation entropies were evaluated for $[\text{Ln}(\text{TEDGA})_n]^{3+}$ complexes ($\text{Ln} = \text{Pr, Nd, Sm, Ho, Er}$), demonstrating a greater preference for $[\text{Ln}(\text{TEDGA})_3]^{3+}$ for later lanthanides. In a chromatographic system, TEDGA was found to increase separations between adjacent actinides.

TABLE OF CONTENTS

ABSTRACT.....	iii
LIST OF FIGURES.....	vii
LIST OF TABLES.....	xi
LIST OF EQUATIONS.....	xii
ACKNOWLEDGMENTS.....	xiii
CHAPTER 1	INTRODUCTION.....1
1.1	Separations.....5
1.2	Solvent Extraction.....8
1.3	Extraction Chromatography.....9
1.4	Trivalent f-element Chemistry & Separations.....10
1.4.1	Organophosphorus Reagents.....10
1.4.2	Diglycolamide Reagents.....11
1.5	TEDGA.....14
1.6	Hypothesis.....18
1.7	Goal.....19
1.8	References.....19
CHAPTER 2	EXPERIMENTAL DETAILS.....23
2.1	Reagents.....23
2.1.1	Nitric Acid Solutions.....23
2.1.2	Lanthanide Solutions.....24
2.1.3	TEDGA Solutions.....25

	2.1.4	Radiochemicals.....	25
2.2		Methods.....	26
	2.2.1	Spectrophotometry.....	26
	2.2.2	Calorimetry.....	28
	2.2.3	Chromatography Studies.....	29
2.3		References.....	30
CHAPTER 3		OBSERVATIONS AND DATA.....	31
3.1		Thermodynamic Data.....	31
	3.1.1	Early Lanthanides (Pr, Nd, Sm)	32
	3.1.2	Late Lanthanides (Ho and Er)	36
3.2		Chromatography Results.....	41
	3.2.1	Acid Dependence.....	41
	3.2.2	TEDGA Dependence.....	43
3.3		References.....	45
CHAPTER 4		DISCUSSION.....	46
4.1		Thermodynamic Selectivity for Lanthanides.....	46
	4.1.1	Conditional Stability Constants of [Ln(TEDGA) _n] ³⁺ Complexes.....	46
	4.1.2	Thermodynamic Constants of [Ln(TEDGA) _n] ³⁺ Complexes.....	50
	4.1.3	Comparison to Diglycolic Acid (DGAc).....	53
4.2		Improving Chromatographic Actinide Separations with TEDGA.....	57
	4.2.1	Actinide Uptake TEDGA Dependence.....	57
	4.2.2	Adjacent Actinide Separation Factors.....	59

4.3	References.....	61
CHAPTER 5	FUTURE WORK.....	62
APPENDIX A	PRINCIPAL COMPONENT ANALYSIS OF SPECTROPHOTOMETRIC DATA.....	64
APPENDIX B	FITS TO SPECTROPHOTOMETRIC DATA IN HYPESPEC.....	67
APPENDIX C	EXTINCTION COEFFICIENTS OF $[\text{Ln}(\text{TEDGA})_n]^{3+}$ COMPLEXES...	72
APPENDIX D	FITS TO CALORIMETRIC DATA IN HYPICAL.....	75

LIST OF FIGURES

Figure 1.1	Asymmetric fission yield curve for thermal fissions of ^{235}U , as occurs in traditional nuclear reactors (Williams, 2019).....	2
Figure 1.2	Spent nuclear fuel waste management timelines.....	2
Figure 1.3	A solvent extraction step (or “stage”).....	8
Figure 1.4	Extraction chromatography. Analytes can be separated based on their Interaction strength with a stationary phase, typically loaded with a complexant. The mobile phase can also contain another complexant to improve selectivity.....	9
Figure 1.5	Common organophosphorus-based complexants for trivalent f-element Separations: bis-diethylphosphoric acid (HDEHP, left), and 2-ethylhexyl phosphonic acid monoethylhexyl ester (HEH[EHP], right).....	11
Figure 1.6	Diglycolamide backbone structure. R-groups are typically alkyl chains of varying lengths.....	12
Figure 1.7	Molecular dynamics image of an $\text{Ln}(\text{TODGA})_3(\text{NO}_3)_3$ complex. Note the nitrate anions coordinated in the outer sphere allowing water to hydrogen bond, possibly leading to micelles and third phase formation (Baldwin et al., 2018).....	13
Figure 1.8	Structure of ethylhexyl-ADAAM (left) and increasing selectivity with increasing TEDGA concentration in a system with 1.5 M HNO_3 and 0.75 M of ethylhexyl-ADAAM (right; Suzuki et al., 2017).....	15
Figure 1.9	A spectrophotometric titration of TEDGA into 0.05 M $\text{Pr}(\text{NO}_3)_3$ at 1 M NaNO_3 , pH 2, 25°C from Charbonnel et al., 2012. The ratio r denotes TEDGA:Ln for each scan, beginning from pure lanthanide (r=0) and ending with a 10:1 TEDGA excess (r=10).....	16
Figure 1.10	Acid-dependency of Eichrom RE Resin for lanthanide uptake. k' is a parameter linearly proportional to K_d (Huff and Huff, 1993).....	18
Figure 2.1	Erroneous extinction coefficient spectra for 0.035 M $\text{Pr}(\text{NO}_3)_3$ titrated with TEDGA at 1 M HNO_3 acidity.....	27
Figure 2.2	Reasonable extinction coefficient spectra for 0.035 M $\text{Pr}(\text{NO}_3)_3$ titrated with TEDGA at 1 M HNO_3 acidity. All species demonstrate positive absorbance on the order of 10^0 - $10^1 \text{ M}^{-1}\text{cm}^{-1}$, centered around unique wavelengths.....	28

Figure 3.1	Principal Component Analysis of $[\text{Pr}(\text{TEDGA})_n]^{3+}$ spectrophotometric data. All four eigenvectors have significant nonzero features, indicating the presence of four species: Pr^{3+} , $[\text{Pr}(\text{TEDGA})]^{3+}$, $[\text{Pr}(\text{TEDGA})_2]^{3+}$, and $[\text{Pr}(\text{TEDGA})_3]^{3+}$	33
Figure 3.2	A sample experimental fit for a calorimetric titration of 0.25 M TEDGA into 1 mL of 13.73 mM $\text{Pr}(\text{NO}_3)_3$ at 1 M HNO_3 constant ionic strength and acidity in both solutions and 25°C reaction cell temperature.....	34
Figure 3.3	HypSpec fit for the Ho^{3+} absorption peak at 451.5 nm, titrating TEDGA into 1.5 mL of 11.27 mM $\text{Ho}(\text{NO}_3)_3$ at 1 M HNO_3 constant ionic strength and acidity.....	37
Figure 3.4	Extinction coefficient spectra for fits to 11.27 mM $\text{Ho}(\text{NO}_3)_3$ titrated with TEDGA at 1 M HNO_3 acidity.....	38
Figure 3.5	A sample experimental fit for a calorimetric titration of 0.25 M TEDGA into 1 mL of 11.27 mM $\text{Ho}(\text{NO}_3)_3$ at 1 M HNO_3 constant ionic strength and acidity in both solutions and 25°C reaction cell temperature.....	39
Figure 3.6	Acid-dependence of actinide uptake into 10-20 mg RE Resin in the absence of TEDGA. Error bars are reported to 1σ for both $[\text{HNO}_3]$ and K_d	42
Figure 3.7	TEDGA-dependence of actinide uptake into 30 mg RE Resin at 1 M H^+ and 2 M NO_3^- . Error bars are reported to 1σ	44
Figure 4.1	Speciation plots for Pr (left), Nd (right), and Sm (bottom) based off 1 M HNO_3 conditional stability constants and 10 mM $\text{Ln}(\text{NO}_3)_3$ concentration from 0 to 100 mM TEDGA concentration.....	47
Figure 4.2	Speciation plots of Ho and Er during complexation with TEDGA based off conditional stability constants at 1 M HNO_3 , 10 mM $\text{Ln}(\text{NO}_3)_3$, and TEDGA ranging from 0 to 250 mM.....	49
Figure 4.3	Structure of diglycolic acid (DGAc).....	53
Figure 4.4	Formation enthalpies (ΔH) for $[\text{Ln}(\text{DGAc})_n]^{3-2n}$ complexes (Grenthe, 1963).....	54
Figure 4.5	Formation entropies (ΔS) for $[\text{Ln}(\text{DGAc})_n]^{3-2n}$ complexes (Grenthe, 1963).....	55
Figure 4.6	Formation free energies (ΔG) for $[\text{Ln}(\text{DGAc})_n]^{3-2n}$ complexes (Grenthe, 1963).....	57
Figure 4.7	Partitioning coefficients of lanthanides with an ADAAM and a diglycolamide (Suzuki et al., 2017).....	60
Figure A.1	Principal Component Analysis of $[\text{Pr}(\text{TEDGA})_n]^{3+}$ spectrophotometric data.....	64

Figure A.2	Principal Component Analysis of $[\text{Nd}(\text{TEDGA})_n]^{3+}$ spectrophotometric data.....	64
Figure A.3	Principal Component Analysis of $[\text{Sm}(\text{TEDGA})_n]^{3+}$ spectrophotometric data....	65
Figure A.4	Principal Component Analysis of $[\text{Ho}(\text{TEDGA})_n]^{3+}$ spectrophotometric data.....	65
Figure A.5	Principal Component Analysis of $[\text{Er}(\text{TEDGA})_n]^{3+}$ spectrophotometric data.....	66
Figure B.1	HypSpec fit for the titration of TEDGA into 1.5 mL of 0.034 M $\text{Pr}(\text{NO}_3)_3$ at 1 M HNO_3 constant ionic strength and acidity.....	67
Figure B.2	HypSpec fit for the titration of TEDGA into 1.5 mL of 0.028 M $\text{Nd}(\text{NO}_3)_3$ at 1 M HNO_3 constant ionic strength and acidity.....	68
Figure B.3	HypSpec fit for the titration of TEDGA into 1.5 mL of 0.024 M $\text{Sm}(\text{NO}_3)_3$ at 1 M HNO_3 constant ionic strength and acidity.....	69
Figure B.4	HypSpec fit for the titration of TEDGA into 1.5 mL of 0.011 M $\text{Ho}(\text{NO}_3)_3$ at 1 M HNO_3 constant ionic strength and acidity.....	70
Figure B.5	HypSpec fit for the titration of TEDGA into 1.5 mL of 0.012 M $\text{Er}(\text{NO}_3)_3$ at 1 M HNO_3 constant ionic strength and acidity.....	71
Figure C.1	Extinction coefficient curves for 0.035 M $\text{Pr}(\text{NO}_3)_3$ titrated with TEDGA at 1M HNO_3 acidity.....	72
Figure C.2	Extinction coefficient curves for 0.028 M $\text{Nd}(\text{NO}_3)_3$ titrated with TEDGA at 1M HNO_3 acidity.....	72
Figure C.3	Extinction coefficient curves for 0.024 M $\text{Sm}(\text{NO}_3)_3$ titrated with TEDGA at 1M HNO_3 acidity.....	73
Figure C.4	Extinction coefficient curves for 0.011 M $\text{Ho}(\text{NO}_3)_3$ titrated with TEDGA at 1M HNO_3 acidity.....	73
Figure C.5	Extinction coefficient curves for 0.012 M $\text{Er}(\text{NO}_3)_3$ titrated with TEDGA at 1M HNO_3 acidity.....	74
Figure D.1	Experimental fits for calorimetric titrations of 0.25 M TEDGA, 10 μL injections into 1 mL of 0.013 M $\text{Pr}(\text{NO}_3)_3$ at 1 M HNO_3 constant ionic strength and acidity in both solutions and 25°C reaction cell temperature.....	75
Figure D.2	Experimental fits for calorimetric titrations of 0.25 M TEDGA, 10 μL injections into 1 mL of 0.011 M $\text{Nd}(\text{NO}_3)_3$ at 1 M HNO_3 constant ionic	

	strength and acidity in both solutions and 25°C reaction cell temperature.....	76
Figure D.3	Experimental fits for calorimetric titrations of 0.25 M TEDGA, 10 µL injections into 1 mL of 0.012 M Sm(NO ₃) ₃ at 1 M HNO ₃ constant ionic strength and acidity in both solutions and 25°C reaction cell temperature.....	77
Figure D.4	Experimental fits for calorimetric titrations of 0.25 M TEDGA, 10 µL injections into 1 mL of 0.011 M Ho(NO ₃) ₃ at 1 M HNO ₃ constant ionic strength and acidity in both solutions and 25°C reaction cell temperature.....	78
Figure D.5	Experimental fits for calorimetric titrations of 0.25 M TEDGA, 10 µL injections into 1 mL of 0.012 M Er(NO ₃) ₃ at 1 M HNO ₃ constant ionic strength and acidity in both solutions and 25°C reaction cell temperature.....	79
Figure D.6	Dilution correction of 0.25 M TEDGA, 10 µL injections into 1 mL of H ₂ O at 1 M HNO ₃ constant ionic strength, 25°C.....	80

LIST OF TABLES

Table 1.1	Previous speciation and thermodynamic parameters for TEDGA complexation with f-elements. All values are from Charbonnel et al., except for the stability constants for $[\text{Cm}(\text{TEDGA})_n]^{3+}$ complexes, which are from Klauf et al., 2019.....	17
Table 3.1	Thermodynamics of lanthanide-TEDGA complexes collected at 1 M HNO_3	32
Table 3.2	Resin uptake (K_d) and standard deviation (σ) of uptake for actinides at different TEDGA concentrations with 30 mg of RE resin and 0.5 mL of 1 M H^+ , 2 M NO_3^- solution.....	43
Table 4.1	Separation factors of lanthanide combinations based off of stability constants for $[\text{Ln}(\text{TEDGA})_3]^{3+}$ complexes.....	50
Table 4.2	Gibbs free energy (ΔG) for formation of $[\text{Ln}(\text{TEDGA})_3]^{3+}$ complexes at 25°C...	52
Table 4.3	Separations factors at increasing TEDGA concentrations for Am/Cm and Cf/Bk at 1 M HNO_3	59

LIST OF EQUATIONS

Equation 1.1	Equilibrium for formation of a 1:1 AB complex from A and B.....	6
Equation 1.2	Equilibrium for formation of a 1:2 AB ₂ complex from A and B.....	6
Equation 1.3	Equilibrium for formation of a 1:3 AB ₃ complex from A and B.....	6
Equation 1.4	Definition of a stability constant (β).....	6
Equation 1.5	Definition of a distribution ratio (D).....	6
Equation 1.6	Definition of an equilibrium distribution (K_d).....	7
Equation 1.7	Separation factor of two analytes in a liquid-liquid system.....	7
Equation 1.8	Separation factor of two analytes in a solid-liquid system.....	7
Equation 1.9	Separation factor of analytes based on stability constants.....	7
Equation 4.1	Calculating free energy (ΔG) from enthalpy, entropy, and temperature.....	51
Equation 4.2	Calculating free energy (ΔG) from stability constants and temperature.....	51

ACKNOWLEDGEMENTS

I am immensely grateful for all the support and compassion that I have received from my friends, family, labmates, and teachers. I would particularly like to thank Dr. Jenifer Shafer for her guidance and dedication, without which this work would not have been possible. I am thankful for the innumerable opportunities and learning experiences that occurred during and alongside this research, and for the personal growth that I have experienced as a result.

CHAPTER ONE

INTRODUCTION

Nuclear power is a high-output, low-carbon electricity source. First commercially implemented in the 1950s and 60s, nuclear provides around 10% of electricity globally today (IEA, 2019). One byproduct of nuclear electricity generation is used nuclear fuel (UNF), colloquially known as nuclear waste. Each year, 10,000 metric tons of UNF are produced globally, adding to a stockpile of over 300,000 tons that has accumulated over decades of energy production (Ewing, 2015). Management of nuclear fuel is a challenge due to the long-term (~100,000 year) waste management timeline, the lack of a potential geological repository that could store all produced and projected U.S.-owned UNF, and the complex elemental and isotopic composition (Tsoulfandis, 2013).

Nuclear waste contains a wide variety of materials due to the unspecific alchemy of the fission process (Robinson and Krause, 1956). The fission process that produces power in nuclear fuel produces at least two-thirds of the elements on the periodic table (Choppin and Rydberg, 1980). The asymmetric fission yield curve (Figure 1) captures the broad distribution of radioisotopes produced from thermal fission of uranium-235 (Williams, 2019). All isotopes produced following fission are immediately radioactive and some of them are radioactive for some time after the fission event. Within a few hundred years (or sooner) the lighter fission products have decayed to stability. The actinide elements, however, provide >95% of UNF mass and are responsible for the ~100,000 year waste management timeline (Figure 2; Ewing, 2015). The most significant weight constituents of UNF are uranium (as ^{238}U and unreacted ^{235}U) and plutonium

(with isotopes ranging from ^{238}Pu to ^{244}Pu); however, neptunium, americium and curium contribute to the waste management timeline significantly (Choppin et al., 2013).

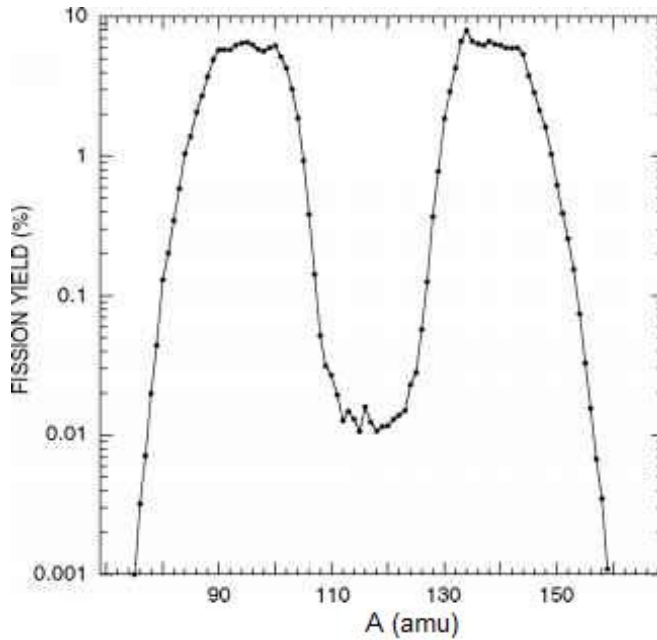


Figure 1.1. Asymmetric fission yield curve for thermal fissions of ^{235}U , as occurs in traditional nuclear reactors (Williams, 2019).

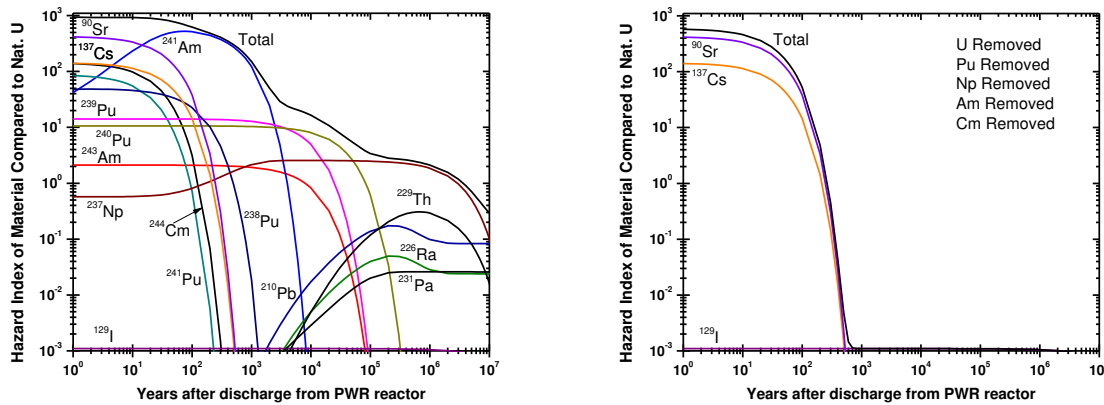


Figure 1.2. Spent nuclear fuel waste management timeline. The radioactivity hazard of all significant isotopes is shown, demonstrating the need for waste management on the order of 10^6 years (left). If all actinides are removed from the fuel, then the hazard becomes significantly less, on the order of 10^3 years (right) (modified from Choppin et al, 2013).

The most successful UNF management strategy envisioned to date would both shorten waste management timelines and reduce the amount of UNF that needs to be stored in a high-level (i.e. actinide) waste repository. This would be done via a partitioning and transmutation strategy (IAEA, 2004). Partitioning separates elements from each other using chemical processes. This involves both separating the actinides from all fission products and separating actinides from each other. For efficient storage, isolation of individual actinides is of great benefit as their half-lives span several orders of magnitude and contribute significantly to the long-term waste management burden. In particular, removing Am and Cm from U, Np, and Pu greatly decreases the long-term radiotoxicity of nuclear waste (Salvatores, 2005).

Even if they are isolated, storing actinides for hundreds of thousands of years while they slowly decay away is not ideal. The longest surviving human-engineered structures, the Egyptian pyramids and Stonehenge, are several orders of magnitude shorter lived than the repository would need to be if transmutation were not completed. All actinide isotopes are fissionable at high neutron energies, and transmutation thus provides a pathway to shortening the used nuclear fuel half-life to a more manageable timeline. After partitioning and isolation, next-generation reactor designs seek to capitalize on this by burning nontraditional fuels containing Am, Cm, or Np (in addition to the traditional U and Pu) by using a more energetic “fast” neutron spectrum. In doing so, these waste isotopes are transmuted into shorter-lived fission product isotopes, providing energy in the process (Edlund, 1983). By transmuting the actinides, the long-term radiotoxicity of nuclear waste can be decreased immensely, to more manageable timescales on the order of hundreds or thousands of years. Waste burners are capable of reducing actinide isotope inventories by upwards of 140-fold for Am and Cm (Croft et al., 1980). While commercial-scale fast neutron spectrum waste

burning reactors have not been implemented yet, they provide a promising solution for nuclear waste management that could be realized in the coming decades (Ohta et al., 2008).

Thus, there is great interest in isolating individual actinide elements. Currently, the Plutonium Uranium Redox Extraction (PUREX) process is used to separate U and Pu from all other elements (Lanham and Runion, 1949). From a chemistry standpoint, this process can be explained in a fairly straightforward fashion. Tributyl phosphate can extract U and Pu based on their 4+ and 6+ oxidation states (O'Boyle et al., 1997). Neptunium can also be easily extracted by oxidizing or reducing Np^{5+} to one of these states (Kolarik and Dressler, 1989). U, Np, and Pu can then be selectively stripped by controlling their redox environments – ultimately providing a pathway to isolating them from fission products (Chen et al., 2017). On the other hand, Am, Cm, and heavier actinides favor the trivalent oxidation state. While immediately following reactor discharge, they only comprise 0.1% of UNF by mass, these elements provide a large fraction of the long-term radiotoxicity (Figure 2; Choppin et al., 2013). While actinides heavier than Cm (i.e. Bk, Cf) do not present as much of an issue in UNF because they are produced in smaller quantities and have shorter half-lives, these elements are still of interest due to their trivalent f-element chemistry. Historically, isolating trivalent f-elements has proven to be a unique challenge due to their similar chemistry (Nash, 1993).

Besides the actinides, lanthanide elements are an important component of UNF that must be addressed. These elements are produced in large quantities in nuclear fission, with over 40% of fissions yielding a lanthanide isotope (Choppin and Rydberg, 1980). While these isotopes have shorter half-lives than the actinides, they are still problematic due to their high neutron capture cross sections. The high neutron capture cross sections cause parasitic neutron absorption and lanthanides must therefore be removed from used nuclear fuel if all actinides are going to be

efficiently fissioned in a fast spectrum reactor (Whittaker et al., 2018). Beyond nuclear applications, the lanthanide elements are also of the utmost importance to global electronics industries. Due to their unique electronic properties, these elements are found in devices such as batteries, catalytic converters, fiber optics, permanent magnets, and many others (Xie et al., 2014). Every lanthanide element except radioactive promethium can be found in a narrow spread of modern Smartphones (Rohrig, 2015). Currently, over 90% of the world's supply of lanthanides comes from China, despite their nearly-ubiquitous and distributed presence in the Earth's crust (Bridge et al., 2018). Because of their widespread use and importance, the United States Department of Energy has labeled the supply of several of these elements as critically important (US Department of Energy, 2010).

As with Am and Cm, lanthanide element isolation has proven challenging. Thus, trivalent f-element chemistry must be better understood for isolation of both the lanthanides and actinides.

1.1 Separations

Separations processes are necessary for elemental isolation. The separations of f-elements are frequently accomplished through selective metal-ligand interactions, usually metal-ligand complexation (Xie et al., 2014). By manipulating the slight differences in chemistry between elements, a single stage isolation can be achieved using a selective complexant. Repeating this complexation equilibrium multiple times allows for a cascade to yield increasingly pure streams of desired products (Tsoulfandis, 2013).

Complexation occurs through an equilibrium process between an analyte and a complexant. By nature of this equilibrium, complexation thus varies in relation to conditions. As an example, suppose a metal A and a ligand B. When A and B are in roughly a 1:1 concentration ratio, the complex AB forms according to Equation 1.1.



As B's concentration is increased, the complexes AB₂ and AB₃ also form in significant quantities, as in Equations 1.2 and 1.3.



These equilibria are combined in a parameter known as a stability constant (β_N), defined as the equilibrium constant for forming the complex AB_N from free A and B in solution, expressed in Equation 1.4.

$$\beta_N = \frac{[AB_N]}{[A][B]^N} \quad (1.4)$$

When complete stability constant information is available, speciation, and separations efficiency, can be predicted if the ratio of A and B is known (Harris, 2010). Therefore, stability constants can be useful in optimizing separations system design.

Mathematical ratios can be used to describe and compare the effectiveness of separations. A distribution ratio (D) is defined as the concentration of an analyte in one phase divided by its concentration in another phase. As an example, distribution of an analyte M between an organic and aqueous phase is expressed in Equation 1.5.

$$D_M = \frac{[D]_{org}}{[D]_{aq}} \quad (1.5)$$

D values reflect the affinity a given metal or metal-ligand complex has for a given phase relative to another phase, as reflected through the analyte's partitioning when in equilibrium. A D value around 1 implies no affinity or specificity between phases, while D values with magnitudes much greater or less than 1 imply high affinity for a particular phase. Note that since D values are generally used to describe the system under equilibrium, they indicate thermodynamic selectivity and do not effectively describe kinetic effects. This thesis will consider two separations methods:

solvent extraction and extraction chromatography (*vide infra*, Sections 1.3 and 1.4). While D values are typically used in the description of solvent extraction systems, partitioning in extraction chromatography is usually expressed as an equilibrium distribution K_d , defined in Equation 1.6, instead of as a D value.

$$K_d = \frac{[M]_i - [M]_{eq}}{[M]_{eq}} * \frac{V}{m} \quad (1.6)$$

Where $[M]_i$ is the initial concentration of analyte, $[M]_{eq}$ is the concentration of the analyte remaining in solution at equilibrium, V is the volume of the solution, and m is the mass of the solid phase. K_d ratios effectively express the uptake of an analyte into the solid phase, with higher K_d values implying greater uptake (Harris, 2010).

A separation factor is defined as the single-stage ratio of distribution values for two different analytes as shown in Equations 1.7 (for liquid-liquid systems) and 1.8 (for solid-liquid systems), where x and y represent two different analytes.

$$SF_{x/y} = \frac{D_x}{D_y} \quad (1.7)$$

$$SF_{x/y} = \frac{[K_d]_x}{[K_d]_y} \quad (1.8)$$

Separation factors can also be defined as a ratio of stability constants if a particular species can be selectively extracted, as shown in equation 1.9.

$$SF_{x/y} = \frac{\beta_{N_x}}{\beta_{N_y}} \quad (1.9)$$

A separation factor of 1 indicates no separation, whereas a separation factor greater or less than 1 indicates some selectivity. Generally, separation factors of greater than 10 are very good, while separation factors between 2-10 are useable, and separation factors between 1-2 are poor. It will be shown, though, that some methods can provide good selectivity despite poor separation factors by using repetition.

1.2 Solvent Extraction

Historically, most separations associated with the nuclear fuel cycle and the lanthanides have been accomplished using solvent extraction (Figure 1.3; Clark et al., 2018). In solvent extraction, two immiscible liquid phases are mixed. Analytes have an affinity for one phase or the other based on their chemistry and compatibility with complexants in one or both phases. After mixing, equilibrium is reached, and species have partitioned into one phase or the other. Partitioning can be defined using a D value according to Equation 1.5, as discussed in section 1.1. The phases are allowed to settle and are separated. Metals or analytes that are extracted into an organic phase can then be stripped back into a fresh aqueous phase by manipulating conditions to reverse the extraction equilibrium. This can be used to purify the analytes by partitioning them into a new aqueous phase in the absence of the initially-present contaminants. The process can be repeated to provide an equilibrium cascade, yielding higher purities (Wilson et al., 2014).

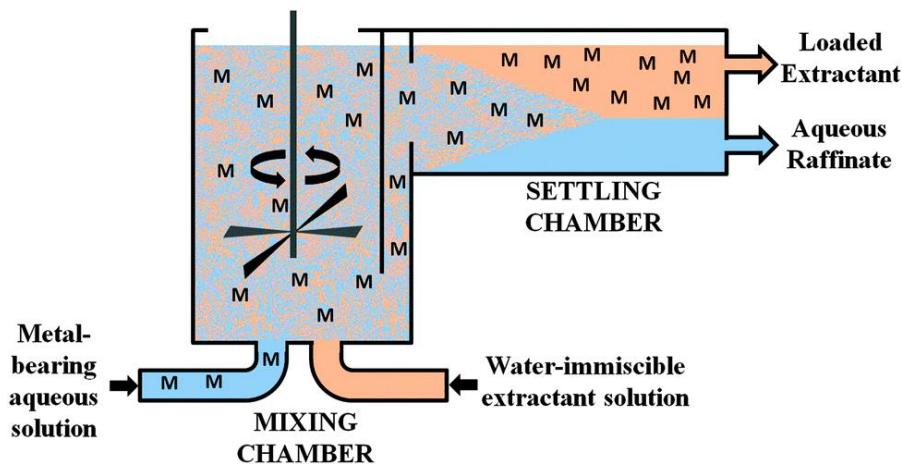


Figure 1.3. A solvent extraction step (or “stage”). Immiscible phases are mixed, allowing for analytes to load into one phase or the other based on their chemistry. Then, the phases are settled out and separated, providing greater purity. Repeating this process yields more pure products (Wilson et al., 2014).

While solvent extraction can provide relatively pure streams of product with high throughput, this method is very energy intensive and requires significant amounts of capital and materials. Solvent extraction also produces large quantities of liquid waste that have presented problems in the past. In the case of nuclear fuel cycle separations, this liquid waste has the added challenge of being radioactive (Ansari and Mohapatra, 2017).

1.3 Extraction Chromatography

Extraction chromatography (also known as column chromatography) presents another route to separation. In extraction chromatography, an analyte-rich liquid phase is passed through a complexant-laden solid (stationary) phase (Figure 1.4). Analytes are then eluted at different times from the solid phase based on their affinity to the complexant (expressed as K_d , see Section 1.1) and their physical properties. The solid phase can then be reused, with more analytes passed through it and separated (Horwitz, 1998).

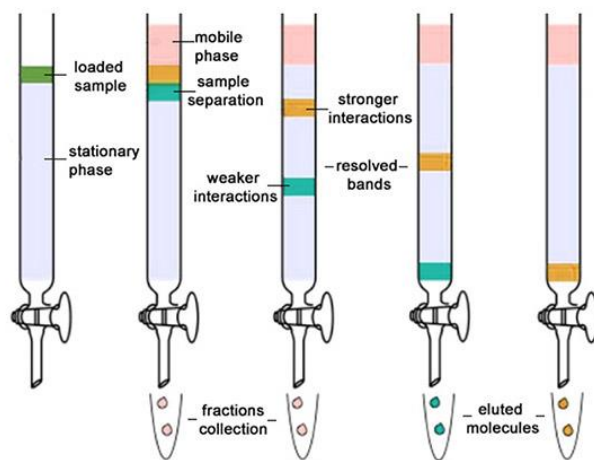


Figure 1.4. Extraction chromatography. Analytes can be separated based on their interaction strength with a stationary phase, typically loaded with a complexant. The mobile phase can also contain another complexant to improve selectivity (Horwitz, 1998).

Extraction chromatography has distinct advantages and disadvantages from solvent extraction. By utilizing a solid phase, the amount of liquid volume required to achieve the same purity is substantially less. However, the throughput of this technique is also much smaller. Still, small and efficient materials are significantly easier to dispose of and less capital intensive for fuel cycle applications by minimizing the amount of contaminated material (Ansari and Mohapatra, 2017). Currently, acrylic resins coated with a variety of extractants are commercially available from companies such as Eichrom Technologies. These chromatographic materials are generally well-characterized and effective for extracting a wide variety of analytes (Horwitz et al., 2006).

1.4 Trivalent f-element Chemistry & Separations

This section will examine systems that have previously demonstrated selectivity for trivalent f-elements. Particularly, a focus is placed on organophosphorus reagents and diglycolamides.

1.4.1 Organophosphorus Reagents

Trivalent f-elements provide a unique challenge for designing separations systems. These elements all have roughly the same ionic radii and are persistent in the trivalent oxidation state, making their chemistry very similar (Krishnamurthy and Gupta, 1992). For example, the ionic radii of lanthanide elements decrease from around 106.1 pm to 84.8 pm from La^{3+} to Lu^{3+} , for an average of just under 2 pm per element. Am^{3+} and Cm^{3+} have similar ionic radii of 98.2 pm and 97.0 pm, respectively, making them difficult to differentiate from the lanthanides (Boatner and Abraham, 1978). Separations processes thus must be very selective to account for these small changes in chemistry. Thus, a complexant is needed that is sufficiently sensitive to the very slight changes in polarizability that occur between trivalent f-elements.

Organophosphorus based complexants (Figure 1.5) provide decent separations for trivalent f-elements. The average separation factor for adjacent lanthanides provided by HDEHP, for example, is around 2.5 at optimized conditions, and for HEH[EHP] this number is closer to 2 (Sato 1989). While some complexants have demonstrated much higher SFs, organophosphorus based complexants are easily scalable to commercial levels, adding to their utility. These complexants have been used in both solvent extraction in organic phases and extraction chromatography when coated to acrylic resins, such as Eichrom's LN or LN2 Resin (which contain HDEHP or HEH[EHP], respectively). Commercial level processes for lanthanide element separations in China, the world's largest supplier, mostly use HDEHP as a complexant in solvent extraction. As mentioned above, this is quite energy and capital intensive. To provide good purities, hundreds of mixer-settler stages are required, producing massive amounts of organophosphorus wastes (Xie et al, 2014). Phosphorus-containing liquid wastes are undesirable because their runoff into groundwater can greatly disrupt ecosystems (US EPA, 2019).

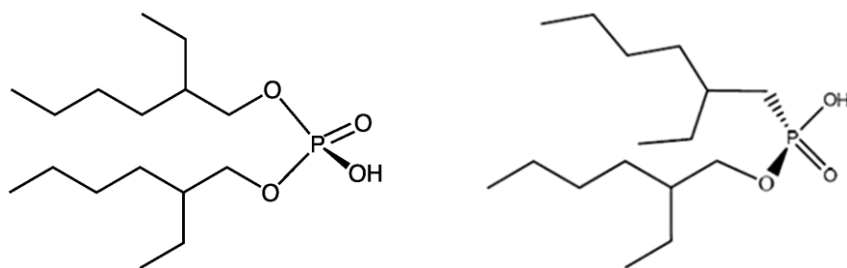


Figure 1.5. Common organophosphorus-based complexants for trivalent f-element separations: bis-diethylphosphoric acid (HDEHP, left), and 2-ethylhexyl phosphonic acid monoethylhexyl ester (HEH[EHP], right).

1.4.2. Diglycolamide Reagents

A relatively new class of complexants is the diglycolamides (DGAs, Figure 1.6). Diglycolamides have several advantages over organophosphorus-based complexants. DGAs only

contain carbon, hydrogen, oxygen, and nitrogen (thus following the “CHON principle”), meaning they are safely incinerable. This avoids large quantities of hazardous liquid wastes to deal with (Husain 2008). DGAs are also commercially scalable, and can provide good separations under optimal conditions (Ansari et al., 2012).

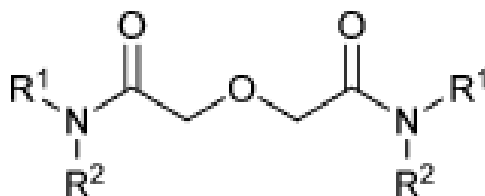


Figure 1.6. Diglycolamide backbone structure. R-groups are typically alkyl chains of varying lengths.

Tetraoctyldiglycolamide (TODGA) has demonstrated selectivity for lanthanides. In the early part of the lanthanide series (La-Eu), TODGA provides an average separation factor of around 3 at optimized conditions. In the later part of the series (Gd-Lu), TODGA does not provide any significant separation (Husain 2008). Nonetheless, TODGA has begun to be used for adjacent early lanthanide separations, particularly in extraction chromatography, where TODGA-coated resin beads can be used to selectively bind and elute lanthanides to isolate them (Horwitz et al., 2005).

The success of TODGA can be attributed to two factors. First, TODGA binds to trivalent f-elements as a tridentate ligand, bonding through the two carbonyl and one ether oxygens. The strain provided by the diglycolamide backbone makes TODGA more sensitive to the small variance in metal size. Second, TODGA’s lengthy octyl chain substituents make it soluble in organic diluents. This allows TODGA to be used as an organic extractant, which can be coupled with an aqueous phase complexant to provide very good separations (Ansari et al., 2012).

Despite its advantages, TODGA and other long-chained diglycolamides have shown vulnerability to third phase and micelle formation when metal loading is high. It is thought that to achieve charge neutrality in organic diluents, nitrates must coordinate in an outer-sphere to $[\text{Ln}(\text{TODGA})_3]^{3+}$ complexes, as the three tridentate TODGA ligands occupy all eight or nine coordination sites of the Ln^{3+} (Figure 1.7). This allows water to form hydrogen bonds to the complex through the outer-sphere nitrate anions, forming a hybrid organic third phase. When third phase formation occurs, separations are effectively impossible and ineffective; thus, third phase formation is highly problematic (Baldwin et al., 2018). Usage of phase modifiers can mitigate this issue, but this is undesirable because it significantly complicates solution and interface chemistry. Because of these factors, other DGAs are of great interest, particularly those with improved solubility properties that can avoid forming third phases while still providing selectivity for trivalent f-elements (Whittaker et al., 2018).

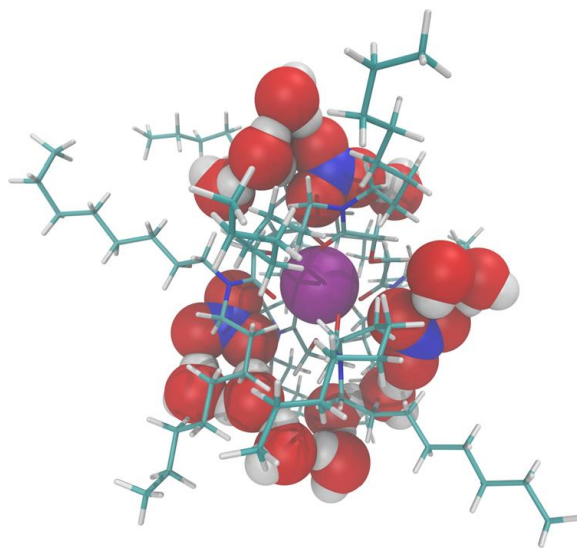


Figure 1.7. Molecular dynamics image of an $\text{Ln}(\text{TODGA})_3(\text{NO}_3)_3$ complex. Note the nitrate anions coordinated in the outer sphere allowing water to hydrogen bond, possibly leading to micelles and third phase formation (Baldwin et al., 2018).

1.5 TEDGA

While long-chained diglycolamides are organic-soluble, the short-chained diglycolamides tetramethyl diglycolamide (TMDGA) and tetraethyl diglycolamide (TEDGA) are aqueous-soluble and thus do not require complex charge neutrality to drive metal-ligand interaction (Ansari et al., 2012). Relatively little research has been done on these DGAs as trivalent f-element complexants. These ligands are attractive because they share the DGA backbone that likely provides selectivity to TODGA, while their short-chained substituents are not likely to form problematic third phases since there is less need for counterion proximity in aqueous media. Preliminary studies of TEDGA in particular are promising (*vide infra*).

Both TEDGA and TMDGA demonstrated stronger binding affinity to Pu^{4+} and Am^{3+} than ethylenediamine tetraacetic acid (EDTA), a common holdback reagent for separating lanthanides from actinides (Ansari et al., 2012). Because of this, TMDGA and TEDGA have been used as masking agents in lanthanide-actinide separations, holding the actinides in the aqueous phase while another extractant removes the lanthanides into the organic phase (Sasaki et al., 2007). TEDGA has also been used as a complexant to separate Am^{3+} and Cm^{3+} in an ionic liquid, 1-butyl-3-methylimidazolium bis(trifluoromethanesulfonyl)imide (Gujar et al., 2016).

In another process, EXAm (EXtraction of Americium), trivalent f-elements are separated using N,N'-dimethyl-N,N'-dioctyl-2-(2-hexyloxyethyl)malonamide (DMDOHEMA) and HDEHP from a highly acidic feed stream. It was found that addition of TEDGA to the aqueous phase increased $\text{Am}^{3+}/\text{Cm}^{3+}$ selectivity by withholding Cm^{3+} and the heavier lanthanides in the aqueous phase while Am^{3+} is extracted. This study did not demonstrate very good selectivity though, with a maximum reported separation factor of $\text{SF}_{\text{Am}/\text{Cm}} = 2.3$. Furthermore, small but significant amounts of TEDGA partitioned into the organic phase, with a maximum $D_{\text{org}/\text{aq}} = 0.14$

(Chapron et al., 2015). This could decrease TEDGA's effectiveness at specifically partitioning actinides into the aqueous phase.

More recently, TEDGA has been utilized as a masking agent for adjacent trivalent actinide separations in other systems, separating Am^{3+} from Cm^{3+} with good selectivity ($SF_{\text{Am/Cm}}$ as high as 41, Figure 1.8) by withholding Cm^{3+} in the aqueous phase while Am^{3+} is extracted by alkyl diamide amines (ADAAMs; Suzuki et al., 2017). Since Am^{3+} and Cm^{3+} have similar ionic radii and are both trivalent – like the lanthanides – TEDGA potentially presents a novel pathway for adjacent f-element separations. Particularly, note that TEDGA bonds more favorably to Cm^{3+} than Am^{3+} , and presumably heavier lanthanides than lighter ones.

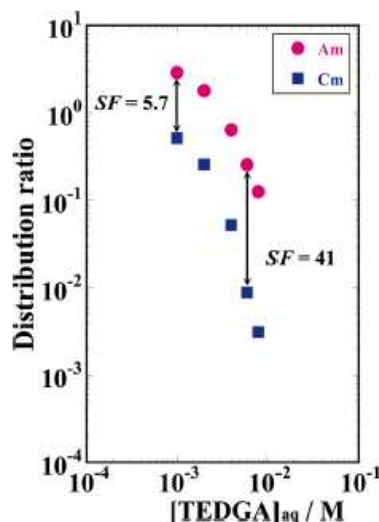
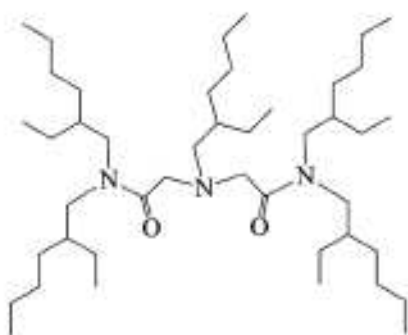


Figure 1.8. Structure of ethylhexyl-ADAAM (left) and increasing selectivity with increasing TEDGA concentration in a system with 1.5 M HNO_3 and 0.75 M of ethylhexyl-ADAAM (right; Suzuki et al., 2017).

While some scoping studies of TEDGA Am and Cm separations have been considered, the complexation properties of aqueous DGAs are very poorly characterized with only a few studies having examined their consideration. One 2012 study presented by Charbonnel et al. examined

and postulated on speciation of TEDGA when complexed with trivalent f-elements. It was predicted that the early lanthanides (La-Sm) do not strongly form 1:3 Ln:TEDGA complexes, instead favoring the 1:1 complex, while later lanthanides (Eu-Lu) prefer to form the 1:3 complex. Initial stability constant estimates for La, Pr, Yb, and Am were reported to support this claim. Formation enthalpies (ΔH) were also reported for $[\text{La}(\text{TEDGA})]^{3+}$, $[\text{La}(\text{TEDGA})_2]^{3+}$, and $[\text{Lu}(\text{TEDGA})_3]^{3+}$ complexes (Charbonnel et al., 2012).

Unfortunately, the sparseness of the UV-Vis data collected by Charbonnel et al. limits the confidence in the assessed stability constants (Figure 1.9). While these parameters provide a useful preliminary benchmark, further verification is necessary to arrive at definitive conclusions regarding thermodynamic trends for $[\text{Ln}(\text{TEDGA})_n]^{3+}$ and $[\text{An}(\text{TEDGA})_n]^{3+}$ complexes. Recently, stability constants were also reported for $[\text{Cm}(\text{TEDGA})_n]^{3+}$ complexes based off of Time-Resolved Laser-Induced Fluorescence Spectroscopy (TRLIFS; Klafß et al., 2019). The results from both studies are compiled in Table 1.1.

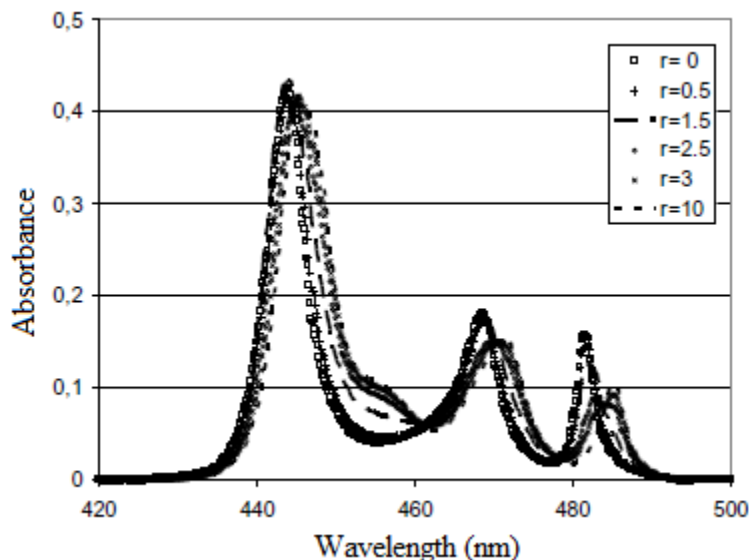


Figure 1.9. A spectrophotometric titration of TEDGA into 0.05 M $\text{Pr}(\text{NO}_3)_3$ at 1 M NaNO_3 , pH 2, 25°C from Charbonnel et al., 2012. The ratio r denotes TEDGA:Ln for each scan, beginning from pure lanthanide ($r=0$) and ending with a 10:1 TEDGA excess ($r=10$).

Table 1.1. Previous speciation and thermodynamic parameters for TEDGA complexation with f-elements. All values are from Charbonnel et al., except for the stability constants for $[\text{Cm}(\text{TEDGA})_n]^{3+}$ complexes, which are from Klauf et al., 2019.

Metal	$\log \beta_1$	$\log \beta_2$	$\log \beta_3$	Metal	ΔH_1 (kJ/mol)	ΔH_2 (kJ/mol)	ΔH_3 (kJ/mol)
<i>La</i>	2.9	5.4	-	<i>La</i>	-9.8	-12.7	-
<i>Pr</i>	2.03	3.51(5)	-	<i>Lu</i>	-	-	-18.3
<i>Yb</i>	-	-	9.2				
<i>Am</i>	2.9	6.07	8.33(5)				
<i>Cm</i>	3.3(3)	6.3(3)	8.3(3)				

Outside of these two studies, very little is known about the physical constants governing binding between TEDGA and trivalent f-elements. The sparseness of data collected across the lanthanide series by Charbonnel (*La*, *Pr*, *Yb*, *Lu*), make assessing trends and intralanthanide separation factors difficult.

Chromatographic separations with TEDGA are also of interest. Acid dependency for uptake of lanthanides into Eichrom RE Resin has previously been studied at 0.2, 1.0, 4.0, and 8.0 M HNO_3 (Figure 1.10; Huff and Huff, 1993). At 0.2, 1.0, and 4.0 M HNO_3 , greater uptake was demonstrated for earlier lanthanides, which is expected to complement the aqueous-loaded TEDGA. This is because TEDGA is anticipated to show stronger complexation for heavier trivalent f-elements (Suzuki et al., 2017). TEDGA is also expected to behave similarly to TODGA, which is selective for early lanthanides, so the combined TEDGA-RE resin system could have very good selectivity in this region (Husain et al., 2008). The early lanthanides *Nd*-*Eu* are often treated as analogs for the actinides *Am*-*Cf* due to their similar ionic radii and trivalent oxidation state (Boatner and Abraham, 1978). Therefore, TEDGA may demonstrate selectivity for *Am*-*Cf* in chromatographic systems containing RE Resin.

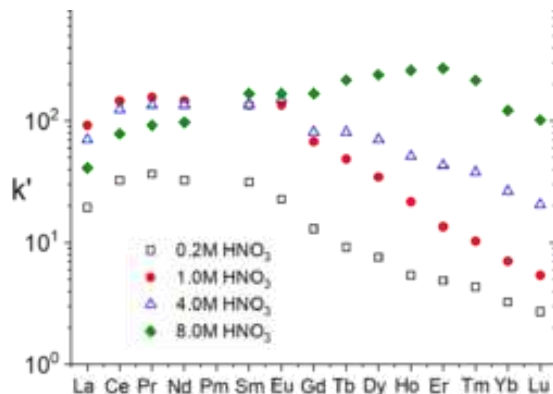


Figure 1.10. Acid-dependency of Eichrom RE Resin for lanthanide uptake. k' is a parameter linearly proportional to K_d (Huff and Huff, 1993).

Thus, the motivation behind this work is to more completely assess TEDGA stability constants across the lanthanide series and examine other opportunities for intragroup f-element separations using TEDGA. The properties examined, in particular, are stability constants, demonstrating speciation of $[\text{Ln}(\text{TEDGA})_n]^{3+}$ species; formation enthalpies (ΔH) and entropies (ΔS), describing thermodynamics of $[\text{Ln}(\text{TEDGA})_n]^{3+}$ species; and equilibrium distributions (K_d) of $[\text{An}(\text{TEDGA})_n]^{3+}$ species when using a chromatographic resin at varying TEDGA concentrations.

1.6 Hypothesis

TEDGA will form 1:3 complexes for all lanthanides considered and these complexes will increase in strength across the series. The Am/Cm separations work completed by Suzuki suggests that heavier trivalent f-elements are complexed more strongly by TEDGA than lighter f-elements. This will be reflected in stability constants (β), which will demonstrate a stronger tendency to form 1:3 complexes for later lanthanides. Additionally, formation enthalpies (ΔH) are expected to be more exothermic for later lanthanides, due to the stronger interaction of TEDGA with the heavier f-element.

1.7 Goal

Chromatographic trivalent actinide separations schemes can be improved by using TEDGA as an aqueous complexant with the RE Resin. As has been previously shown, TEDGA shows selectivity for the actinides Am and Cm in liquid-liquid extraction systems (Chapron et al., 2015; Suzuki et al., 2017). It is anticipated that TEDGA is selective for these and the heavier actinides Bk and Cf in extraction chromatography systems, where increasing TEDGA concentration in the liquid (mobile) phase will increase differences in K_d ratios between elements, thus increasing separation factors.

1.8 References

- Ansari, S.A.; Mohapatra, P.K. A review on solid phase extraction of actinides and lanthanides with amide based extractants. *J. Chromatogr. A.* 2017, *1499*, 1-20.
- Ansari, S.A.; Pathak, P.; Mohapatra, P.K.; Manchanda, V.K. Chemistry of diglycolamides: promising extractants for actinide partitioning. *Chem. Rev.* 2012, *112*, 1751-1772.
- Baldwin, A.G.; Ivanov, A.S; Williams, N.J.; Ellis, R.J.; Moyer, B.A.; Bryantsev, V.S.; Shafer, J.C. Outer-sphere water clusters tune the lanthanide selectivity of diglycolamides. *ACS Cent. Sci.* 2018, *4*, 739-747.
- Boatner, L.A.; Abraham, M.M. Electron paramagnetic resonance from actinide elements. *Rep. Prog. Phys.* 1978, *41*(1), 87-155.
- Bridge, G.; Barr, S.; Bouzarovski, S.; Bradshaw, M.; Brown, E.; Bulkeley, H.; Walker, G. *Energy and Society: A Critical Perspective*; Routledge: New York, NY, 2018.
- Chapron, S.; Marie, C.; Arrachart, G.; Miguiditchian, M.; Pellet-Rostaing, S. New insight into the americium/curium separation by solvent extraction using diglycolamides. *Solvent Extr. Ion Exc.* 2015, *33*, 236-248.
- Charbonnel, M.C.; Berthon, C.; Berthon, L.; Boubals, N.; Burdet, F.; Duchesne, M.T.; Guilbaud, P.; Mabile, N.; Petit, S.; Zorz, N. Complexation of Ln(III) and An(III) with hydrosoluble TEDGA: speciation and thermodynamics studies. *Procedia Chem.* 2012, *7*, 20-26.
- Chen, H.; Taylor, R.J.; Jobson, M.; Woodhead, D.A.; Boxall, C.; Masters, A.J.; Edwards, S. Simulation of neptunium extraction in an advanced PUREX process-model improvement. *Solvent Extr. Ion Exc.* 2017, *35*(1), 1-18.

- Choppin, G.; Liljenzin, J.; Rydberg, J.; Ekberg, C. "Chapter 21: The Nuclear Fuel Cycle." In *Radiochemistry and Nuclear Chemistry (Fourth Edition)*, 685-751. Oxford: Academic Press, 2013.
- Choppin, G.; Rydberg, J. *Nuclear Chemistry: Theory and Applications*. Pergamon Press, 1980, Appendix H.
- Clark, A.E.; Yang, P.; Shafer, J.C. "Coordination of Actinides and the Chemistry Behind Solvent Extraction." In *Experimental and Theoretical Approaches to Actinide Chemistry*, edited by J.K. Gibson and W.A. de Jong, John Wiley & Sons LTD, 2018, 237-282.
- Croft, A.G.; Tedder, D.W.; Drago, J.P.; Blomeke, J.O.; Perona, J.J. "Actinide partitioning-transmutation program final report: I, overall assessment." ORNL-5566, 1980. Oak Ridge National Laboratory, Oak Ridge, Tennessee.
- Edlund, M. C. "Transmutation of Radioactive Wastes: An Assessment." In *Nuclear Technologies in a Sustainable Energy System*, edited by G. S. Bauer and A. McDonald, Springer-Verlag, 1983, 305–310.
- Ewing, R. C. Long-term storage of spent nuclear fuel. *Nat. Mater.* 2015, 14, 252-257.
- Gujar, R. B.; Ansari, S. A.; Mohapatra, P. K.; Leoncini, A.; Verboom, W. Solid phase extraction of Am(III) and Cm(III) from acidic feeds using tetraethyl diglycolamide (TEDGA) in ionic liquid. *J. Radioanal. Nucl. Ch.* 2016, 309, 819-825.
- Harris, D.C. "Chapter 22: Introduction to Analytical Separations." *Quantitative Chemical Analysis*, 8th ed., W.H. Freeman, 2010, 537–564.
- Horwitz, E.P. Extraction chromatography of actinides and selected fission products: Principles and achievement of selectivity. In *Proceedings of the International Workshop on the Application of Extraction Chromatography in Radionuclide Measurement*, 1998, 27 – 37.
- Horwitz, E.P.; McAlister, D.R.; Bond, A.H.; Barrans, R.E. Novel Extraction Chromatographic Resins Based on Tetraalkyldiglycolamides: Characterization and Potential Applications, *Solvent Extr. Ion Exc.* 2005, 23, 319-344.
- Horwitz, E.P.; McAlister, D.R.; Dietz, M.L. Extraction chromatography versus solvent extraction: how similar are they? *Sep. Sci. Technol.* 2006, 41(10), 2163-2182.
- Huff, E.A.; Huff, D.R., "TRU Spec and RE Spec Chromatography: Basic Studies and Applications," 34th ORNL/DOE Conference On Analytical Chemistry In Energy Technology. Gatlinburg TN, 1993.
- Husain, M.; Ansari, S.A.; Mohapatra, P.K.; Gupta, R.K.; Parmar, V.S.; Manchanda, V.K. Extraction chromatography of lanthanides using N,N,N',N'-tetraoctyl diglycolamide (TODGA) as the stationary phase. *Desalination.* 2008, 229, 294-301.

- IAEA. "Implications of Partitioning and Transmutation in Radioactive Waste Management." Technical Report Series No. 435; International Atomic Energy Agency: Vienna, Austria, 2004.
- IEA. "Nuclear Power in a Clean Energy System." *International Energy Agency*, 2019, www.iea.org/publications/nuclear/.
- Klaß, L.; Wilden, A.; Kreft, F.; Wagner, C.; Geist, A.; Panak, P.J.; Herdzyk-Konieczko, I.; Narbutt, J.; Modolo, G. Evaluation of the hydrophilic complexant N,N,N',N'-tetraethyldiglycolamide (TEDGA) and its methyl-substituted analogues in the selective Am(III) separation. *Solvent Extr. Ion Exc.* 2019, 37(5), 297-312.
- Kolarik, Z.; Dressler, P. Extraction and coextraction of Tc(VII), Zr(IV), Np(IV,VI), Pa(V), and Nb(V) with tributyl phosphate from nitric acid solutions. *Solvent Extr. Ion Exc.* 1989, 7(4), 625-644.
- Krishnamurthy, N.; Gupta, C. K. Extractive metallurgy of rare earths. *Int. Mater. Rev.* 1992, 37, 197-248.
- Lanham, W.B.; Runion, T.C. "Purex Process for Plutonium and Uranium Recovery." ORNL-479, 1949. Oak Ridge National Laboratory, Oak Ridge, Tennessee.
- Nash, K. A review of the basic chemistry and recent developments in trivalent f-elements separations. *Solvent Extr. and Ion Exc.* 1993, 11, 729-768.
- O'Boyle, N.C.; Nicholson, G.P.; Piper, T.J.; Taylor, D.M.; Williams, D.R.; Williams, G. A review of plutonium(IV) selective ligands. *Appl. Radiat. Isot.* 1997, 48(2), 183-200.
- Ohta, H.; Ogata, T.; Yokoo, T.; Ougier, M.; Glatz, J.; Fontaine, B.; Breton, L. Low-burnup irradiation behavior of fast reactor metal fuels containing minor actinides. *Nucl. Technol.* 2009, 165, 96-110.
- Robinson, M. T.; Krause, J. F. The yields of the chemical elements in thermal neutron fission of U-235. *Nucl. Sci. and Engr.* 1956, 1, 216-221.
- Rohrig, B. "Smartphones: Smart Chemistry." American Chemical Society, 2015, www.acs.org/content/acs/en/education/resources/highschool/chemmatters/past-issues/archive-2014-2015/smartphones.html.
- Salvatores, M. Nuclear fuel cycle strategies including partitioning and transmutation. *Nucl. Eng. Des.* 2005, 235, 805-816.
- Sasaki, Y.; Sugo, Y.; Kitatsuji, Y.; Kirishima, A.; Kimura, T.; Choppin, G. R. Complexation and back extraction of various metals by water-soluble diglycolamide. *Anal. Sci.* 2007, 23, 727-31.

- Sato, T. Liquid-liquid extraction of rare-earth elements from aqueous acid solutions by acid organophosphorus compounds. *Hydrometallurgy*, 1989, 22, 121-140.
- Suzuki, H.; Tsubata, Y.; Matsumura, T. High-performance alkyl diamide amine and water-soluble diamide ligand for separating of Am(III) from Cm(III). *Anal. Sci.* 2017, 33, 239-242.
- Tsoufanidis, Nicholas. *The Nuclear Fuel Cycle*. American Nuclear Society, 2013.
- US Department of Energy. Critical Materials Strategy. US Department of Energy, 2010, Washington, DC, 1–191.
- US EPA. “Nutrient Pollution.” EPA, Environmental Protection Agency, 2019, www.epa.gov/nutrientpollution/issue.
- Whittaker, D.; Geist, A.; Modolo, G.; Taylor, R.; Sarsfield, M.; Wilden, A. Applications of diglycolamide based solvent extraction processes in spent nuclear fuel reprocessing, Part 1: TODGA. *Solvent Ex. and Ion Exc.* 2018, 36, 223-256.
- Williams, Brian. “Mass Distribution of Fission Fragments - Nuclear Energy.” *Global Warming Causes*, 2019, www.briangwilliams.us/nuclear-energy-3/mass-distribution-of-fission-fragments.html.
- Wilson, A. M.; Bailey, P. J.; Tasker, P. A.; Turkington, J. R.; Grant, R. A.; Love, J. B. Solvent extraction: the coordination chemistry behind extractive metallurgy. *Chem. Soc. Rev.* 2014, 43, 123-134.
- Xie, F.; Zhang, T. A.; Dreisinger, D.; Doyle, F. A critical review on solvent extraction of rare earths from aqueous solutions. *Miner. Eng.* 2014, 56, 10-28.

CHAPTER TWO

EXPERIMENTAL DETAILS

2.1 Reagents

TEDGA was synthesized by and purchased from Marshallton Laboratories LLC at above 99% purity and confirmed by NMR spectroscopy. Previously made lanthanide nitrate stock solutions were standardized using ICP-OES. Nitric acid was purchased from Macron Fine Chemicals. Sodium nitrate solutions were made by dissolving solid anhydrous NaNO_3 purchased from Fisher Scientific. Chromatographic RE resin (50-100 μm mesh size) was purchased from Eichrom Technologies. Ultima Gold liquid scintillation cocktail was purchased from Perkin Elmer.

2.1.1 Nitric Acid Solutions

Concentrated nitric acid was purchased from Macron. The concentrated acid was diluted to 250 mL quantities of 0.2, 0.4, 0.6, 0.8, 1.0, and 2.0 M HNO_3 using 18 $\text{M}\Omega$ water in volumetric flasks. Acid solutions were stored in Nalgene bottles, and it was assumed that concentration remained constant over the months of experimentation.

Potentiometric measurements were completed using Orion Series Ross Semi-micro Electrodes. Electrodes were calibrated using standards at pH 4, 7, and 10, supplied by Fisher Scientific. Potassium hydrogen phthalate (KHP) (~0.20 g) were used to standardize a 0.52 ± 0.07 M NaOH solution. Each day that the NaOH solution was used, at least one more KHP standardization was completed to assay NaOH concentration. The NaOH was consistently found to be within the concentration and uncertainties listed above.

To standardize HNO_3 solutions, 5 mL quantities were stirred and titrated with the standardized NaOH solution under nitrogen atmosphere, held at 25.0°C using a water jacket. The

only exception to this was the 2.0 M solution, where 2.5 mL was mixed with 2.5 mL of water prior to the titration. This was done to enable the equivalence point to be reached within 20 mL of base additions due to the volume constraint of working in a 25 mL vial. Acid solutions were confirmed to have approximately the desired concentrations: 0.21 ± 0.02 M, 0.42 ± 0.02 M, 0.62 ± 0.02 M, 0.83 ± 0.01 M, 1.01 ± 0.01 M, and 1.99 ± 0.04 M.

2.1.2 Lanthanide Solutions

Lanthanide stock standardization was completed using ICP-OES in partnership with Eichrom Technologies. Volumetric flasks (100 mL) were calibrated gravimetrically by filling to the line with 18 M Ω water of known temperature (typically around 22.0°C, measured with a Thermo Scientific thermocouple thermometer). Using precise water density literature, the exact volume of water in the flask was then determined (Handbook of Chemistry and Physics, 1971). This was done three times for each flask. Samples were then prepared in triplicate containing an estimated 10 ppm of Ln(NO₃)₃ (Ln = La, Pr, Nd, Sm, Eu, Gd, Dy, Ho, Er, Tm, Yb, Lu) in 2% w/w nitric acid using previous estimates of stock concentration and precise dilution factors for the calibrated glassware. After ICP-OES determined each sample's concentration, the dilution factors were then applied to back-calculate the stock concentrations. Stock concentrations were all around 0.5 M Ln(NO₃)₃.

Lanthanide working solutions were prepared by diluting stocks to 20 mL using a combination of 2 M HNO₃ and 18 M Ω water. All lanthanide stocks had approximately 1 M HNO₃ acidity for the experiments for two reasons: first, to ensure constant ionic strength, and second, to prevent lanthanide hydrolysis (Brown and Eckberg, 2016). The stock lanthanides had an unknown acid concentration; however, it was assumed that this would be negligible based on the volume ratios used in diluting to form working solutions.

2.1.3 TEDGA Solutions

TEDGA working solutions were made by gravimetrically measuring liquid TEDGA into volumetric glassware, and then diluting with 2 M NaNO₃ or 1 M HNO₃. This yielded 10 mL solutions of approximately 2, 10, 20, 50, 100, and 200 mM TEDGA with 2 M NaNO₃ ionic strength, and 100 mL solutions of 100 mM and 250 mM TEDGA solutions in 1 M HNO₃. The 100 mM and 250 mM solutions were used for spectrophotometry and calorimetry as produced, respectively; the other solutions were diluted by a factor of 2 using HNO₃ solutions when used for chromatography experiments.

2.1.4 Radiochemicals

Radiotracer quantities of ^{152,154}Eu, ²⁴⁹Bk, and ²⁴⁹Cf were used from stocks previously made at the Colorado School of Mines Radiochemistry Laboratory. ²⁴⁹Bk and ²⁴⁹Cf were produced and supplied by the High Flux Isotope Reactor at Oak Ridge National Laboratory. ^{152,154}Eu was produced by neutron irradiation of Eu at the USGS 1 MW TRIGA Reactor at the Denver Federal Center. ²⁴¹Am and ²⁴⁴Cm were supplied by Eckert and Ziegler. New 500 μL stocks were made of ²⁴¹Am and ²⁴⁴Cm in 1 M HNO₃, with concentrations of approximately 4,000 dpm/μL and 7,500 dpm/μL, respectively.

The ²⁴⁹Bk and ²⁴⁹Cf were used from a single dual-label solution. This is possible because ²⁴⁹Bk is a β-emitter, while ²⁴⁹Cf is an α-emitter. With a sensitive scintillation cocktail such as Ultima Gold and an energy discriminator provided by the HIDEX scintillation counter, the activity of each isotope in a mixture can be determined. The ²⁴¹Am and ²⁴⁴Cm are also α-emitters and were counted using Ultima Gold scintillation cocktail with a HIDEX scintillation counter for consistency.

2.2 Methods

2.2.1 Spectrophotometry

Spectrophotometric measurements were completed on a Cary 300 dual beam spectrophotometer. Spectrophotometric titrations were completed by titrating a 100 mM TEDGA solution into 1.5 mL of 10-35 mM $\text{Ln}(\text{NO}_3)_3$ ($\text{Ln} = \text{Pr}, \text{Nd}, \text{Sm}, \text{Ho}, \text{Er}$) solutions at 1 M HNO_3 constant ionic strength and acidity. Injection sizes were 10, 25, 50, 75, and 100 μL , with the larger volumes used during the later stages of the titration. These lanthanides were selected because they have absorption bands in the visible region of the spectrum that shift in energy and intensity during complexation with TEDGA (Henrie et al., 1976). Over the course of each titration, Ln:TEDGA ratios were gradually increased from pure lanthanide to around 1:10 to provide an opportunity for 1:1, 1:2, and 1:3 Ln:TEDGA complex formation. The titrand solution was mixed in the cuvette using a pipette. Spectrophotometric data was manually baselined and normalized in Microsoft Excel. Principle Component Analysis (Appendix A) was done using Sixpack to determine how many stability constants could be fit to the baselined and normalized spectrophotometric data, as indicated by the number of significant eigenvectors to predict variability in the main photoppeak over the course of the titration. The stability constants of 1:1, 1:2, and 1:3 Ln:TEDGA complexes were then determined by fitting the data in HypSpec software (Appendix B). Fitting used the built-in regression iteration method for Ho and Er, and was done manually for Pr, Nd, and Sm complexes (*vide infra*).

HypSpec typically fits data using an automated regression iteration process. However, when left to its own devices, this would lead to overfitting of the data for the early lanthanides Pr, Nd, and Sm. One or more stability constants would be fit to negative extinction coefficients in order to provide a better fit to the remaining constants (Figure 2.1). Furthermore, extinction coefficient vs.

wavelength curves sometimes showed separate species to be multiples of each other, centered around the same peaks. Both of these suggest errors to the fit. Negative extinction coefficients are unreasonable under the conditions of this experiment, and each species is expected to have its own extinction coefficient spectrum with unique peaks and intensities. By manipulating stability constants manually, fits could be determined with reasonable extinction coefficient curves for each species (Pr shown in Figure 2.2; all lanthanides in Appendix C). For Pr and Sm, HypSpec's error regression analysis could still be performed to estimate the errors in each stability constant. These values probably underestimate the errors because of this, as there is no way to be sure that a stability constant has been adequately fit other than a minimization of regression error while maintaining reasonable speciation and extinction parameters. For unknown reasons, error could not be estimated for Nd.

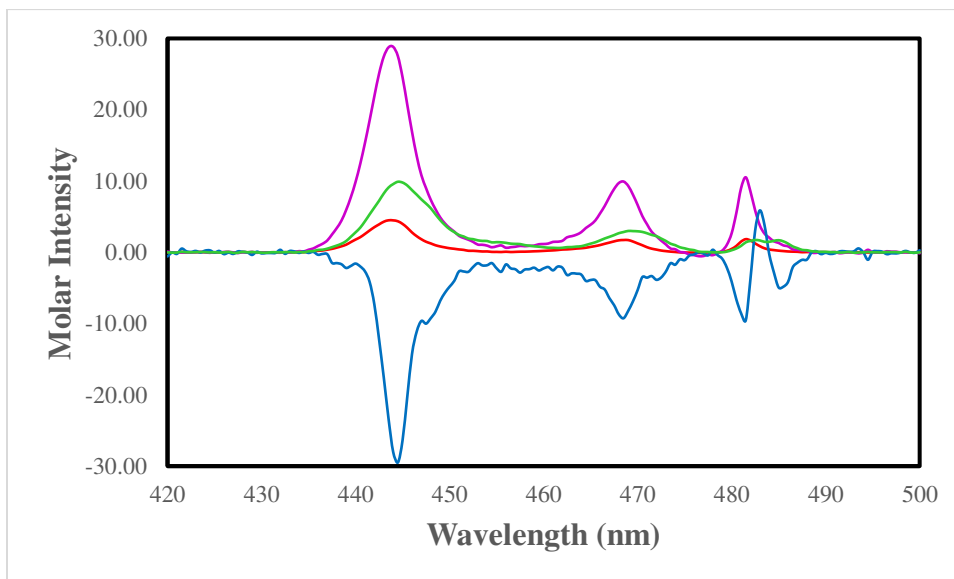


Figure 2.1. Erroneous extinction coefficient spectra for 0.035 M $\text{Pr}(\text{NO}_3)_3$ titrated with TEDGA at 1 M HNO_3 acidity. Free Pr^{3+} is shown in red, $[\text{Pr}(\text{TEDGA})]^{3+}$ in green, $[\text{Pr}(\text{TEDGA})_2]^{3+}$ in blue, and $[\text{Pr}(\text{TEDGA})_3]^{3+}$ in purple. Note the strongly negative coefficient for $[\text{Pr}(\text{TEDGA})_2]^{3+}$, which is unreasonable under these conditions.

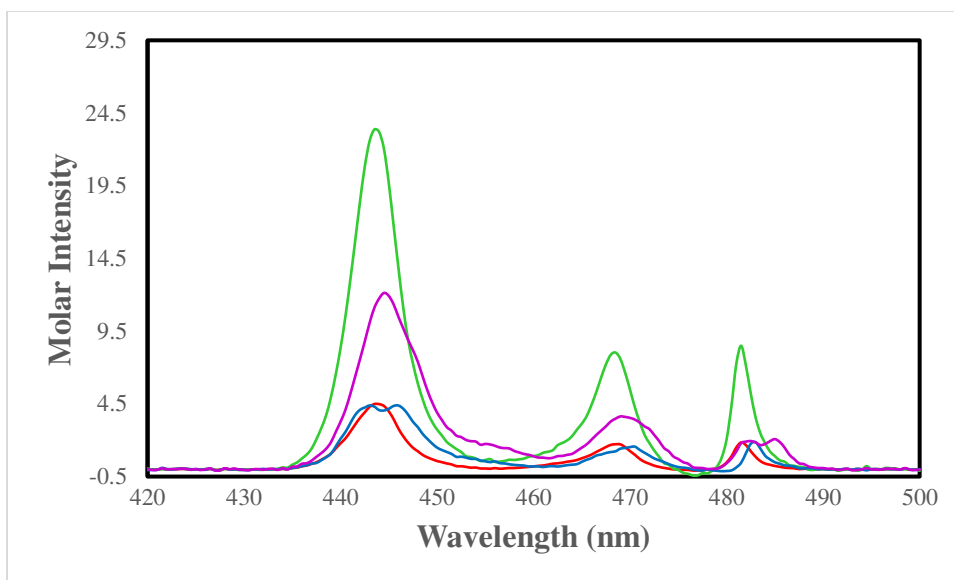


Figure 2.2. Reasonable extinction coefficient spectra for 0.035 M $\text{Pr}(\text{NO}_3)_3$ titrated with TEDGA at 1 M HNO_3 acidity. Free Pr^{3+} is shown in red, $[\text{Pr}(\text{TEDGA})]^{3+}$ in green, $[\text{Pr}(\text{TEDGA})_2]^{3+}$ in blue, and $[\text{Pr}(\text{TEDGA})_3]^{3+}$ in purple. All species demonstrate positive absorbance on the order of 10^0 - $10^1 \text{ M}^{-1}\text{cm}^{-1}$, centered around unique wavelengths.

2.2.2 Calorimetry

Calorimetric titrations were completed using a TA Instruments Affinity ITC. Calorimetric titrations were done by injecting a 250 mM TEDGA solution into a 1 mL cell solution of approximately 10 mM $\text{Ln}(\text{NO}_3)_3$ ($\text{Ln} = \text{Pr}, \text{Nd}, \text{Sm}, \text{Ho}, \text{Er}$) solutions at 1 M HNO_3 constant ionic strength and acidity. Injection size was 10 μL , and 25 injections were completed in each titration at 25°C. Over the course of each titration, Ln:TEDGA ratios were increased from pure lanthanide to around 1:6 to enable formation of the 1:1, 1:2, and 1:3 Ln:TEDGA complexes. Heat rates into the reaction cell after each injection are compared to an identical blank cell, recorded, and integrated to provide the heats released in each reaction step. The first reaction step is always discarded due to diffusion effects between the cell and the injection needle. Data was corrected for dilution effects by titrating a 250 mM TEDGA solution into water at 1 M HNO_3 constant ionic strength. It was determined that a lanthanide dilution correction (water into 10 mM $\text{Ln}(\text{NO}_3)_3$ at 1

M HNO₃ constant ionic strength) was negligible and unnecessary for all metals, releasing heats approximately two orders of magnitude less than the [Ln(TEDGA)_n]³⁺ complexation reactions in all cases. The HypCal fitting software was then used to determine ΔH, ΔS, and ΔG values for stepwise formation of [Ln(TEDGA)₃]³⁺ complexes (Appendix D). While HypCal fits stability constants, it is generally a less reliable method of doing so compared to spectrophotometry. When significant disagreement arose between stability constants from HypSpec and HypCal, those provided by HypSpec are expected to be more accurate.

2.2.3 Chromatography Studies

Chromatography batch studies were performed to measure uptake of radioisotopes into Eichrom RE resin under various conditions.

First, acid-dependency was measured. Resin (10-20 mg quantities) were weighed into 2 mL vials. To each vial, 0.5 mL of 0.2 M, 0.4 M, 0.6 M, 0.8 M, or 1.0 M HNO₃ and a spike of radiotracer were then added. Solutions were vortexed for 1 hour and then centrifuged for 5 minutes. Samples were then filtered with a luer-slip syringe filter to remove the resin, and 200 μL aliquots were counted by LSC (α- and β-emitters) and Gamma Scintillation (γ-emitters).

To assess the TEDGA dependency, a range of TEDGA concentrations was used at constant acidic strength. Resin (30 mg quantities) were weighed into 2 mL vials. Each vial contained 1 mM, 5 mM, 10 mM, 25 mM, 50 mM, or 100 mM TEDGA at 1 M acidity and 1.5 M NO₃⁻. A spike of radiotracer was then added. Solutions were vortexed for 1 hour and then centrifuged for 5 minutes. Samples were then filtered to remove the resin, and 200 μL aliquots were counted by LSC (α- and β-emitters) and Gamma Scintillation (γ-emitters). Gamma counting was completed using a Cobra II NaI Crystal Scintillator Gamma Detector. Alpha and beta counting was performed using a Hidex

Liquid Scintillation Counter. K_d ratios were calculated using Equation 1.6 in the Introduction.
Higher K_d values imply greater uptake of the radiotracer into the resin.

2.3 References

Brown, P.L. and Ekberg, C. "Chapter 8: Scandium, Yttrium, and the Lanthanide Metals." In *Hydrolysis of Metal Ions*. John Wiley & Sons Ltd, 2016, 225-324.

"Handbook of Chemistry and Physics." Handbook of Chemistry and Physics, 53rd ed., Chemical Rubber Co, 1971, p. F4.

Henrie, D.E.; Fellows, R.L.; Choppin, G.R. Hypersensitivity in the electronic transitions of lanthanide and actinide complexes. *Coordin. Chem. Rev.*, 1976, 18(2), 199-224.

CHAPTER THREE

OBSERVATIONS AND DATA

In this chapter, TEDGA complexation with trivalent f-elements is discussed. In section 3.1, thermodynamic titrations of TEDGA with lanthanide elements are used to assess conditional stability constants (β), formation enthalpies (ΔH), and formation entropies (ΔS) of $[\text{LnTEDGA}]^{3+}$, $[\text{Ln}(\text{TEDGA})_2]^{3+}$, and $[\text{Ln}(\text{TEDGA})_3]^{3+}$ complexes in aqueous media. In section 3.2, TEDGA is shown to improve the quality of a chromatographic material for trivalent actinide separations by increasing differences in K_d values for adjacent elements.

3.1 Thermodynamic Data

TEDGA solutions were injected into $\text{Ln}(\text{NO}_3)_3$ solutions at 1 M HNO_3 strength and 25°C , yielding $[\text{LnTEDGA}]^{3+}$, $[\text{Ln}(\text{TEDGA})_2]^{3+}$, and $[\text{Ln}(\text{TEDGA})_3]^{3+}$ complexes according to their stepwise equilibria. In spectrophotometric titrations, shifts in the hypersensitive electronic transition peaks for each metal demonstrated complexation and yielded isosbestic points, indicating multiple species. In calorimetric titrations, variations in reaction step heats yielded the stoichiometry of complexation. As was proposed, there was a significant difference between the early and late lanthanides; these are addressed separately in sections 3.1.1 and 3.1.2, respectively (Charbonnel et al., 2012). Relevant thermodynamic data, including conditional stability constants, ΔH , and ΔS are reported in Table 3.1. Conditional stability constants were calculated for both spectrophotometric (HypSpec) and calorimetric (HypCal) titrations. Spectrophotometric and calorimetric fits can be found in Appendix B and Appendix D, respectively. For the early lanthanides, there is good agreement between both; for the later lanthanides, the spectrophotometrically determined stability constants appear to be more robust.

Table 3.1. Thermodynamics of lanthanide-TEDGA complexes collected at 1 M HNO₃.

Metal	log β (HypSpec)	log β (HypCal)	ΔH (kJ/mol)	ΔS (J/mol*K ⁻¹)
<i>Pr</i>				
1:1	3.07(7)	3.4(2)	-5.6(2)	46(3)
1:2	6.3(2)	6.4(3)	-9.4(3)	91(5)
1:3	8.4(3)	8.5(5)	-7.7(5)	137(9)
<i>Nd</i>				
1:1	3.46 ^x	3.5(3)	-5.8(3)	48(5)
1:2	6.59 ^x	6.6(3)	-9.8(3)	93(6)
1:3	9.54 ^x	9.1(5)	-8.6(5)	150(10)
<i>Sm</i>				
1:1	3.50(4)	3.5(3)	-5.5(3)	49(5)
1:2	6.70(9)	6.7(4)	-11.6(4)	89(8)
1:3	9.6(1)	9.6(5)	-11.8(5)	140(10)
<i>Ho</i>				
1:1	3.73(7)	1.9 ^x	--	--
1:2	7.6(2)	7(2)	-8.8(6)	100(30)
1:3	8.6(2)	9(3)	-11(2)	140(60)
<i>Er</i>				
1:1	2.68(3)	2 ^x	--	--
1:2	5.86(6)	7(2)	-8.5(7)	110(30)
1:3	7.89(7)	10(2)	-10(2)	160(40)

^xErrors not provided as they could not be accurately estimated.

3.1.1 Early Lanthanides (Pr, Nd, Sm)

The early lanthanides Pr, Nd, and Sm all clearly indicated the stepwise formation of 1:1, 1:2, and 1:3 Ln:TEDGA complexes. The formation of all three complexes was confirmed by Principal Component Analysis of spectrophotometric data (Pr shown in Figure 3.1; all metals shown in Appendix A). Shifts in visible absorption spectra over the course of the titrations were

calculated to be multiples of four significant eigenvectors; thus, the visible spectra can be mathematically calculated based on the equilibria of the free metal ion and the 1:1, 1:2, and 1:3 Ln:TEDGA complexes. These results were then manually fit in the HypSpec software as the HypSpec software, when ran in an automated mode, did not yield sufficiently specific results (see section 2.2.1).

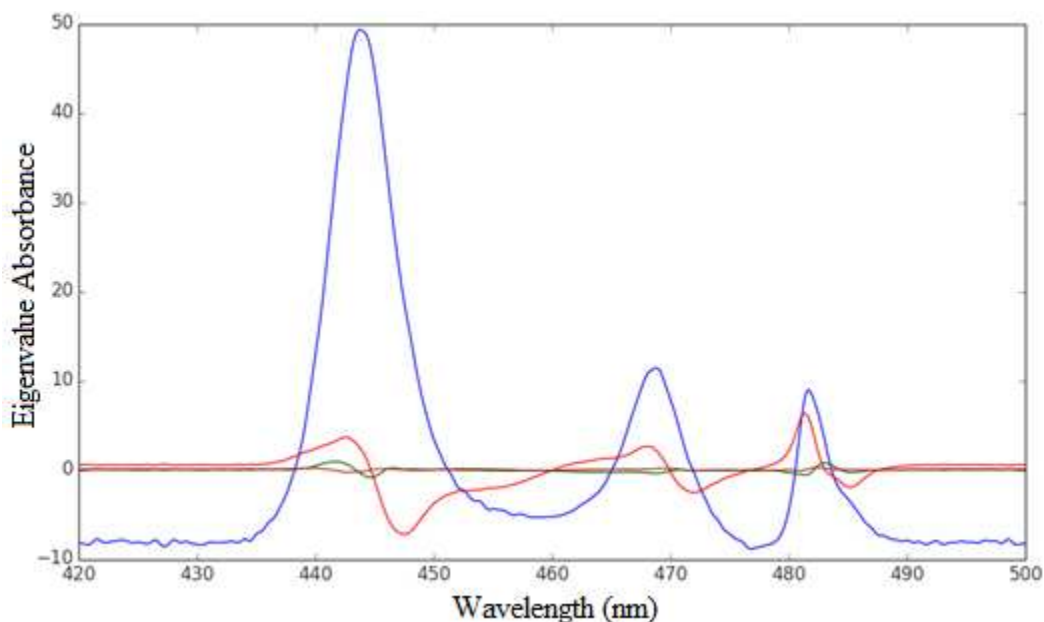


Figure 3.1. Principal Component Analysis of $[\text{Pr}(\text{TEDGA})_n]^{3+}$ spectrophotometric data. The first (blue), second (red), third (green) and fourth (yellow) eigenvectors are shown. All four eigenvectors have significant nonzero features, indicating the presence of four species: Pr^{3+} , $[\text{Pr}(\text{TEDGA})]^{3+}$, $[\text{Pr}(\text{TEDGA})_2]^{3+}$, and $[\text{Pr}(\text{TEDGA})_3]^{3+}$.

Spectrophotometrically determined conditional stability constants demonstrate large degrees of similarity between the early lanthanide elements in their complexation with TEDGA. All metals demonstrate stepwise formation of 1:1, 1:2, and 1:3 Ln:TEDGA complexes. All 1:1 complexes have a $\log \beta_1$ around 3.5, while all 1:2 complexes have a $\log \beta_2$ around 6.5, and all 1:3 complexes have a $\log \beta_3$ of around 9. Errors could not be estimated for the Nd complexes. For Pr and Sm, $\log \beta_1$ and $\log \beta_2$ are each within error. Thus, no clear trends are immediately discernable based upon

the β_1 and β_2 conditional stability constants for each metal. However, β_3 steadily increases from Pr to Nd to Sm. Thus, the speciation of the 1:3 Ln:TEDGA complex becomes more dominant relative to the 1:1 and 1:2 complex for later (i.e. smaller) lanthanides. Though, it is only when TEDGA is in a large excess that the 1:3 complex becomes favored.

Calorimetric data was fit using HypCal, which first fits a titration curve's stoichiometry (based on stability constants), and then from this fits ΔH and ΔS for each species. For the early lanthanides (Pr, Nd, and Sm) thermodynamic fits appeared to be quite accurate (Figure 3.2). For these metals, conditional stability constant estimates from both HypCal and HypSpec were consistent with each other. Fits for all calorimetric titrations can be found in Appendix D.

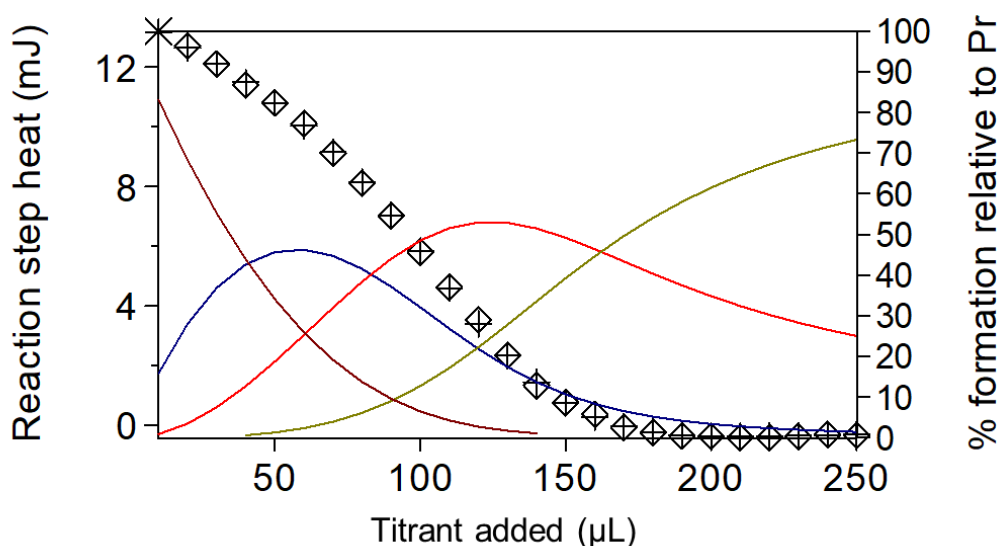


Figure 3.2. A sample experimental fit for a calorimetric titration of 0.25 M TEDGA into 1 mL of 13.73 mM $\text{Pr}(\text{NO}_3)_3$ at 1 M HNO_3 constant ionic strength and acidity in both solutions and 25°C reaction cell temperature. Speciation of free Pr^{3+} is shown in brown, $[\text{Pr}(\text{TEDGA})]^{3+}$ in blue, $[\text{Pr}(\text{TEDGA})_2]^{3+}$ in red, and $[\text{Pr}(\text{TEDGA})_3]^{3+}$ in yellow. There is good agreement between measurements (squares) and calculated values (crosses).

Each of the early lanthanides demonstrated stepwise formation of 1:1, 1:2, and 1:3 Ln:TEDGA complexes. At first glance, ΔH_3 became more exothermic for later lanthanides and

suggests an enthalpic favoring of the later lanthanide 1:3 Ln:TEDGA complexes; however, ΔH_2 and ΔH_3 for Pr and Nd are each within error. All ΔH_1 values appear approximately equal and are within error, each around -5.6 kJ/mol. For Pr and Nd, ΔH_2 is greater in magnitude than ΔH_3 , while for Sm, ΔH_2 and ΔH_3 are approximately equal and within error of each other. The ΔH_2 values are around -10 kJ/mol for each metal, and ΔH_3 values increase in magnitude from around -8 to -12 kJ/mol.

The general pattern appears to be a greater enthalpic favoring of the $[\text{Ln}(\text{TEDGA})_3]^{3+}$ complex for later lanthanides, while no clear trend is discernable for 1:1 and 1:2 complexes. This is consistent with stability constant estimates in both HypCal and HypSpec, which were in good agreement for the early lanthanides.

The entropies of each complex demonstrate a much clearer trend. For these lanthanides, $\Delta S_3 > \Delta S_2 > \Delta S_1 > 0$, indicating that complexation becomes more entropically favored as the TEDGA number increases. This is probably due to the increase in molecular freedom associated with water molecules being liberated due to metal-TEDGA coordination. Free Pr^{3+} , Nd^{3+} , and Sm^{3+} ions in solution are expected to be 9-coordinate, with nine bound water molecules. During complexation with TEDGA, these water molecules are freed into solution, increasing the overall disorder of the system.

For the early lanthanides, thermodynamic trends suggest the smaller lanthanide cations more readily form the 1:3 Ln:TEDGA complex than the larger lanthanides. Pr and Nd seem to enthalpically favor the 1:2 complex over the 1:3 complex, in agreement with previous work (Charbonnel et al., 2012). For Sm, the 1:2 and 1:3 complexes appear to have approximately the same formation enthalpy, so neither is intrinsically favored. This could be the transition point to the later lanthanides (*vide infra* section 3.1.2). Lastly, all early lanthanides demonstrated the

greatest entropic favoring when forming the 1:3 complex compared to the 1:1 and 1:2 complexes, likely because formation of this complex releases nine water molecules into solution.

3.1.2 Late Lanthanides (Ho and Er)

The late lanthanides Ho and Er did not clearly demonstrate stepwise formation of 1:1, 1:2, and 1:3 complexes. Principal component analyses of these elements suggested that $[\text{Ho}(\text{TEDGA})_n]^{3+}$ absorption spectra result from the combination of three eigenvectors, while $[\text{Er}(\text{TEDGA})_n]^{3+}$ absorption spectra could be calculated with two or three eigenvectors (Appendix A). While one eigenvector must correspond to the free Ho^{3+} and Er^{3+} ions, it is not obvious what the other eigenvectors indicate. When attempting to fit the data in HypSpec, several different fits were attempted. When only a 1:1 or a 1:3 complex was fit to the data, results differed greatly from attempts to fit a 1:1, 1:2, and 1:3 complex, and so on. The most confident fits include formation of 1:1, 1:2, and 1:3 complexes; however, these fits have some noteworthy errors (*vide infra*).

For Ho and Er, conditional stability constant estimates varied significantly and do not demonstrate a clear trend. Both spectra were fit iteratively in HypSpec to minimize errors, but errors remained large in a few cases (particularly, $\log \beta_2$ and $\log \beta_3$ had errors greater than 0.1 for Ho). More significantly, variations in conditional stability constants were much greater than would be realistically expected for adjacent lanthanides. Going from Ho to Er, $\Delta \log \beta_1 \approx -1$, $\Delta \log \beta_2 \approx -2$, and $\Delta \log \beta_3 \approx -1$. While not impossible, it seems unlikely that a ligand such as TEDGA would have selectivity of this magnitude for adjacent late lanthanides. It seems more likely that these variations are artifacts of the fitting.

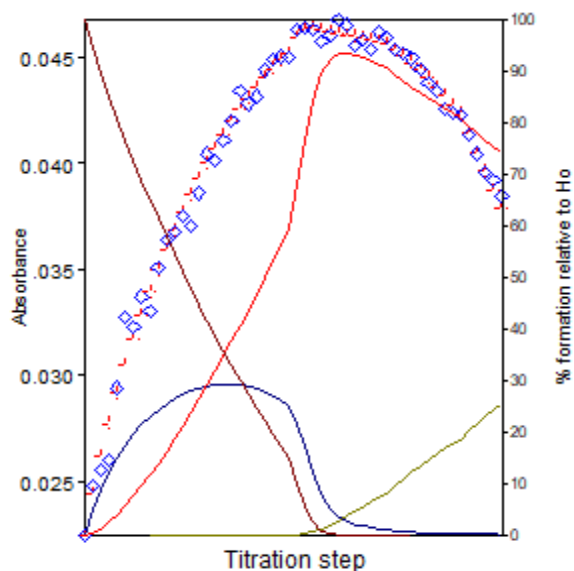


Figure 3.3. HypSpec fit for the Ho^{3+} absorption peak at 451.5 nm, titrating TEDGA into 1.5 mL of 11.27 mM $\text{Ho}(\text{NO}_3)_3$ at 1 M HNO_3 constant ionic strength and acidity. Speciation of free Ho^{3+} is shown in brown, $[\text{Ho}(\text{TEDGA})]^{3+}$ in blue, $[\text{Ho}(\text{TEDGA})_2]^{3+}$ in red, and $[\text{Ho}(\text{TEDGA})_3]^{3+}$ in yellow. Visually, there is good agreement between measurements (squares) and calculated values (crosses), suggesting the fit is accurate.

At first glance, a visual comparison of simulated and measured data suggests a good fit for both elements (Ho in Figure 3.3; all metals in Appendix B). However, the extinction coefficient curves illuminate errors. For Ho, it appears that $[\text{Ho}(\text{TEDGA})]^{3+}$ and $[\text{Ho}(\text{TEDGA})_2]^{3+}$ have nearly identical extinction coefficients (Figure 3.4). This is an indicator that one species has been erroneously fit as two. For Er, it appears that $[\text{Er}(\text{TEDGA})]^{3+}$, $[\text{Er}(\text{TEDGA})_2]^{3+}$, and possibly the free Er^{3+} ion are multiples of each other (Appendix C). Here again, this suggests that a single species has erroneously been fit as two or three separate species. Recall that these errors are consistent with the Principal Component Analysis, which suggested three species for the Ho-TEDGA titration data and two or three for the Er-TEDGA titration data. In summary, the stability constant estimates for Ho and Er reported in Table 3.1 are reported while treading with light feet. Alternative assessments under different conditions might provide some insight. Assessment of

separations chemistry for the heaviest lanthanides could also provide some indication of differences in stability constants.

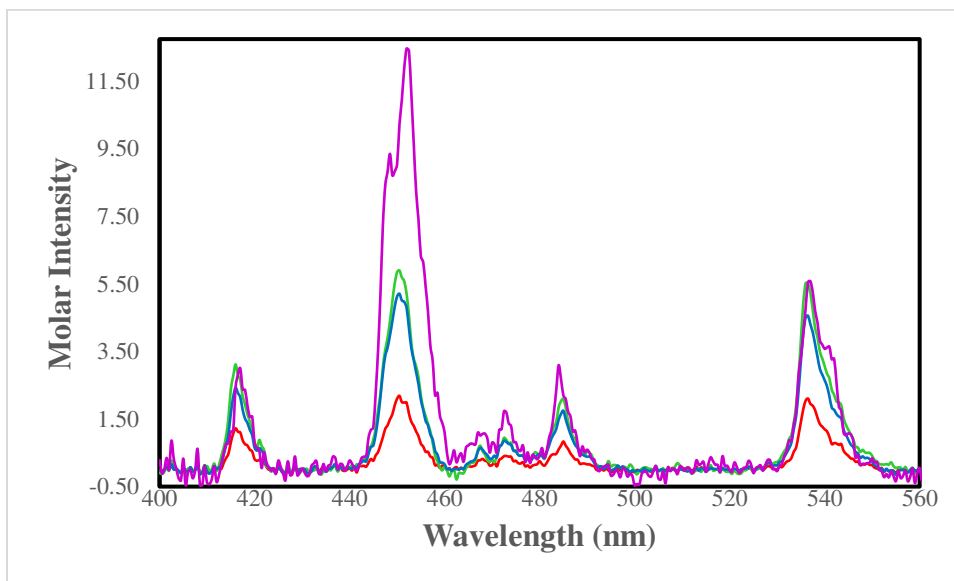


Figure 3.4. Extinction coefficient spectra for fits to 11.27 mM $\text{Ho}(\text{NO}_3)_3$ titrated with TEDGA at 1 M HNO_3 acidity. Free Ho^{3+} is shown in red, $[\text{Ho}(\text{TEDGA})]^{3+}$ in green, $[\text{Ho}(\text{TEDGA})_2]^{3+}$ in blue, and $[\text{Ho}(\text{TEDGA})_3]^{3+}$ in purple. Large degrees of similarity between curves suggest confounding and misidentification of species.

It should be noted, though, that second and third order fits to spectrophotometric data appear to have even greater systematic errors. Leaving out $[\text{Ho}(\text{TEDGA})]^{3+}$ and fitting $[\text{Ho}(\text{TEDGA})_2]^{3+}$ and $[\text{Ho}(\text{TEDGA})_3]^{3+}$ failed to provide any results that could approximate the titration data. Fitting to only a $[\text{Ho}(\text{TEDGA})_3]^{3+}$ complex similarly led to results that did not remotely demonstrate any accuracy. The same was true for additional Er fits.

Thus, spectrophotometric results for Ho and Er did not appear very reliable. While it is possible that each of Er's conditional stability constants are an order of magnitude less than those of Ho, it seems very unlikely that such a drastic change would be observed. It remains possible that $\log \beta_3$ is less for Er than Ho based on calorimetry data. From the spectrophotometric fits, though, the extent of this difference is not clear.

Consistent with the spectrophotometric titrations, calorimetric titrations of the late lanthanides (Ho and Er) were also difficult to resolve (Appendix D). The experimental thermograms fit a combination of 1:1, 1:2, and 1:3 Ln:TEDGA complexes after a great deal of persistence. The errors in these fits are large. Nonetheless, the most confident fitting results are reported in Table 3.1 and elaborated on below. The conditional stability constants fit in HypCal were mostly dependent on the initial input value for $\log \beta_1$. The best fits (minimizing regression error) were achieved with the reported values; however, the formation enthalpy and entropy of the 1:1 complex $[\text{Ln}(\text{TEDGA})]^{3+}$ could not be fit for Ho nor Er. Visually, the fits do not accurately represent the data, as is similarly reflected by the large uncertainties (Figure 3.5). It is postulated that, while the 1:1 complex was formed in the titration, its heat signature was not significant enough to be distinguished from the other complexes.

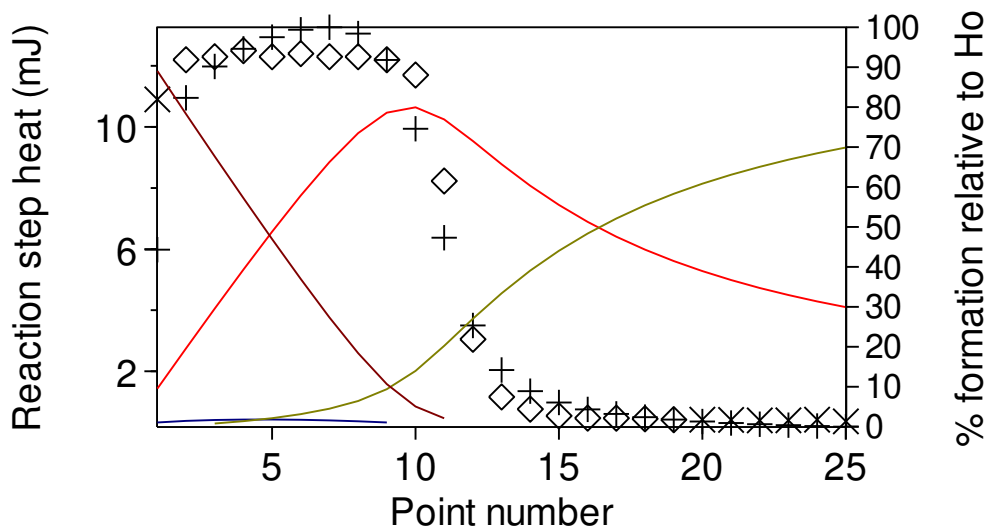


Figure 3.5. A sample experimental fit for a calorimetric titration of 0.25 M TEDGA into 1 mL of 11.27 mM $\text{Ho}(\text{NO}_3)_3$ at 1 M HNO_3 constant ionic strength and acidity in both solutions and 25°C reaction cell temperature. Speciation of free Ho^{3+} is shown in brown, $[\text{Ho}(\text{TEDGA})]^{3+}$ in blue, $[\text{Ho}(\text{TEDGA})_2]^{3+}$ in red, and $[\text{Ho}(\text{TEDGA})_3]^{3+}$ in yellow. There is poor agreement between measurements (squares) and calculated values (crosses).

Both Ho and Er demonstrated a more exothermic heat of formation for the 1:3 complex than the 1:2 complex, though both ΔH values are within error for both metals. This suggests that the 1:3 complex is enthalpically favored for these elements, rather than the 1:2 complex which was favored for the early lanthanides. Interestingly, ΔH_3 was smaller for Er than for Ho (within error), and both were smaller than ΔH_3 of Sm. Recall that for the early lanthanides, smaller elements had larger ΔH_3 values. It appears that for the late lanthanides, the opposite is true. The reasons for this are not obvious at this time, though steric crowding is anticipated to be more relevant for the smaller, heavier lanthanides and this may be inhibiting interactions between the lanthanide metal center and TEDGA for these elements.

No comment can realistically be made on the standard entropies for formation of late lanthanide complexes. Both complexes demonstrated ΔS_2 around $105 \text{ J/mol}\cdot\text{K}^{-1}$ and ΔS_3 around $150 \text{ J/mol}\cdot\text{K}^{-1}$, but errors for both numbers are very large.

For the late lanthanides, thermodynamic trends suggest that larger elements favor the 1:3 complex more than smaller ones. Furthermore, for all the late lanthanides, the 1:3 complex seems enthalpically favored over the 1:2 complex. However, the thermodynamics governing these systems is hardly clear. Despite the stoichiometric ratios used, the 1:1 complex was not sufficiently detected to be well fit from the data.

To summarize the thermodynamic data presented in section 3.1, it seems that TEDGA provides the most selectivity for early lanthanides. For Pr, Nd, and Sm, a much larger proportion of the 1:2 complex is formed relative to the 1:3 complex, with ΔH_3 becoming steadily more exothermic and ΔS_3 steadily increasing as lanthanide size decreases. It is likely that somewhere between Sm and Ho, there is a transition from favoring the 1:2 Ln:TEDGA complex to the 1:3 complex. This could occur as early as Sm, which demonstrated roughly the same ΔH for formation

of both the 1:2 and 1:3 complexes. While the data for lanthanides following this point is unclear, it seems that for later lanthanides ΔH_3 is greater than ΔH_2 , with ΔH_3 possibly decreasing in magnitude with lanthanide size. It is thus anticipated that later lanthanides show greater enthalpic favoring of the 1:3 complex relative to the 1:1 and 1:2 complexes.

3.2 Chromatography Results

Actinide (Am, Cm, Bk, Cf) uptake into Eichrom RE resin was studied in relation to acid concentration in the absence of TEDGA, and then in relation to TEDGA concentration at constant acidity (1 M HNO₃). Acid-dependence is reported in section 3.2.1, while TEDGA-dependence is reported in section 3.2.2. TEDGA appears to increase the selectivity of the chromatographic system, as will be shown in these sections.

3.2.1 Acid Dependence

All actinides demonstrated increasing uptake into resin with increasing acidity, signified by the increase in K_d values at higher acid concentrations. For each isotope, plotting $\log K_d$ vs. \log HNO₃ led to a linear relationship (Figure 3.6), as is typical of well-behaved resin systems. The only exception to this is Bk (*vide infra*). This demonstrates that there are not significant competing equilibria with the uptake of trivalent actinide ions into the resin.

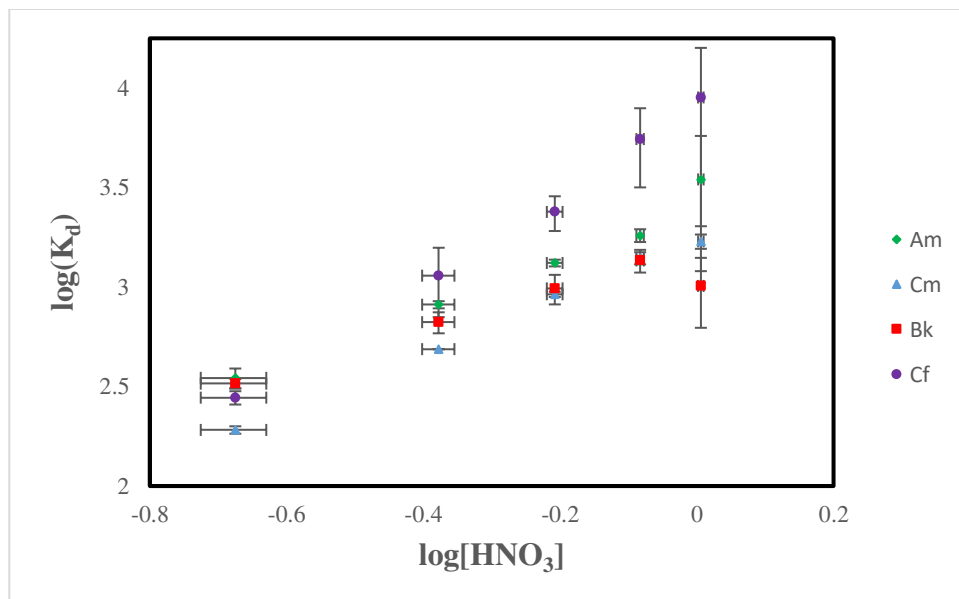


Figure 3.6. Acid-dependence of actinide uptake into 10-20 mg RE Resin in the absence of TEDGA. Error bars are reported to 1σ for both $[\text{HNO}_3]$ and K_d .

As Figure 3.6 demonstrates, actinide uptake into resin increases with increasing acid concentration. For all isotopes, the uptake is mostly linear. There is not a clear relationship between actinide ionic radius and uptake into resin. Californium, the smallest ion, demonstrates the greatest uptake, followed by americium, the largest ion. Berkelium demonstrates a decrease in uptake at 1.0 M HNO_3 compared to its maximum uptake at 0.8 M HNO_3 . This data is from a solution containing both Bk^{3+} and Cf^{3+} , so counting errors (i.e. Cf being counted as Bk) could possibly skew these values. This could be remedied by using unique solutions containing either Cf or Bk to determine these K_d values. All actinides show large and overlapping errors at 1.0 M HNO_3 . This is attributed to low count rates in the aqueous phase at this acidity, since almost all activity was concentrated in the resin.

3.2.2 TEDGA Dependence

TEDGA is expected to bond to actinides and hold them in the aqueous phase, preventing uptake in the resin and decreasing the measured K_d ratio. This effect is expected to be more pronounced for smaller actinides based on previous results (Suzuki et al., 2017).

Distribution coefficients (K_d) and their standard deviations (σ) are summarized in Table 3.2. For all actinides, increasing TEDGA concentration led to smaller K_d values, as expected (Figure 3.7). This signifies that TEDGA is bonding to actinides and holding them in the liquid phase instead of bonding to the resin. Interestingly, the effect is more pronounced for larger, not smaller, actinides. The greatest decreases in K_d with increasing TEDGA concentration are observed for Am^{3+} , followed by Cm^{3+} , Bk^{3+} , and then Cf^{3+} . This signifies that TEDGA is most strongly bonding with larger, rather than smaller, actinides.

Table 3.2. Resin uptake (K_d) and standard deviation (σ) of uptake for actinides at different TEDGA concentrations with 30 mg of RE resin and 0.5 mL of 1 M H^+ , 2 M NO_3^- solution. Berkelium and californium were not studied at 0.005 M TEDGA concentration.

[TEDGA]	K_d Am	σ_{Am}	K_d Cm	σ_{Cm}	K_d Bk	σ_{Bk}	K_d Cf	σ_{Cf}
0.001	1433.40	190.74	1397.74	88.79	391.18	57.05	863.18	88.12
0.005	250.07	47.16	295.07	15.71	-	-	-	-
0.010	173.61	53.24	214.56	10.63	67.73	5.18	292.68	12.55
0.025	89.80	4.59	153.43	1.32	60.67	12.70	304.03	58.72
0.050	85.04	7.34	142.49	13.22	49.65	3.88	272.11	24.09
0.100	67.36	4.62	129.35	3.11	55.38	2.10	287.31	28.17

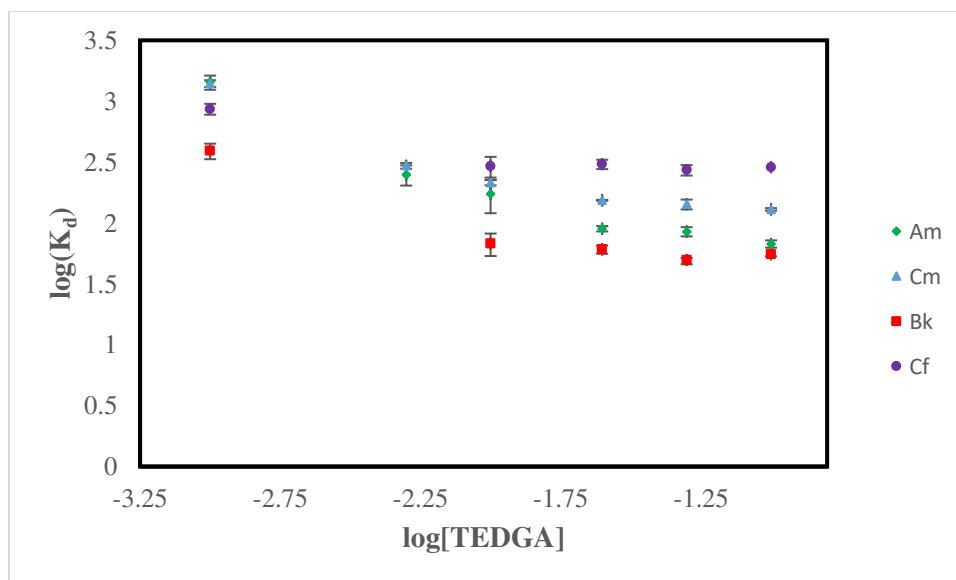


Figure 3.7. TEDGA-dependence of actinide uptake into 30 mg RE Resin at 1 M H⁺ and 2 M NO₃⁻. Error bars are reported to 1σ.

Differences between actinides are not immediately clear. Americium demonstrates a larger decrease in uptake than curium at identical conditions. This suggests that TEDGA is more effectively holding-back Am³⁺ than Cm³⁺. This was not expected, since TEDGA is thought to bond more strongly to Cm³⁺ than Am³⁺ based on previous results (Chapron et al., 2012; Suzuki et al., 2017). At low TEDGA concentrations, Am³⁺ and Cm³⁺ demonstrate virtually the same uptake into the resin, so it seems unlikely that the selectivity between these elements is due to the qualities of the resin itself. Further experimentation will be necessary to fully understand why Am³⁺ and Cm³⁺ behaved in this way.

Both Bk³⁺ and Cf³⁺, which were examined in the same dual-label solution, demonstrate a “flat-lining” of data for TEDGA concentrations greater than 10 mM, which could indicate a saturation of either the aqueous or the solid phase. Am³⁺ and Cm³⁺ demonstrate the same effect, but only after a higher concentration of TEDGA (25 mM). It is not clear why this occurs. The most likely explanation is that TEDGA provides diminishing selectivity returns above a certain

concentration. Furthermore, it seems that this concentration is inversely related to actinide size, with larger actinides showing selectivity to higher TEDGA concentrations.

3.3 References

Chapron, S.; Marie, C.; Arrachart, G.; Miguirditchian, M.; Pellet-Rostaing, S. New insight into the americium/curium separation by solvent extraction using diglycolamides. *Solvent Extr. Ion Exc.* 2015, *33*, 236-248.

Charbonnel, M.C.; Berthon, C.; Berthon, L.; Boubals, N.; Burdet, F.; Duchesne, M.T.; Guilbaud, P.; Mabilille, N.; Petit, S.; Zorz, N. Complexation of Ln(III) and An(III) with hydrosoluble TEDGA: speciation and thermodynamics studies. *Procedia Chem.* 2012, *7*, 20-26.

Suzuki, H.; Tsubata, Y.; Matsumura, T. High-performance alkyl diamide amine and water-soluble diamide ligand for separating of Am(III) from Cm(III). *Anal. Sci.* 2017, *33*, 239-242.

CHAPTER FOUR

DISCUSSION

TEDGA appears to have selectivity for trivalent f-elements. In section 4.1, lanthanide selectivity will be discussed based on thermodynamic data; then, in section 4.2, actinide selectivity will be discussed based on improvements to a chromatographic system.

4.1 Thermodynamic Selectivity for Lanthanides

Based on the results reported in Chapter Three, TEDGA demonstrates thermodynamic selectivity for lanthanides. From trends in both the speciation and thermodynamic parameters governing complexation, TEDGA shows a greater tendency to form 1:3 complexes with later lanthanides than earlier ones, supporting the hypothesis. This selectivity could be capitalized on for lanthanide separations processes.

4.1.1 Conditional Stability Constants of $[\text{Ln}(\text{TEDGA})_n]^{3+}$ Complexes

Stability constants provide useful information regarding speciation of $[\text{Ln}(\text{TEDGA})_n]^{3+}$ complexes. For the early lanthanides (Pr, Nd, and Sm), conditional stability constant estimates are consistent from both HypSpec and HypCal. For these elements, $\log \beta_1$ and $\log \beta_2$ are constant around 3.5 and 6.6, respectively, while $\log \beta_3$ increases from 8.5 to 9.1 to 9.6 for Pr, Nd, and Sm. This demonstrates an increase in the relative proportion of the 1:3 complex for later (i.e. smaller) lanthanides. The half-order of magnitude difference between adjacent lanthanides Pr and Nd suggests good selectivity, and similar selectivity between Nd and Sm.

Speciation plots can be generated in HySS software using experimental stability constants for each complex and compared. This is shown in Figure 4.1. For each metal, 1:1 and 1:2 complexes form at low concentrations of TEDGA. As TEDGA concentration increases, 1:3

complexes form in significantly greater proportion for Sm than for Nd and Pr. Above a 4:1 TEDGA:Ln excess, the $[\text{Ln}(\text{TEDGA})_3]^{3+}$ complex is the dominant species for all metals. At 4:1 excess, approximately 90% of Sm is bound as $[\text{Sm}(\text{TEDGA})_3]^{3+}$, versus 80% for Nd and 60% for Pr. TEDGA could thus provide a $\text{SF}_{\text{Sm/Pr}} \approx 1.5$, $\text{SF}_{\text{Sm/Nd}} \approx 1.125$, and $\text{SF}_{\text{Nd/Pr}} \approx 1.33$ at this concentration if the 1:3 complexes are extracted. While separation factors of this magnitude are not competitive with industrial processes, they nonetheless are indicative of selectivity, as desired (Xie et al., 2014).

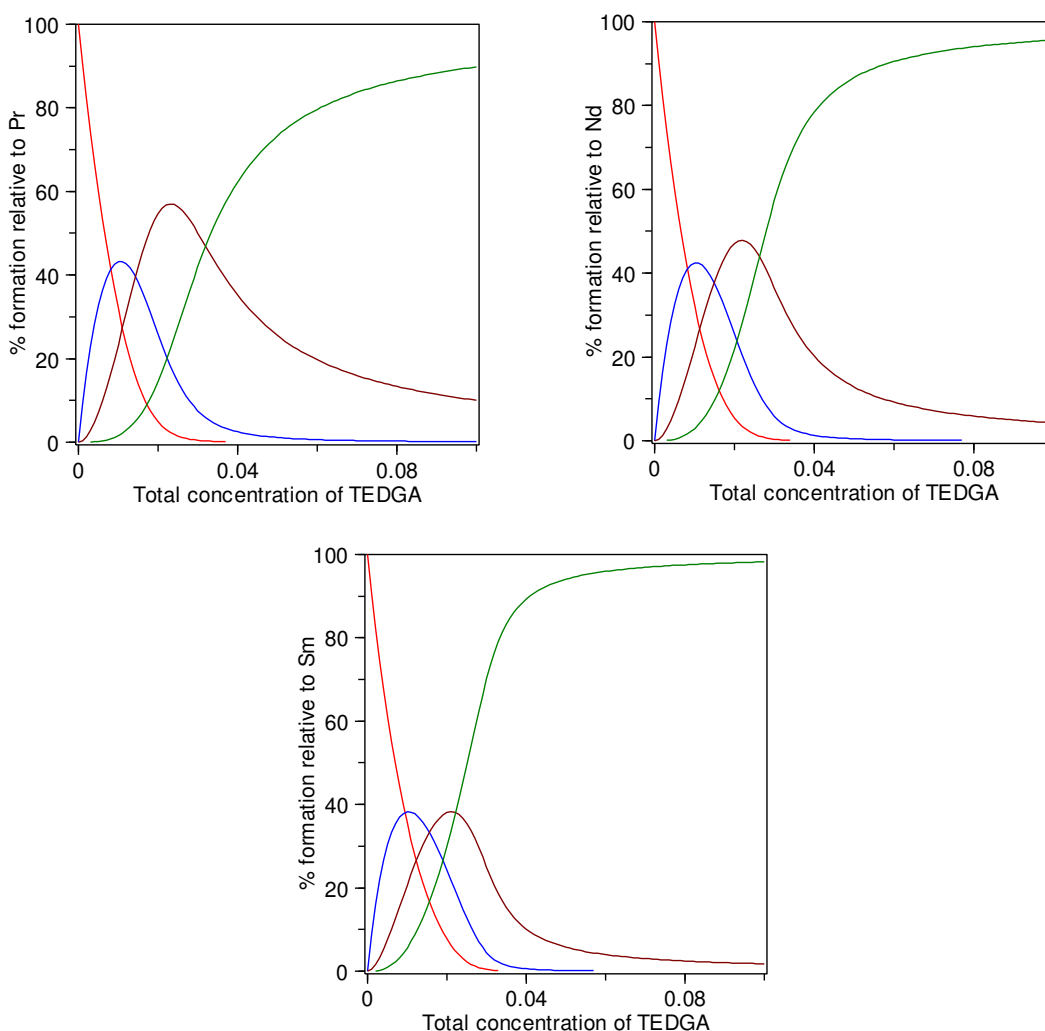


Figure 4.1. Speciation plots for Pr (left), Nd (right), and Sm (bottom) based off 1 M HNO_3 conditional stability constants and 10 mM $\text{Ln}(\text{NO}_3)_3$ concentration from 0 to 100 mM TEDGA concentration. Free metal is shown in red, $[\text{Ln}(\text{TEDGA})]^{3+}$ is shown in blue, $[\text{Ln}(\text{TEDGA})_2]^{3+}$ is shown in brown, and $[\text{Ln}(\text{TEDGA})_3]^{3+}$ is shown in green.

It is worth noting that, to date, no stability constants for $[\text{Ln}(\text{TEDGA})_n]^{3+}$ complexes have been reported in the literature other than the Charbonnel 2012 conference paper. There is thus a dearth of information with which to compare the reported data. The results reported here are in agreement with Charbonnel's results and contribute towards understandings of TEDGA speciation with trivalent f-elements in aqueous media. Results for $\log \beta_1$ and $\log \beta_2$ are also in good agreement with reported stability constants for $[\text{Am}(\text{TEDGA})_n]^{3+}$ complexes from Charbonnel and $[\text{Cm}(\text{TEDGA})_n]^{3+}$ complexes from Klab, assuming that Am^{3+} and Cm^{3+} behave similarly to the lanthanide ions Nd^{3+} and Pm^{3+} , respectively (Charbonnel et al., 2012; Klab et al., 2019). It is not immediately clear whether $\log \beta_3$ values are in good agreement or not, as there is significant error in these values for both experiments. Nonetheless, values appear to be in the right ballpark orders of magnitude for $[\text{Ln}(\text{TEDGA})_n]^{3+}$ complexes.

For the late lanthanides (Ho and Er), conditional stability constant estimates are much less reliable. There is not good agreement between the stability constant estimates from HypSpec and HypCal. Based on the large errors in the fits from HypCal, the HypSpec constants appear the most accurate, but there are errors with these too (see section 3.1.2). Thus, for the late lanthanides, the results and interpretations thereof are conjecture, and further research is necessary to confirm or negate them.

For Ho and Er, it seems that the relative predominance of the 1:3 complex decreases for the smaller lanthanide Er. This trend in $\log \beta_3$ values (8.6 for Ho and 7.89 for Er) is not in good agreement with $\log \beta_3 = 9.2$ for ytterbium provided by Charbonnel. Generally, the decrease in all three stability constants from Ho to Er suggests that all three $[\text{Ln}(\text{TEDGA})_n]^{3+}$ complexes have complexation strengths significantly weaker for Er. This could be because the smaller lanthanide provides greater strain to coordinated TEDGA, which in turn could decrease bond strength. For

ions this late in the series, significant strain is anticipated to reach a nine-coordinate complex. Alternatively, the greater strain could cause less favorable energetics to form the later-lanthanide complex, decreasing its relative speciation. These results agree with the calorimetric studies, noted by the decrease in ΔH_3 from Ho to Er; however, these numbers are similarly in poor agreement with $\Delta H_3 = -18.3$ kJ/mol for Lu reported by Charbonnel.

Experimental stability constants for Ho and Er are used to generate speciation plots in Figure 4.2. Unlike the early lanthanides, the 1:3 complex does not become the preferred species until a large excess (approximately 12:1) of TEDGA for Ho. Additionally, the 1:1 complex does not form as the predominant species anywhere, instead being outweighed by the free ion and the 1:2 species for both Ho and Er. This could explain difficulties of fitting a 1:1 complex for the late lanthanides. For Er, the 1:3 complex becomes dominant around a 5:1 TEDGA excess. Interestingly, this means that the 1:3 complex is more favored for Er than for Ho. This is consistent with the early lanthanides, where the 1:3 complex becomes more favored for the smaller lanthanide.

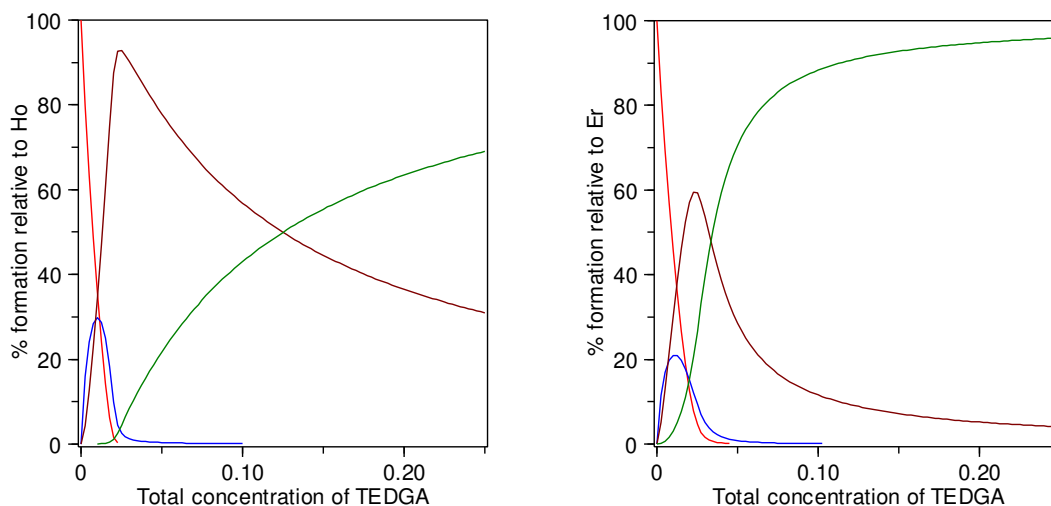


Figure 4.2. Speciation plots of Ho and Er during complexation with TEDGA based off conditional stability constants at 1 M HNO₃, 10 mM Ln(NO₃)₃, and TEDGA ranging from 0 to 250 mM. Free metal ion is shown in red, [Ln(TEDGA)]³⁺ is shown in blue, [Ln(TEDGA)₂]³⁺ is shown in brown, and [Ln(TEDGA)₃]³⁺ is shown in green.

Using Equation 1.9, separation factors for $[\text{Ln}(\text{TEDGA})_3]^{3+}$ complexes can be determined for lanthanides based on the stability constants β_3 (Table 4.1). The average separation factor for adjacent early lanthanides is approximately 3, which is similar to the separations provided by TODGA in this part of the series (Husain et al., 2008). For adjacent lanthanides, a separation factor of 3 is relatively high, and demonstrates good selectivity. The later lanthanides Ho and Er demonstrate a large separation factor of 5.13, though this could be inflated due to large variances in β_3 estimates. Interestingly, little separation is seen between the early and late lanthanides Pr and Ho.

Table 4.1. Separation factors of lanthanide combinations based off of stability constants for $[\text{Ln}(\text{TEDGA})_3]^{3+}$ complexes. Stability constants from calorimetric data were used for the early lanthanides (Pr, Nd, Sm) and from spectrophotometric data for the late lanthanides (Ho, Er).

Metal Combination	Separation Factor
<i>Nd/Pr</i>	3.98
<i>Sm/Nd</i>	3.16
<i>Sm/Pr</i>	12.6
<i>Ho/Er</i>	5.13
<i>Ho/Pr</i>	1.26

Thus, from a speciation standpoint, later lanthanides increasingly favor the 1:3 complex. TEDGA thus provides selectivity from a speciation standpoint, manifesting as a favored or disfavored preference for the 1:3 complex, with a maximum occurring somewhere between Sm and Ho. The selectivity provided by TEDGA is of similar magnitude to the selectivity provided by TODGA, another diglycolamide complexant.

4.1.2 Thermodynamic Constants of $[\text{Ln}(\text{TEDGA})_n]^{3+}$ Complexes

As with the stability constants, the thermodynamic parameters ΔH , ΔS , and ΔG demonstrate TEDGA selectivity for lanthanides.

Enthalpies of formation for $[\text{Ln}(\text{TEDGA})_n]^{3+}$ complexes vary across the lanthanide series. For the earliest lanthanides, formation enthalpy of $[\text{Ln}(\text{TEDGA})]^{3+}$ appears constant, and formation enthalpy of $[\text{Ln}(\text{TEDGA})_2]^{3+}$ is more exothermic than the formation of $[\text{Ln}(\text{TEDGA})_3]^{3+}$, demonstrating an enthalpic preference for the 1:2 complex over the 1:3. Continuing across the lanthanide series, formation of $[\text{Ln}(\text{TEDGA})_3]^{3+}$ relative to $[\text{Ln}(\text{TEDGA})_2]^{3+}$ becomes more favorable as lanthanide size decreases. At Sm, the two complexes appear to have approximately the same formation enthalpy. For elements smaller than Sm, $[\text{Ln}(\text{TEDGA})_3]^{3+}$ is more enthalpically favored than $[\text{Ln}(\text{TEDGA})_2]^{3+}$. It is possible that this favoring increases with decreasing lanthanide size, continuing the trend from the early lanthanides; however, the data presented in this report are not precise enough to support or negate this claim.

Entropies of formation for $[\text{Ln}(\text{TEDGA})_n]^{3+}$ complexes demonstrate interesting trends. For all lanthanides, $\Delta S_3 > \Delta S_2$. This is perhaps expected, as coordination of each tridentate TEDGA releases 2-3 free H_2O molecules into solution. For early lanthanides, ΔS_1 and ΔS_2 are approximately constant around $48 \text{ J/mol}\cdot\text{K}^{-1}$ and $90 \text{ J/mol}\cdot\text{K}^{-1}$. For late lanthanides, ΔS_2 is similarly constant around $105 \text{ J/mol}\cdot\text{K}^{-1}$. ΔS_3 is approximately constant for all lanthanides, around $150 \text{ J/mol}\cdot\text{K}^{-1}$. This signifies that smaller lanthanides have greater complex disorder, and that there is a difference between early and late lanthanides for ΔS_2 but not for ΔS_3 (*vide infra*, section 4.1.3).

From ΔH and ΔS , the free energy for formation of complexes, ΔG , can be calculated at any temperature (T , [K]) according to equation 4.1.

$$\Delta G = \Delta H - T\Delta S \quad (4.1)$$

Similarly, ΔG can be calculated from the equilibrium constant of formation, according to equation 4.2.

$$\Delta G = -RT\ln\beta \quad (4.2)$$

For the purpose of separations and selectivity, ΔG_3 is particularly interesting. Tabulated ΔG_3 values at 25°C are shown in Table 4.2.

Table 4.2. Gibbs free energy (ΔG) for formation of $[\text{Ln}(\text{TEDGA})_3]^{3+}$ complexes at 25°C. Note that an extra significant figure was added to all numbers to demonstrate differences.

Metal	ΔG_3 (kJ/mol)	
	$\Delta H_3 - T\Delta S_3$	$-RT \ln \beta_3$
<i>Pr</i>	-48.5	-48.5
<i>Nd</i>	-53.3	-51.9
<i>Sm</i>	-53.5	-54.8
<i>Ho</i>	-52.7	-51
<i>Er</i>	-57.7	-57

Variations in ΔG_3 illustrate selectivity between TEDGA and lanthanides, particularly early ones. $[\text{Ln}(\text{TEDGA})_3]^{3+}$ complexes become significantly more favored from Pr to Nd to Sm, as indicated by decreases in ΔG_3 of approximately 3 kJ/mol for adjacent elements. For the later lanthanides, variations in ΔG_3 are large, but less reliable due to large errors in each value. Formation entropies for $[\text{Ln}(\text{TEDGA})_3]^{3+}$ complexes are approximately 150 J/mol·K⁻¹, while enthalpies are on the order of -10 kJ/mol. At 25°C, $-T\Delta S_3$ thus contributes around four-times as much to ΔG_3 than ΔH_3 does. Thus, entropy drives $[\text{Ln}(\text{TEDGA})_3]^{3+}$ complex formation.

The large observed entropies are likely due to two causes. First, formation of 1:3 Ln:TEDGA complexes release eight or nine water molecules into solution, which consequently increases disorder significantly. Second, TEDGA is charge-neutral, so Ln-TEDGA interactions are likely weak. Particularly when steric crowding occurs around lanthanides, weak bonds allow for significant freedom of coordinated TEDGA, increasing disorder. This causes entropic favoring for $[\text{Ln}(\text{TEDGA})_3]^{3+}$ complexes.

4.1.3. Comparison to Diglycolic Acid (DGAc)

Besides the few ΔH values provided by Charbonnel, energetic parameters for $[\text{Ln}(\text{TEDGA})_n]^{3+}$ complexes are absent in the literature. Thus, there are few values with which the results can be directly compared. Instead, the reported thermodynamic parameters can be compared to diglycolic acid (DGAc), which shares the coordinating diglycol backbone with TEDGA (Figure 4.3).

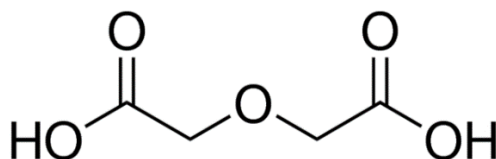


Figure 4.3. Structure of diglycolic acid (DGAc).

There is good agreement for trends in ΔH between Ln-TEDGA and Ln-DGAc complexes (Figure 4.4). Diglycolic acid complexes demonstrate an increasingly exothermic ΔH_1 , ΔH_2 , and ΔH_3 for smaller early lanthanides, reaching a maximum around Eu. Enthalpies then decrease in magnitude for later, smaller lanthanides, especially for formation of 1:1 and 1:2 complexes. Interestingly, formation of $[\text{Ln}(\text{DGAc})]^+$ and $[\text{Ln}(\text{DGAc})_2]^-$ complexes is endothermic for the smallest lanthanides Er, Tm, Yb, and Lu. While ΔH_3 decreases in magnitude slightly from Gd to Lu, it remains relatively constant between -20 kJ/mol and -15 kJ/mol (Grenthe, 1963). Trends in ΔH for formation of Ln-DGAc complexes are in agreement with $[\text{Ln}(\text{TEDGA})_n]^{3+}$ complexes, which also demonstrate more exothermic formation of complexes for smaller early lanthanides with a maximum around Sm, and less exothermic formation of complexes of late lanthanides. While the formation enthalpies of $[\text{Ln}(\text{TEDGA})_2]^{3+}$ complexes appear to decrease in magnitude significantly between Sm and Ho, the formation enthalpies of $[\text{Ln}(\text{TEDGA})_3]^{3+}$ complexes only decrease in magnitude slightly, remaining constant around -10 kJ/mol. ΔH_3 values are greater in

magnitude for DGAc than for TEDGA, presumably because the ionic interaction of DGAc^{2-} ligands leads to stronger binding with the lanthanide metal than the polar interactions of TEDGA ligands. These trends demonstrate an enthalpically-preferential formation of the 1:3 complex relative to the 1:2 and 1:1 complexes that is increasingly pronounced across the lanthanide series for both TEDGA and DGAc.

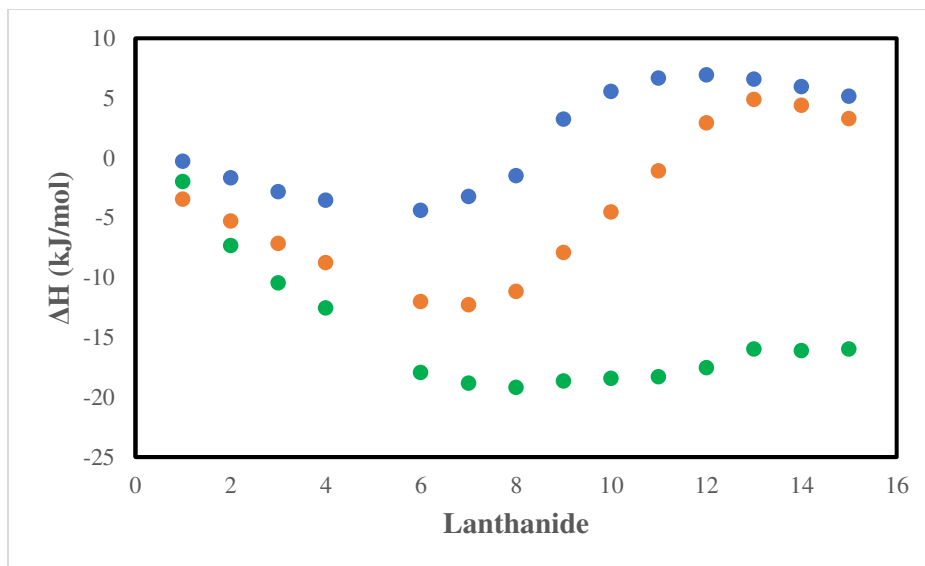


Figure 4.4. Formation enthalpies (ΔH) for $[\text{Ln}(\text{DGAc})_n]^{3-2n}$ complexes (Grenthe, 1963). The 1:1 complex is shown in blue, the 1:2 complex is shown in orange, and the 1:3 complex is shown in green.

Trends in complex formation entropy are similarly in agreement for both $[\text{Ln}(\text{TEDGA})_n]^{3+}$ and $[\text{Ln}(\text{DGAc})_n]^{3-2n}$. Ln-DGAc complexes demonstrate interesting entropy with lanthanide size (Figure 4.5). For $[\text{Ln}(\text{DGAc})]^+$, ΔS_1 is approximately constant at $90 \text{ J/mol}\cdot\text{K}^{-1}$ for early lanthanides and $120 \text{ J/mol}\cdot\text{K}^{-1}$ for late lanthanides, with the increase observed between Eu and Dy. Similarly, for $[\text{Ln}(\text{DGAc})_2]^-$ complexes, entropies of formation are a constant $150 \text{ J/mol}\cdot\text{K}^{-1}$ for the early lanthanides and $210 \text{ J/mol}\cdot\text{K}^{-1}$ for late lanthanides, with an increase observed between Gd and Tm. Entropy of formation of $[\text{Ln}(\text{DGAc})_3]^{3-}$ complexes is constant around $190 \text{ J/mol}\cdot\text{K}^{-1}$ for all lanthanides. It appears that early and late lanthanide-DGAc complexes thus have unique,

constant entropies, with the later lanthanides demonstrating a greater formation entropy and with the increase observed in the middle of the series for 1:1 and 1:2 complexes (Grenthe, 1963).

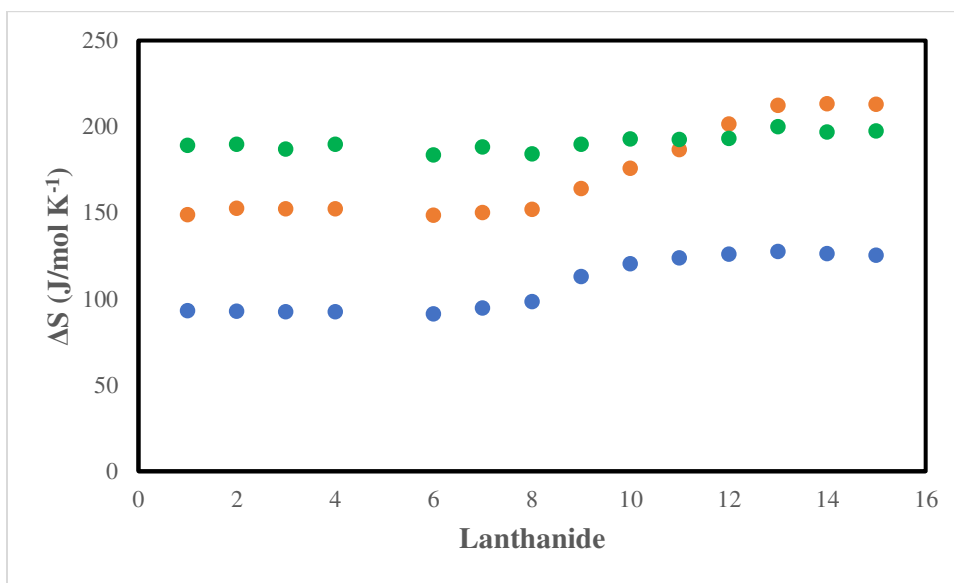


Figure 4.5. Formation entropies (ΔS) for $[\text{Ln}(\text{DGAc})_n]^{3-2n}$ complexes (Grenthe, 1963). The 1:1 complex is shown in blue, the 1:2 complex is shown in orange, and the 1:3 complex is shown in green.

The differences between early and late lanthanides can be attributed to the equilibria of free diglycolate (DGAc^{2-}) ions in solution and complexed diglycolate in $[\text{Ln}(\text{DGAc})_n]^{3-2n}$. Early lanthanide complexes are expected to have a coordination number of nine, so a 1:1 complex contains six water molecules and has the form $[\text{Ln}(\text{DGAc})(\text{H}_2\text{O})_6]^+$. Late lanthanide complexes are expected to have a coordination number of eight, so the 1:1 complex has the form $[\text{Ln}(\text{DGAc})(\text{H}_2\text{O})_5]^+$. The latter complex has greater entropy than the former (Grenthe, 1963). Thus, the complexation of free DGAc^{2-} ions is more entropically favorable for eight-coordinate lanthanides than nine-coordinate lanthanides. The same argument is made for the 1:2 Ln:DGAc complexes $[\text{Ln}(\text{DGAc})_2(\text{H}_2\text{O})_3]^-$ and $[\text{Ln}(\text{DGAc})_2(\text{H}_2\text{O})_2]^-$ for early and late lanthanides, respectively. For both 1:1 and 1:2 complexes, the increase in entropy observed in the middle of the series reflects competitive equilibria in the formation of eight- and nine-coordinate complexes.

Entropy of formation of 1:3 complexes shows very little variance across the lanthanide series, as all lanthanides form the nine-coordinate $[\text{Ln}(\text{DGAc})_3]^{3-}$ complex. The slight increase in complex entropy that is observed is likely due to greater crowding of ligands around the lanthanide, since the metal center decreases in size across the series.

The same trends are observed for $[\text{Ln}(\text{TEDGA})_2]^{3+}$ and $[\text{Ln}(\text{TEDGA})_3]^{3+}$ complexes, though they are less pronounced. For $[\text{Ln}(\text{TEDGA})_2]^{3+}$ complexes, the early lanthanides appear to have a smaller entropy of formation (around $90 \text{ J/mol}\cdot\text{K}^{-1}$) compared to the late lanthanides (around $105 \text{ J/mol}\cdot\text{K}^{-1}$). As with DGAc, this demonstrates a greater entropy of eight-coordinate $[\text{Ln}(\text{TEDGA})_2(\text{H}_2\text{O})_2]^{3+}$ complexes compared to nine-coordinate $[\text{Ln}(\text{TEDGA})_2(\text{H}_2\text{O})_3]^{3+}$ complexes. For $[\text{Ln}(\text{TEDGA})_3]^{3+}$ complexes, formation entropy is approximately constant around $150 \text{ J/mol}\cdot\text{K}^{-1}$. In all instances, reported ΔS values are greater for Ln-DGAc complexes than Ln-TEDGA complexes. As with enthalpic constants, this is likely because DGAc can deprotonate and have a strong ionic interaction with Ln^{3+} , while TEDGA cannot. The decrease in overall charge during formation of $[\text{Ln}(\text{DGAc})_n]^{3-2n}$ complexes increases entropy, while there is no change in overall charge during $[\text{Ln}(\text{TEDGA})_n]^{3+}$ formation. Thus, the results reported for Ln-TEDGA complex formation entropies agree with those reported for Ln-DGAc complexes.

Free energy of formation of Ln-TEDGA and Ln-DGAc complexes are also in agreement. For Ln-DGAc complexes, ΔG becomes more negative for smaller early lanthanides, and constant for lanthanides later than Sm (Figure 4.6; Grenthe, 1963). The same was observed for $[\text{Ln}(\text{TEDGA})_3]^{3+}$ complexes. For the early lanthanides, ΔG_3 became a few kJ/mol more negative for smaller adjacent lanthanides. Following Sm, ΔG_3 was approximately constant. ΔG_3 was smaller in magnitude for $[\text{Ln}(\text{TEDGA})_3]^{3+}$ complexes compared to $[\text{Ln}(\text{DGAc})_3]^{3-}$ complexes, likely

because of the favorability of forming the ionic DGAc complex compared to the neutral TEDGA complex.

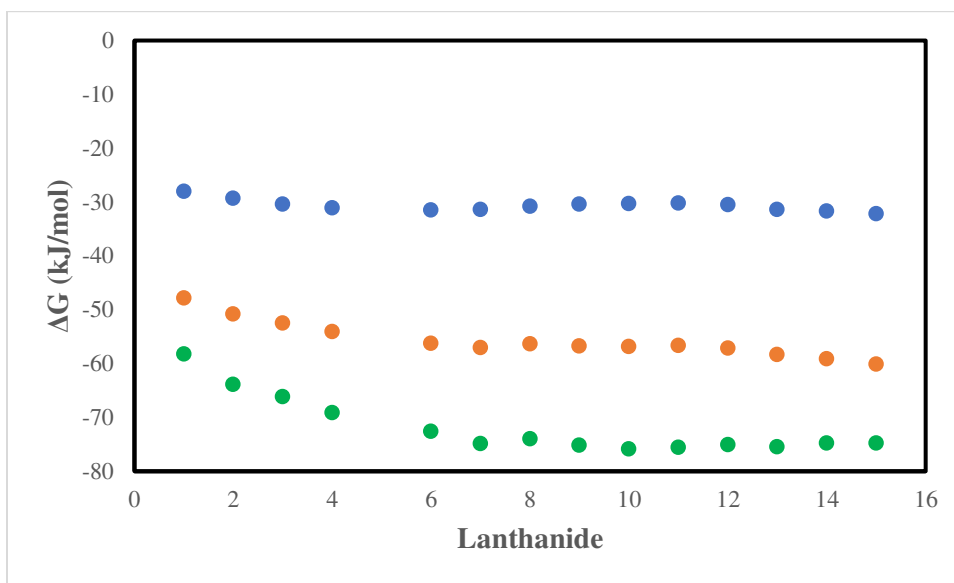


Figure 4.6. Formation free energies (ΔG) for $[\text{Ln}(\text{DGAc})_n]^{3-2n}$ complexes (Grenthe, 1963). The 1:1 complex is shown in blue, the 1:2 complex is shown in orange, and the 1:3 complex is shown in green.

4.2 Improving Chromatographic Actinide Separations with TEDGA

Introducing TEDGA to an actinide separation system based on Eichrom RE Resin caused an increase in selectivity for adjacent actinides. TEDGA thus shows great promise as an aqueous synergist or masking agent for chromatographic actinide separations. Actinide uptake into resin as a function of TEDGA concentration is discussed in section 4.2.1, and adjacent actinide separation factors are discussed in section 4.2.2.

4.2.1 Actinide Uptake TEDGA Dependence

All actinides demonstrated a decrease in K_d with increasing concentration of TEDGA. This was expected, since TEDGA is expected to bind to trivalent actinides in the aqueous phase, preventing them from bonding to the solid chromatographic material.

For all actinides, increasing TEDGA concentration ceased to significantly decrease K_d above a certain concentration. For Bk^{3+} and Cf^{3+} , concentrations above 10 mM had little-to-no effect on K_d , while for Am^{3+} and Cm^{3+} , TEDGA concentrations above 25 mM had no effect on K_d . This likely indicates a saturation of the $[An(TEDGA)_3]^{3+}$ complex in the aqueous phase. At radiotracer quantities, actinide concentrations are anticipated at the nM or μ M level. Usage of TEDGA concentrations above 10 mM thus signifies at least a 10^3 excess. At this level of excess, only the 1:3 complex is realistically expected for the actinides, assuming they behave like the lanthanides. Thus, almost all actinides in solution are expected to be bound as the 1:3 complex. After a certain concentration, equilibria between this complex and the resin remain mostly constant despite increases in TEDGA concentration.

It is interesting that the saturation concentration was higher for Am^{3+} and Cm^{3+} than for Bk^{3+} and Cf^{3+} . These elements also demonstrated a larger decrease in K_d in relation to TEDGA concentration. This signifies that earlier (larger) actinides have greater binding with TEDGA than later (smaller) ones. This is in disagreement with results for the early lanthanides, which are expected to behave analogously to the trivalent actinides. This could be due to systematic errors, as previous work has consistently shown that TEDGA binds more strongly to Cm^{3+} than Am^{3+} in aqueous media (Chapron et al., 2015; Suzuki et al., 2017). The slopes of TEDGA-dependence vs. K_d are also smaller in magnitude than would normally be expected. Further verification of the method is thus necessary.

Nonetheless, increasing TEDGA concentration decreases actinide K_d into Eichrom RE resin, demonstrating affinity between TEDGA and trivalent actinides. Variations in this decrease provide selectivity.

4.2.2 Adjacent Actinide Separation Factors

On its own, Eichrom RE resin does not provide significant separations between adjacent actinides, as demonstrated by the acid uptake curves. This section will demonstrate that introducing TEDGA into the system allows for K_d values to provide separations for adjacent actinides; thus, TEDGA provides selectivity for these trivalent f-elements.

Adjacent actinide separation factors for Am/Cm and Cf/Bk are shown in Table 4.3. Table 4.3 shows that increasing TEDGA concentration increases the separation factors between adjacent trivalent actinides. Separation factors as high as nearly 2 were observed for $SF_{Cm/Am}$ and 5.48 for $SF_{Cf/Bk}$. Thus, TEDGA can provide good separations for adjacent actinides, further demonstrating its selectivity for trivalent f-elements.

Table 4.3. Separations factors at increasing TEDGA concentrations for Am/Cm and Cf/Bk at 1 M HNO_3 .

[TEDGA] (M)	SF(Cm/Am)	SF(Cf/Bk)
0.001	0.98	2.21
0.005	1.18	-*
0.010	1.24	4.32
0.025	1.71	5.01
0.050	1.68	5.48
0.100	1.92	5.19

*Californium and berkelium were not tested at this TEDGA concentration.

It is worth comparing TEDGA to other systems that separate Cm^{3+}/Am^{3+} and Cf^{3+}/Bk^{3+} . These indicate how good of a separation agent TEDGA practically is for these elements.

In the EXAm process, discussed briefly in the Introduction, applying 0.03 M TEDGA in the aqueous phase at 6 M HNO_3 increases $SF_{Cm/Am}$ from approximately 1.6 (for pure DMDOHEMA) to 2.5. This is slightly greater than the separation factor that was found in this work. However, in this work, increasing TEDGA from 0.001 M to 0.100 M caused a two-fold

increase in $SF_{\text{Cm/Am}}$, whereas in EXAm, using TEDGA only increases $SF_{\text{Cm/Am}}$ by approximately 60%. In that sense, TEDGA has more effectively improved the efficiency of the RE Resin system than DMDOHEMA in the EXAm process (Chapron et al., 2015).

As was discussed in the Introduction, and a great motivator for this research, coupling TEDGA with ADAAMs allowed for $SF_{\text{Cm/Am}}$ to increase from around 5 to 41. This eightfold increase is remarkable. ADAAM is very selective for Am^{3+} , and TEDGA is more selective for Cm^{3+} in this system. As a proof of principle, an ethylhexyl-substituted ADAAM was used for partitioning studies of lanthanides (Figure 4.7; Suzuki et al., 2017). It was shown that D_{Ln} steadily decreased across the series, with the greatest negative slope occurring in the early part from Pr-Gd; thus, ADAAM strongly complexes with the larger trivalent f-element. This is compared to tetradodecyl diglycolamide, which has steadily increasing D_{Ln} for the lanthanides, with the greatest positive slope occurring for the early elements, as with most diglycolamides (Ansari and Mohapartra, 2017). Thus, the DGA is expected to mask and bond more strongly to the smaller element, while the ADAAM is expected to strongly extract the larger one. Combining both of these allows for the fantastic adjacent actinide separation that was reported (Suzuki et al., 2017).

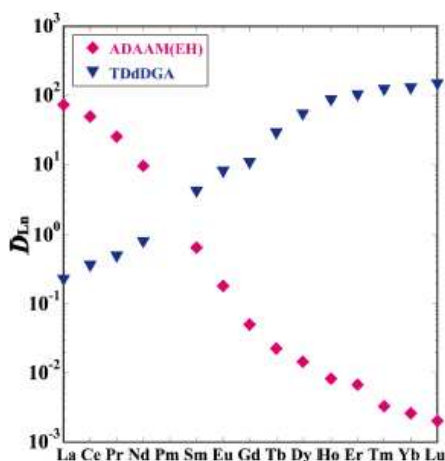


Figure 4.7. Partitioning coefficients of lanthanides with an ADAAM and a diglycolamide. The most selectivity for adjacent lanthanides occurs in the early part of the series, where each extractant demonstrates the largest variation in D (Suzuki et al., 2017).

The same reasoning explains why TEDGA improves selectivity when applied with RE Resin. RE Resin has been shown to have a fairly constant uptake for the lanthanide elements Ce-Eu. These elements are the lanthanide analogs for the actinides; thus, RE resin is expected to have little-to-no selectivity for actinides. TEDGA, on the other hand, demonstrates an increase in uptake (noted in section 4.1 as increasing β_3 from Pr to Sm) for these elements. Thus, it is anticipated that TEDGA is most selective for actinides in this region, leading to the observed selectivity in the coupled resin-TEDGA system.

4.3 References

- Ansari, S.A.; Mohapatra, P.K. A review on solid phase extraction of actinides and lanthanides with amide based extractants. *J. Chromatogr. A*. 2017, *1499*, 1-20.
- Chapron, S.; Marie, C.; Arrachart, G.; Miguiditchian, M.; Pellet-Rostaing, S. New insight into the americium/curium separation by solvent extraction using diglycolamides. *Solvent Extr. Ion Exc.* 2015, *33*, 236-248.
- Charbonnel, M.C.; Berthon, C.; Berthon, L.; Boubals, N.; Burdet, F.; Duchesne, M.T.; Guilbaud, P.; Mabilille, N.; Petit, S.; Zorz, N. Complexation of Ln(III) and An(III) with hydrosoluble TEDGA: speciation and thermodynamics studies. *Procedia Chem.* 2012, *7*, 20-26.
- Grenthe, I. Thermodynamic properties of rare earth complexes II: Free energy, enthalpy, and entropy changes for the formation of rare earth diglycolate and dipicolinate complexes at 25.00°C. *Acta Chem. Scand.* 1963, *17*, 2487-2498.
- Husain, M.; Ansari, S.A.; Mohapatra, P.K.; Gupta, R.K.; Parmar, V.S.; Manchanda, V.K. Extraction chromatography of lanthanides using N,N,N',N'-tetraoctyl diglycolamide (TODGA) as the stationary phase. *Desalination*. 2008, *229*, 294-301.
- Klaß, L.; Wilden, A.; Kreft, F.; Wagner, C.; Geist, A.; Panak, P.J.; Herdzyk-Koniek, I.; Narbutt, J.; Modolo, G. Evaluation of the hydrophilic complexant N,N,N',N'-tetraethyldiglycolamide (TEDGA) and its methyl-substituted analogues in the selective Am(III) separation. *Solvent Extr. Ion Exc.* 2019, *37(5)*, 297-312.
- Xie, F.; Zhang, T. A.; Dreisinger, D.; Doyle, F. A critical review on solvent extraction of rare earths from aqueous solutions. *Miner. Eng.* 2014, *56*, 10-28.

CHAPTER FIVE

FUTURE WORK

It has been shown that TEDGA is selective for trivalent f-elements. Particularly, the lanthanides Pr, Nd, Sm, Ho, and Er were studied. The literature is still lacking for the remaining lanthanides. While spectrophotometry cannot be applied to all of the remaining elements due to a lack of available absorption and emission bands, calorimetry can be done to further evaluate stability constants for the lanthanide series. There appears to be a transition between Sm and Ho after which the 1:3 complex becomes the most thermodynamically favored relative to the 1:1 and 1:2 complexes, but it is not clear when this transition occurs. By probing the elements in this region, insight can be gained into the nature of this transition.

Probing the 1:1 complex for the late lanthanides Ho and Er proved challenging, affecting the reliability of data for these elements. Future experiments could perform titration experiments in reverse, beginning with an excess of TEDGA and titrating in Ln^{3+} ions. At late points in the titration, detectable amounts of 1:1 complex would potentially be formed. This would allow greater precision in determining β_1 , particularly for Ho and Er.

While not examined in this work, other methods such as TRLIFS can be used to probe stability constants of $[\text{Ln}(\text{TEDGA})_n]^{3+}$ complexes for elements that are fluorescent, such as Eu. Radiotracer experiments can also be used to estimate stability constants. Verification of the conditional stability constants using the same and alternative methods to demonstrate trends across the lanthanide series would allow for improved understanding of Ln-TEDGA complexation.

For chromatography, TEDGA-dependence could be tested at other acid concentrations or with other resins. For the RE resin, early lanthanide uptake appears to be approximately constant

at 0.2, 1.0, and 4.0 M HNO₃, but at 0.2 M there could be a slight decrease in uptake. This could complement TEDGA, which increases uptake in this region, to provide greater selectivity for actinides at 0.2 M HNO₃. At 8.0 M HNO₃, the opposite effect is observed. Increasing uptake in the RE resin would cause TEDGA to be less selective, since TEDGA's uptake is also increasing in this region. Other resins could also be examined. The most promising choice would be TRU Resin, which also contains the CMPO extractant that is used in RE Resin. Other Eichrom resin products all demonstrate an increasing K_d for early lanthanides; thus, little selectivity would be expected when used alongside TEDGA.

Lastly, other aqueous diglycolamides could be tested for lanthanide selectivity. It was found that TEDGA had a large entropic favoring for complex formation with these elements at 25°C, so other short-chained DGAs might be expected to demonstrate similar favorability. The shorter-chained tetramethyl diglycolamide would probably have less entropic selectivity, since the shorter methyl chains will exert less strain and have fewer degrees of freedom. Tetrapropyl diglycolamide and tetrabutyl diglycolamide would both be interesting to examine, as their long alkyl chains would be expected to increase entropy of [Ln(DGA)_n]³⁺ complexes. Examining further DGA complexation with lanthanides and actinides might demonstrate relationships between alkyl chain length and selectivity, which would be useful for designing future trivalent f-element separations.

APPENDIX A

PRINCIPAL COMPONENT ANALYSIS OF SPECTROPHOTOMETRIC DATA

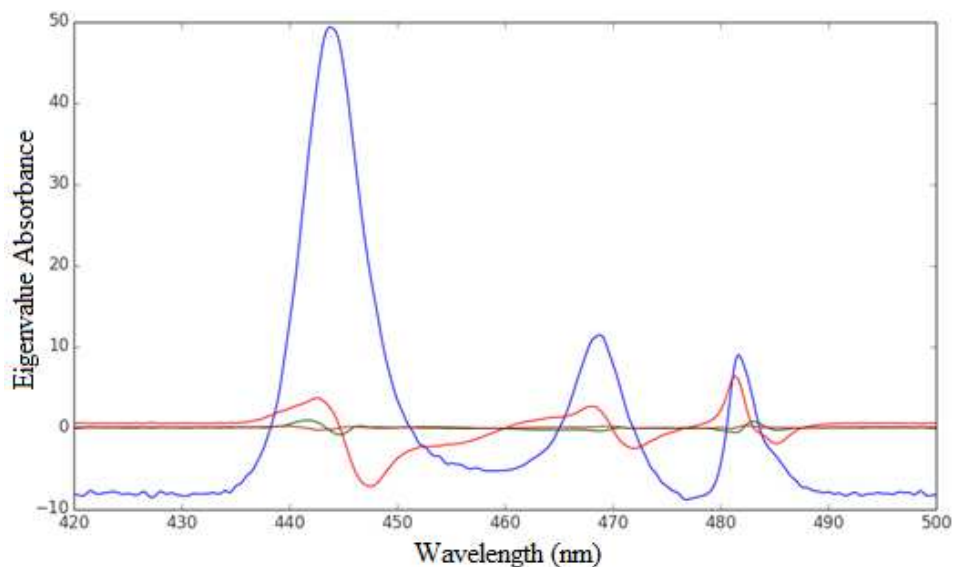


Figure A.1. Principal Component Analysis of $[\text{Pr}(\text{TEDGA})_n]^{3+}$ spectrophotometric data. The first (blue), second (red), third (green) and fourth (yellow) eigenvectors are shown. All four eigenvectors have significant nonzero features, indicating the presence of four species: Pr^{3+} , $[\text{Pr}(\text{TEDGA})]^{3+}$, $[\text{Pr}(\text{TEDGA})_2]^{3+}$, and $[\text{Pr}(\text{TEDGA})_3]^{3+}$.

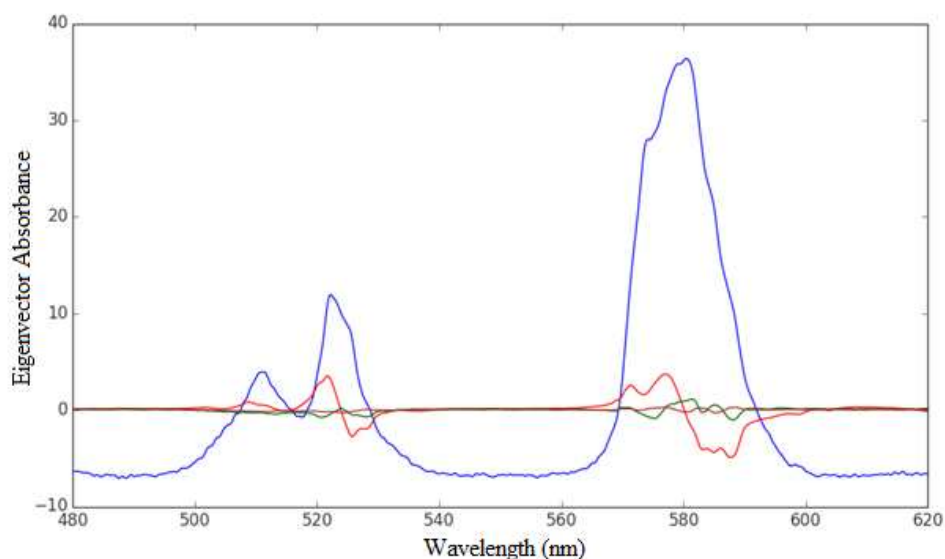


Figure A.2. Principal Component Analysis of $[\text{Nd}(\text{TEDGA})_n]^{3+}$ spectrophotometric data. The first (blue), second (red), third (green), and fourth (brown) eigenvectors are shown. All four eigenvectors have significant nonzero features, indicating the presence of four species: Nd^{3+} , $[\text{Nd}(\text{TEDGA})]^{3+}$, $[\text{Nd}(\text{TEDGA})_2]^{3+}$, and $[\text{Nd}(\text{TEDGA})_3]^{3+}$.

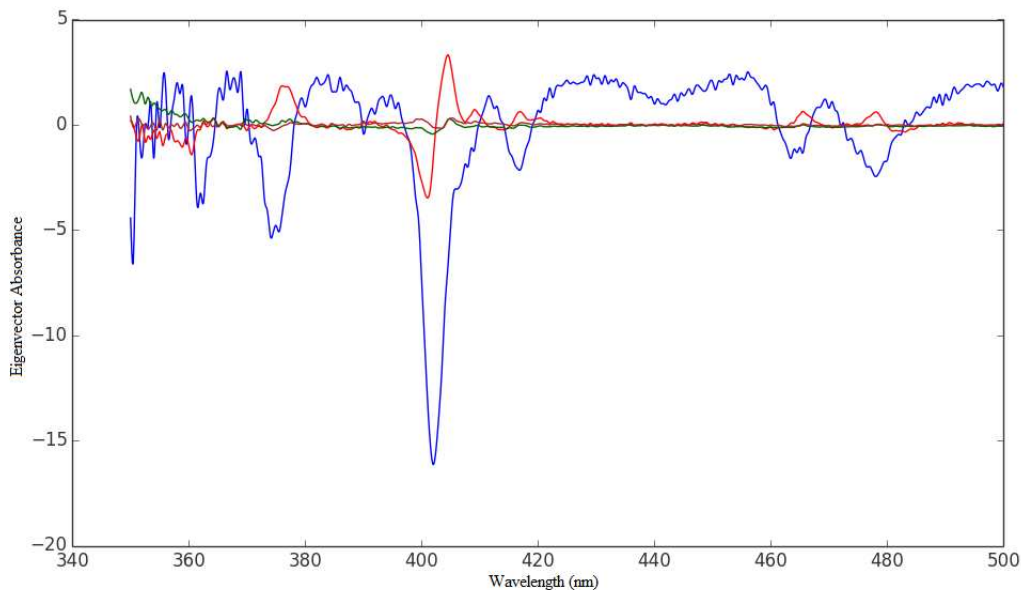


Figure A.3. Principal Component Analysis of $[\text{Sm}(\text{TEDGA})_n]^{3+}$ spectrophotometric data. The first (blue), second (red), third (green), and fourth (brown) eigenvectors are shown. All four eigenvectors have significant nonzero features, indicating the presence of four species: Sm^{3+} , $[\text{Sm}(\text{TEDGA})]^{3+}$, $[\text{Sm}(\text{TEDGA})_2]^{3+}$, and $[\text{Sm}(\text{TEDGA})_3]^{3+}$.

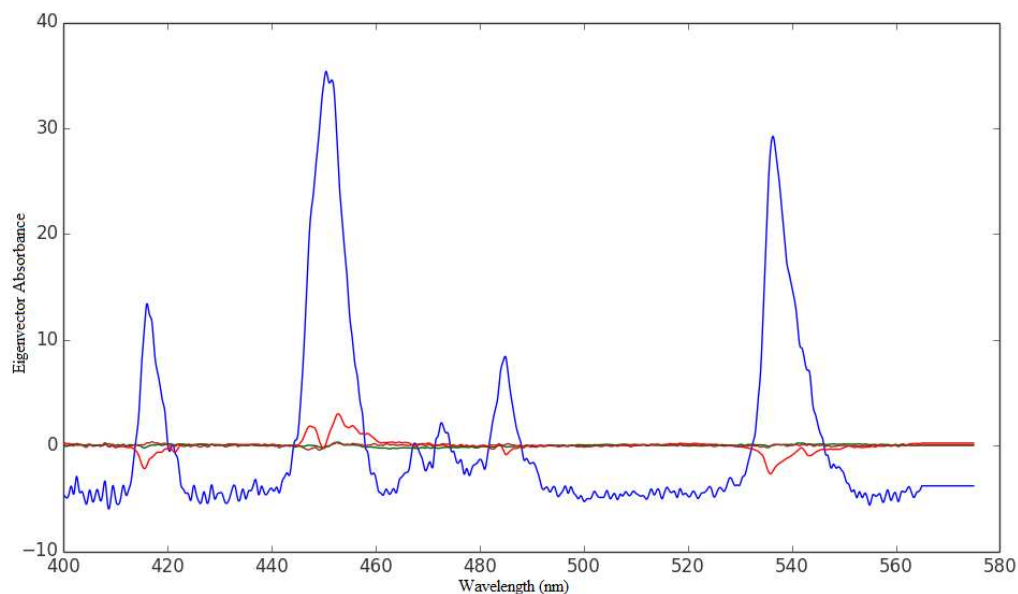


Figure A.4. Principal Component Analysis of $[\text{Ho}(\text{TEDGA})_n]^{3+}$ spectrophotometric data. The first (blue), second (red), third (green), and fourth (brown) eigenvectors are shown. Three eigenvectors are nonzero. This indicates the presence of Ho^{3+} and two other species.

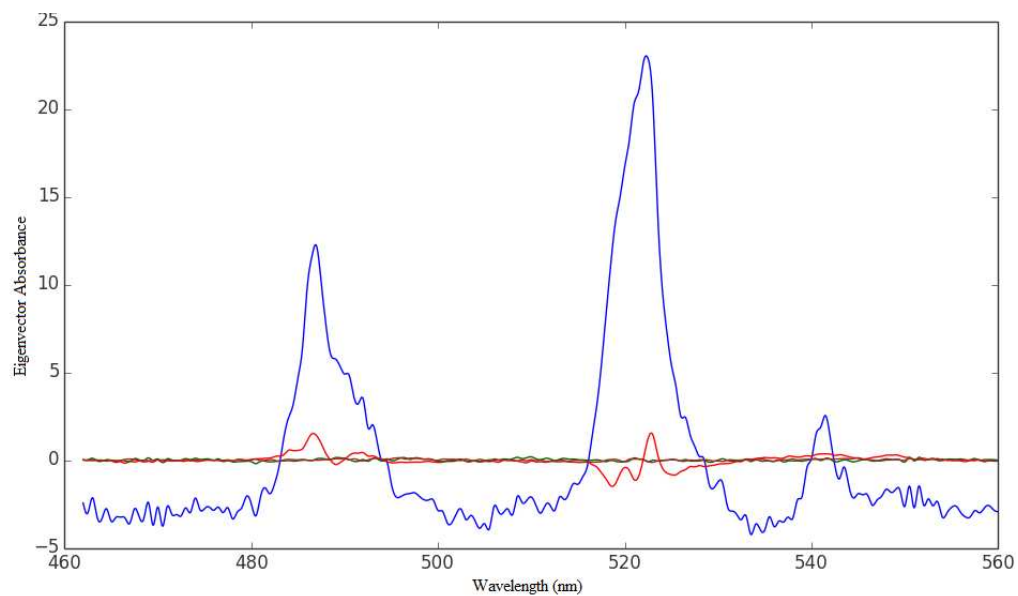


Figure A.5. Principal Component Analysis of $[\text{Er}(\text{TEDGA})_n]^{3+}$ spectrophotometric data. The first (blue), second (red), third (green), and fourth (brown) eigenvectors are shown. Either two or three eigenvectors are nonzero. This indicates the presence of Er^{3+} and one or two other species.

APPENDIX B

FITS TO SPECTROPHOTOMETRIC DATA IN HYPSPPEC

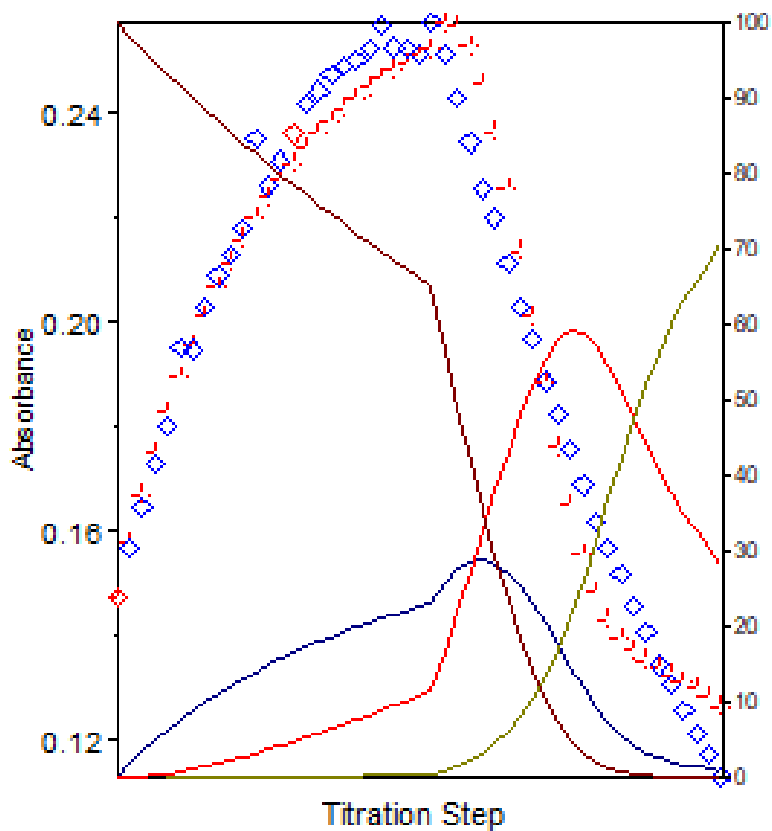


Figure B.1. HypSpec fit for the titration of TEDGA into 1.5 mL of 0.034 M $\text{Pr}(\text{NO}_3)_3$ at 1 M HNO_3 constant ionic strength and acidity. The fit is displayed at 443 nm, where Pr^{3+} has an absorbance peak. Speciation of free Pr^{3+} is shown in brown, $[\text{Pr}(\text{TEDGA})]^{3+}$ in blue, $[\text{Pr}(\text{TEDGA})_2]^{3+}$ in red, and $[\text{Pr}(\text{TEDGA})_3]^{3+}$ in yellow. Experimental data is shown as diamonds; calculated values are shown as crosses.

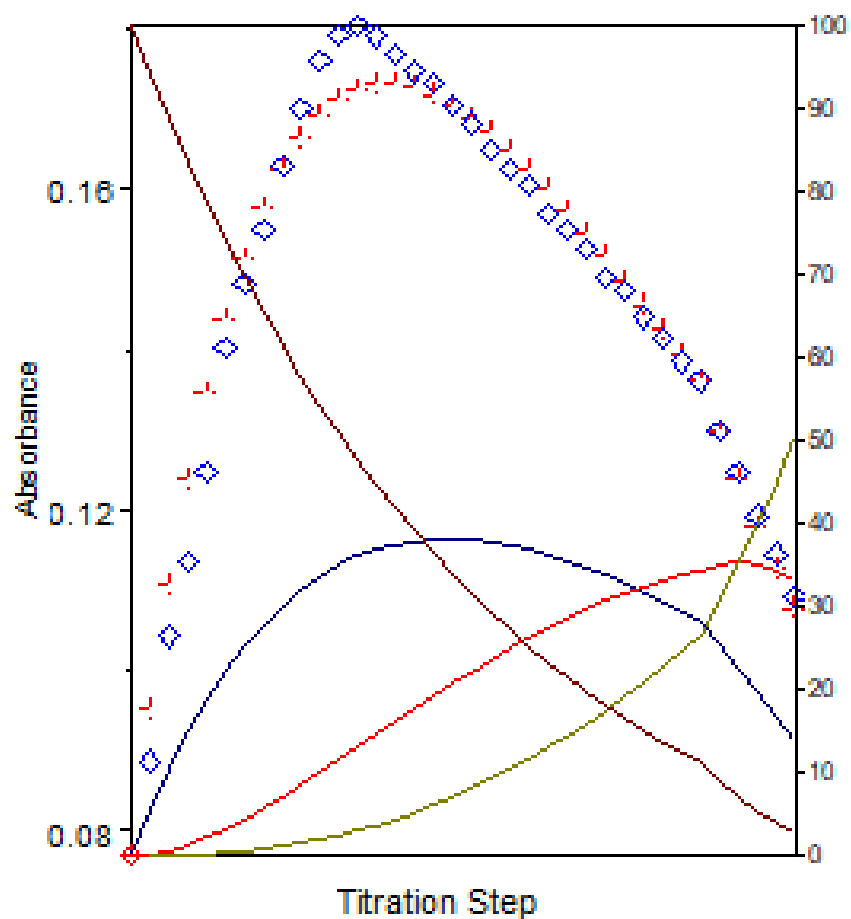


Figure B.2. HypSpec fit for the titration of TEDGA into 1.5 mL of 0.028 M $\text{Nd}(\text{NO}_3)_3$ at 1 M HNO_3 constant ionic strength and acidity. The fit is displayed at 581.5 nm, where Nd^{3+} has an absorbance peak. Speciation of free Nd^{3+} is shown in brown, $[\text{Nd}(\text{TEDGA})]^{3+}$ in blue, $[\text{Nd}(\text{TEDGA})_2]^{3+}$ in red, and $[\text{Nd}(\text{TEDGA})_3]^{3+}$ in yellow. Experimental data is shown as diamonds; calculated values are shown as crosses.

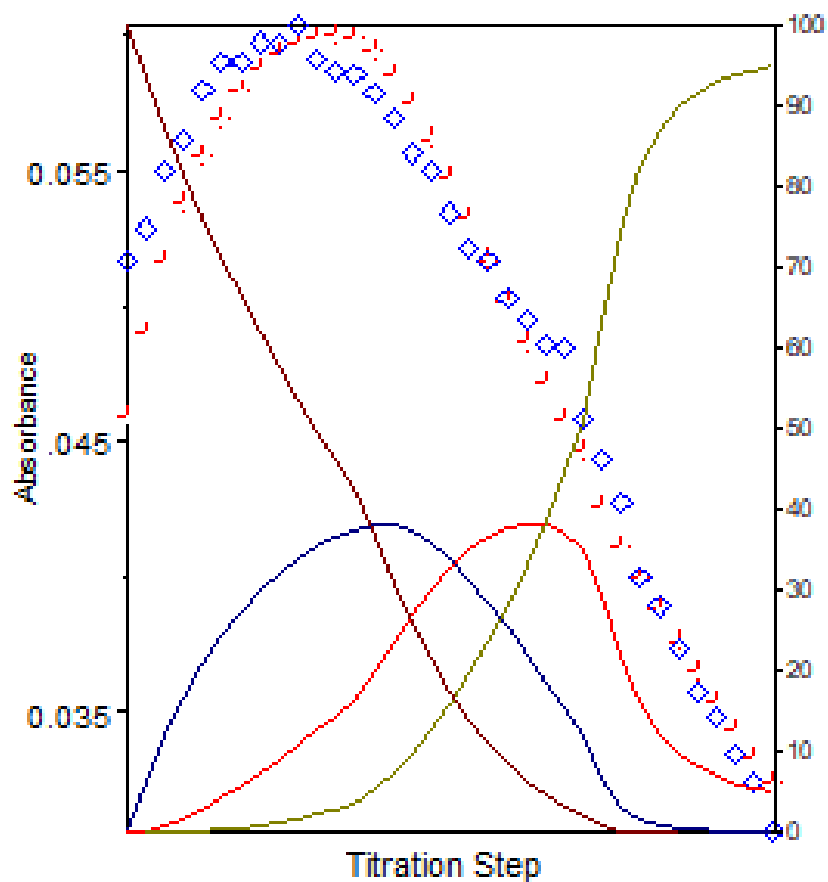


Figure B.3. HypSpec fit for the titration of TEDGA into 1.5 mL of 0.024 M $\text{Sm}(\text{NO}_3)_3$ at 1 M HNO_3 constant ionic strength and acidity. The fit is displayed at 402.5 nm, where Sm^{3+} has an absorption peak. Speciation of free Sm^{3+} is shown in brown, $[\text{Sm}(\text{TEDGA})]^{3+}$ in blue, $[\text{Sm}(\text{TEDGA})_2]^{3+}$ in red, and $[\text{Sm}(\text{TEDGA})_3]^{3+}$ in yellow. Experimental data is shown as diamonds; calculated values are shown as crosses.

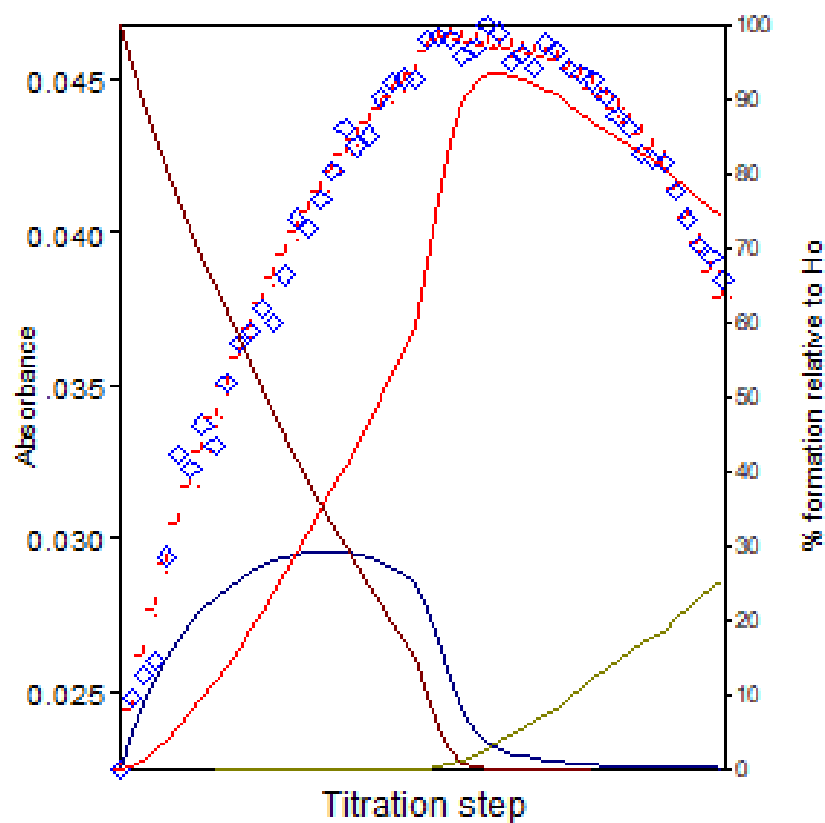


Figure B.4. HypSpec fit for the titration of TEDGA into 1.5 mL of 0.011 M $\text{Ho}(\text{NO}_3)_3$ at 1 M HNO_3 constant ionic strength and acidity. The fit is displayed at 451.5 nm, where Ho^{3+} has an absorption peak. Speciation of free Ho^{3+} is shown in brown, $[\text{Ho}(\text{TEDGA})]^{3+}$ in blue, $[\text{Ho}(\text{TEDGA})_2]^{3+}$ in red, and $[\text{Ho}(\text{TEDGA})_3]^{3+}$ in yellow. Experimental data is shown as diamonds; calculated values are shown as crosses.

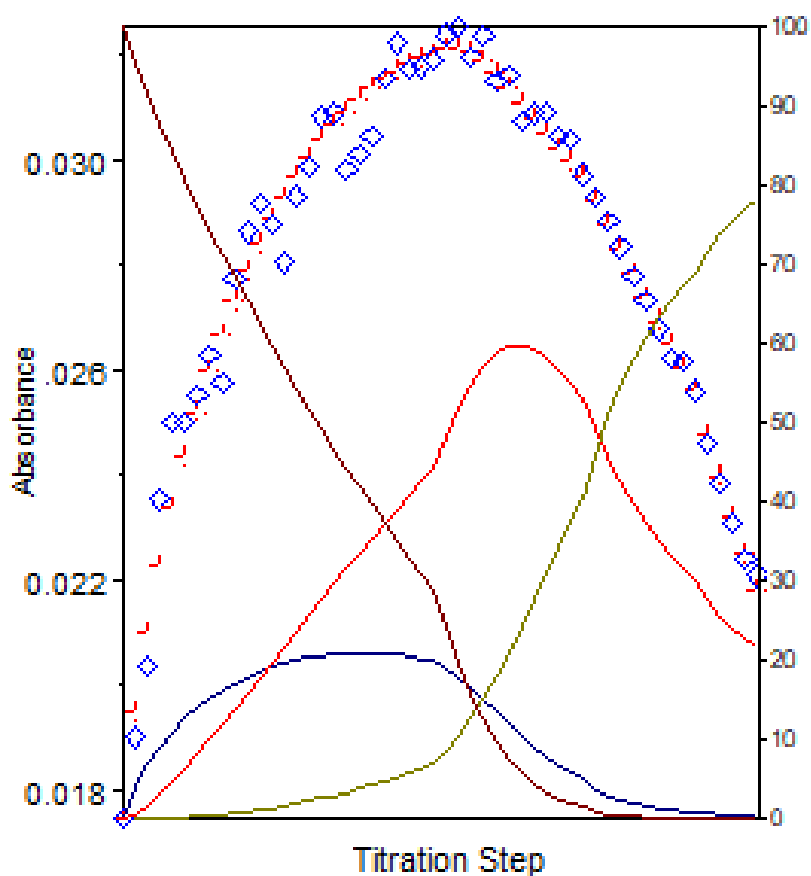


Figure B.5. HypSpec fit for the titration of TEDGA into 1.5 mL of 0.012 M $\text{Er}(\text{NO}_3)_3$ at 1 M HNO_3 constant ionic strength and acidity. The fit is displayed at 522.5 nm, where Er^{3+} has an absorption peak. Speciation of free Er^{3+} is shown in brown, $[\text{Er}(\text{TEDGA})]^{3+}$ in blue, $[\text{Er}(\text{TEDGA})_2]^{3+}$ in red, and $[\text{Er}(\text{TEDGA})_3]^{3+}$ in yellow. Experimental data is shown as diamonds; calculated values are shown as crosses.

APPENDIX C

EXTINCTION COEFFICIENTS OF $[\text{Ln}(\text{TEDGA})_n]^{3+}$ COMPLEXES

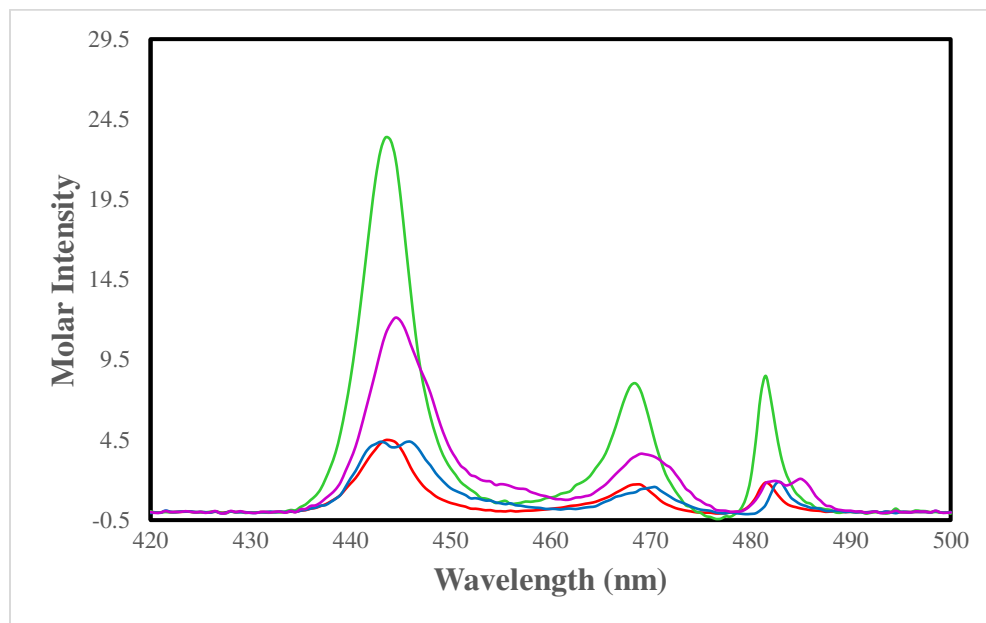


Figure C.1. Extinction coefficient curves for 0.035 M $\text{Pr}(\text{NO}_3)_3$ titrated with TEDGA at 1M HNO_3 acidity. Free Pr^{3+} is shown in red, $[\text{Pr}(\text{TEDGA})]^{3+}$ in green, $[\text{Pr}(\text{TEDGA})_2]^{3+}$ in blue, and $[\text{Pr}(\text{TEDGA})_3]^{3+}$ in purple.

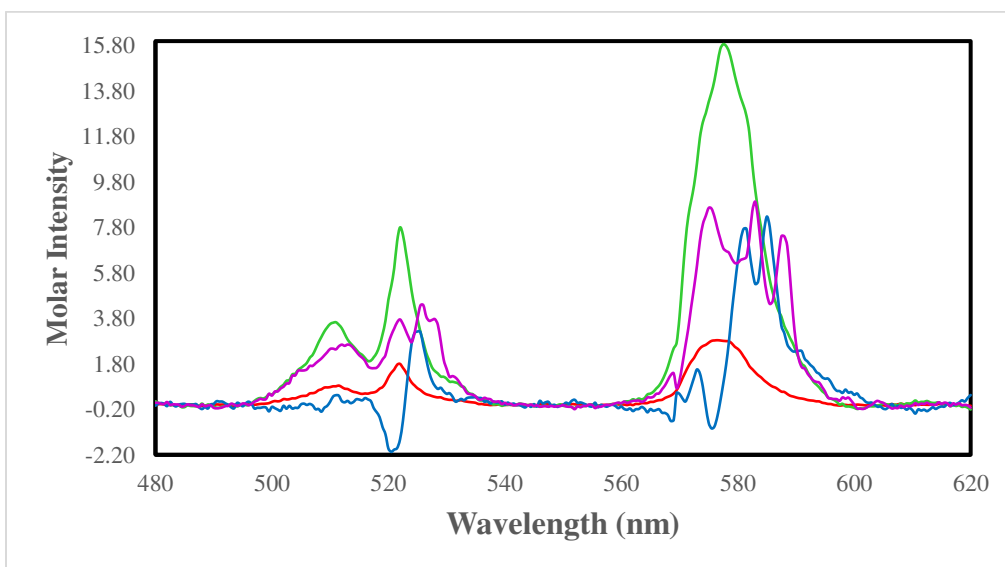


Figure C.2. Extinction coefficient curves for 0.028 M $\text{Nd}(\text{NO}_3)_3$ titrated with TEDGA at 1M HNO_3 acidity. Free Nd^{3+} is shown in red, $[\text{Nd}(\text{TEDGA})]^{3+}$ in green, $[\text{Nd}(\text{TEDGA})_2]^{3+}$ in blue, and $[\text{Nd}(\text{TEDGA})_3]^{3+}$ in purple.

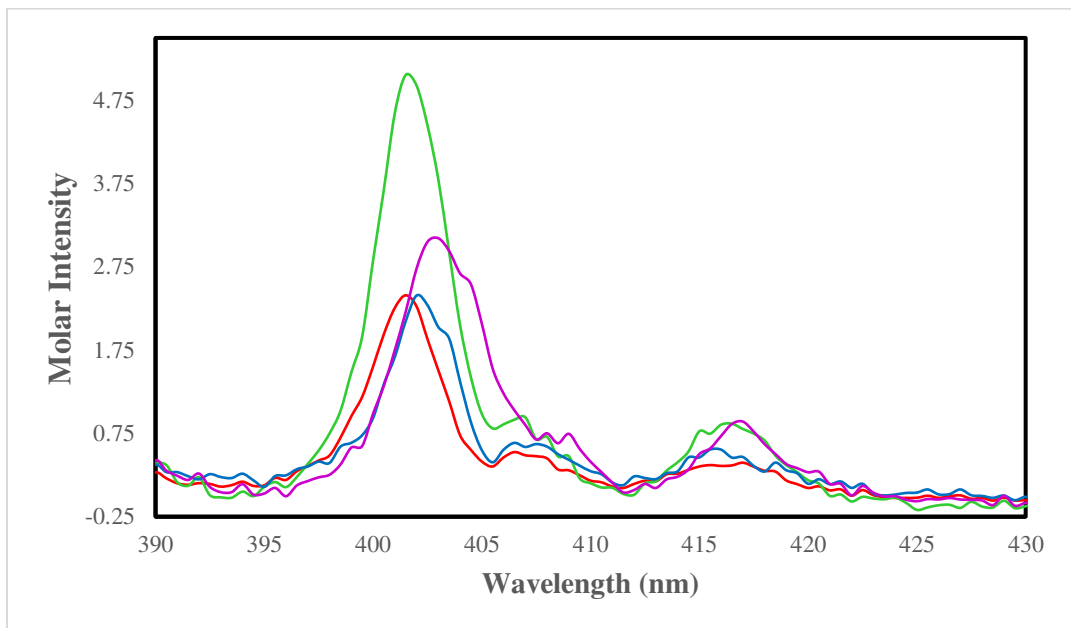


Figure C.3. Extinction coefficient curves for 0.024 M $\text{Sm}(\text{NO}_3)_3$ titrated with TEDGA at 1M HNO_3 acidity. Free Sm^{3+} is shown in red, $[\text{Sm}(\text{TEDGA})]^{3+}$ in green, $[\text{Sm}(\text{TEDGA})_2]^{3+}$ in blue, and $[\text{Sm}(\text{TEDGA})_3]^{3+}$ in purple.

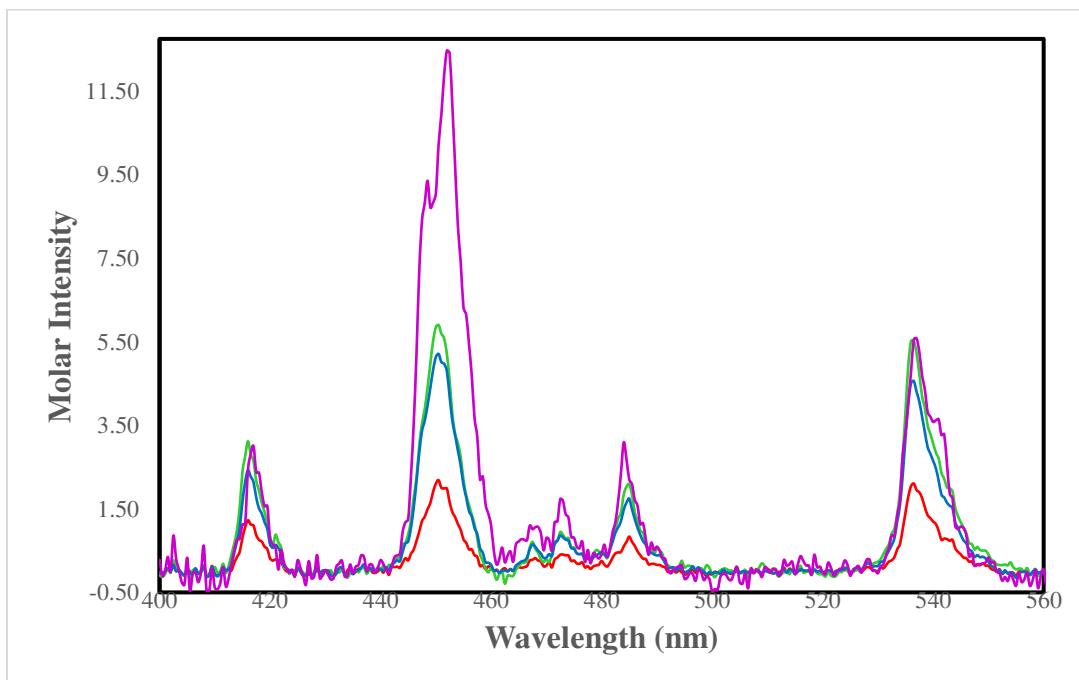


Figure C.4. Extinction coefficient curves for 0.011 M $\text{Ho}(\text{NO}_3)_3$ titrated with TEDGA at 1M HNO_3 acidity. Free Ho^{3+} is shown in red, $[\text{Ho}(\text{TEDGA})]^{3+}$ in green, $[\text{Ho}(\text{TEDGA})_2]^{3+}$ in blue, and $[\text{Ho}(\text{TEDGA})_3]^{3+}$ in purple.

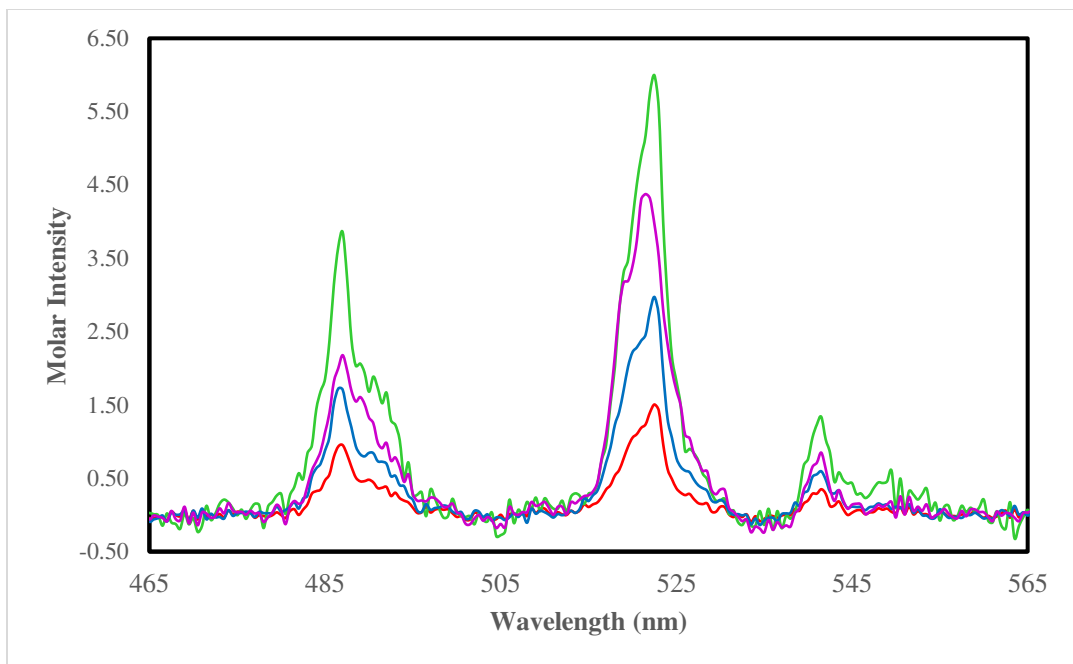


Figure C.5. Extinction coefficient curves for 0.012 M $\text{Er}(\text{NO}_3)_3$ titrated with TEDGA at 1M HNO_3 acidity. Free Er^{3+} is shown in red, $[\text{Er}(\text{TEDGA})]^{3+}$ in green, $[\text{Er}(\text{TEDGA})_2]^{3+}$ in blue, and $[\text{Er}(\text{TEDGA})_3]^{3+}$ in purple.

APPENDIX D

FITS TO CALORIMETRIC DATA IN HYPICAL

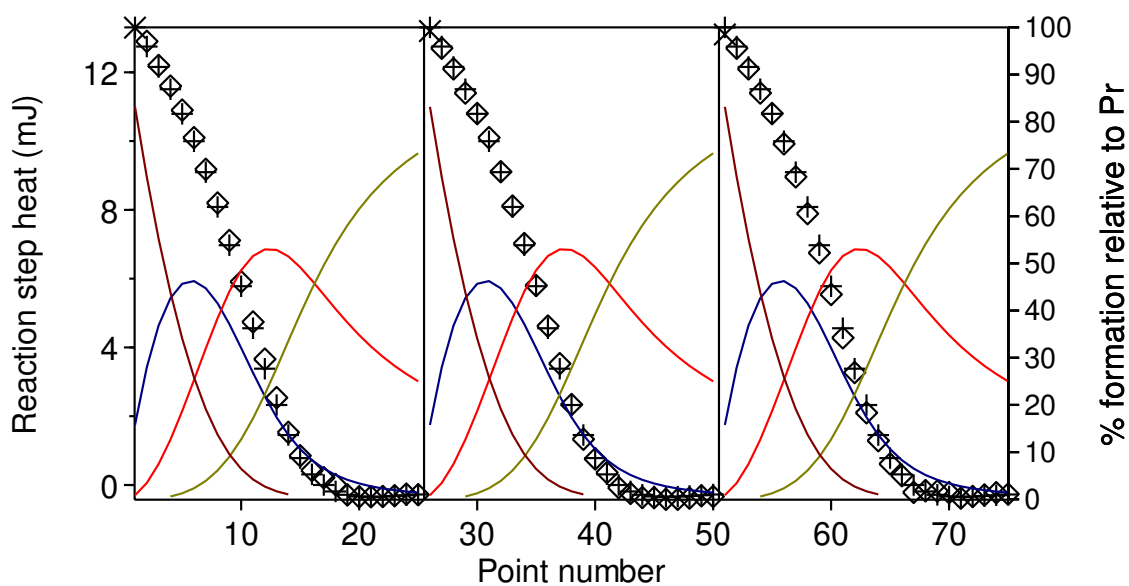


Figure D.1. Experimental fits for calorimetric titrations of 0.25 M TEDGA, 10 μL injections into 1 mL of 0.013 M $\text{Pr}(\text{NO}_3)_3$ at 1 M HNO_3 constant ionic strength and acidity in both solutions and 25°C reaction cell temperature. Speciation of free Pr^{3+} is shown in brown, $[\text{Pr}(\text{TEDGA})]^{3+}$ in blue, $[\text{Pr}(\text{TEDGA})_2]^{3+}$ in red, and $[\text{Pr}(\text{TEDGA})_3]^{3+}$ in yellow. Experimental data is shown as diamonds; calculated values are shown as crosses.

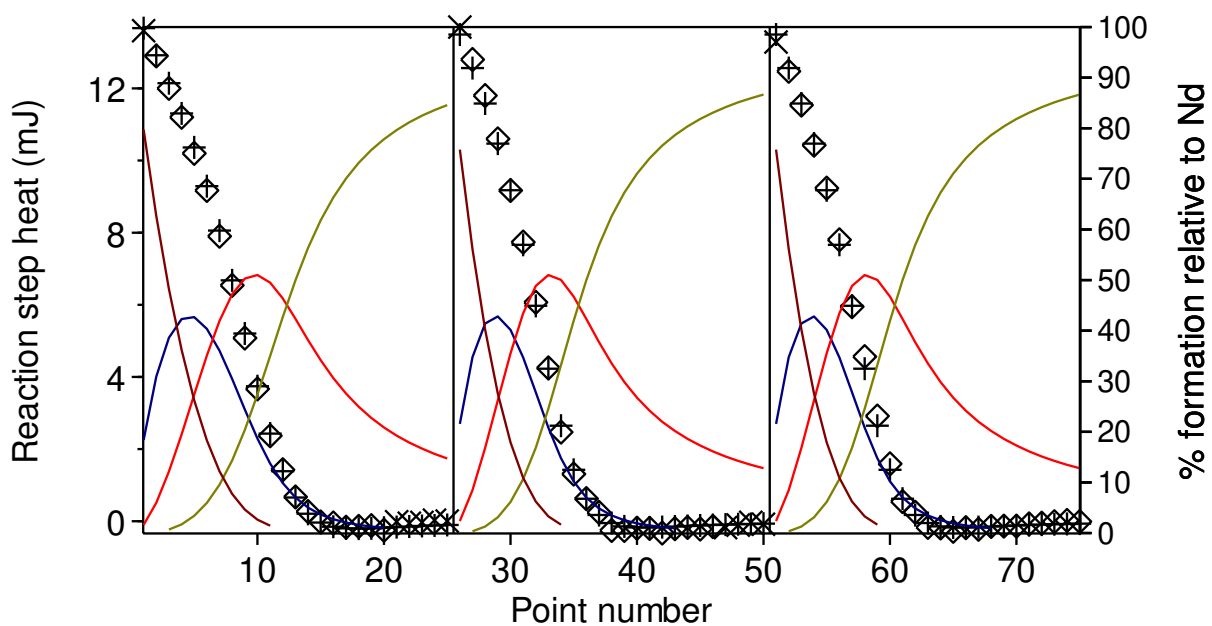


Figure D.2. Experimental fits for calorimetric titrations of 0.25 M TEDGA, 10 μL injections into 1 mL of 0.011 M $\text{Nd}(\text{NO}_3)_3$ at 1 M HNO_3 constant ionic strength and acidity in both solutions and 25°C reaction cell temperature. Speciation of free Nd^{3+} is shown in brown, $[\text{Nd}(\text{TEDGA})]^{3+}$ in blue, $[\text{Nd}(\text{TEDGA})_2]^{3+}$ in red, and $[\text{Nd}(\text{TEDGA})_3]^{3+}$ in yellow. Experimental data is shown as diamonds; calculated values are shown as crosses.

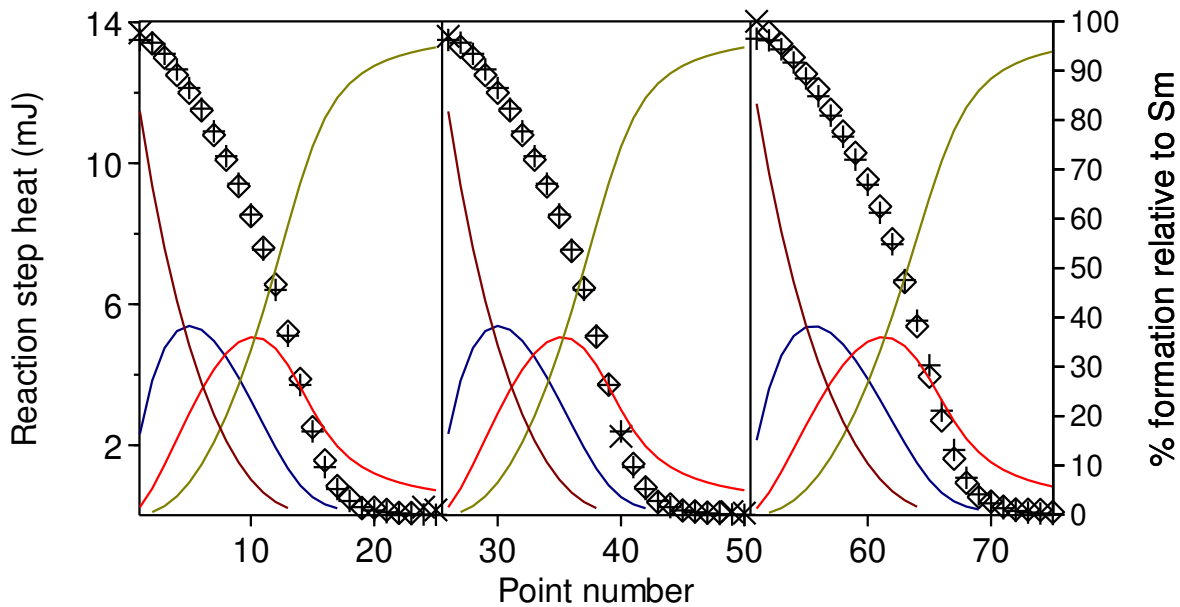


Figure D.3. Experimental fits for calorimetric titrations of 0.25 M TEDGA, 10 μL injections into 1 mL of 0.012 M $\text{Sm}(\text{NO}_3)_3$ at 1 M HNO_3 constant ionic strength and acidity in both solutions and 25°C reaction cell temperature. Speciation of free Sm^{3+} is shown in brown, $[\text{Sm}(\text{TEDGA})]^{3+}$ in blue, $[\text{Sm}(\text{TEDGA})_2]^{3+}$ in red, and $[\text{Sm}(\text{TEDGA})_3]^{3+}$ in yellow. Experimental data is shown as diamonds; calculated values are shown as crosses.

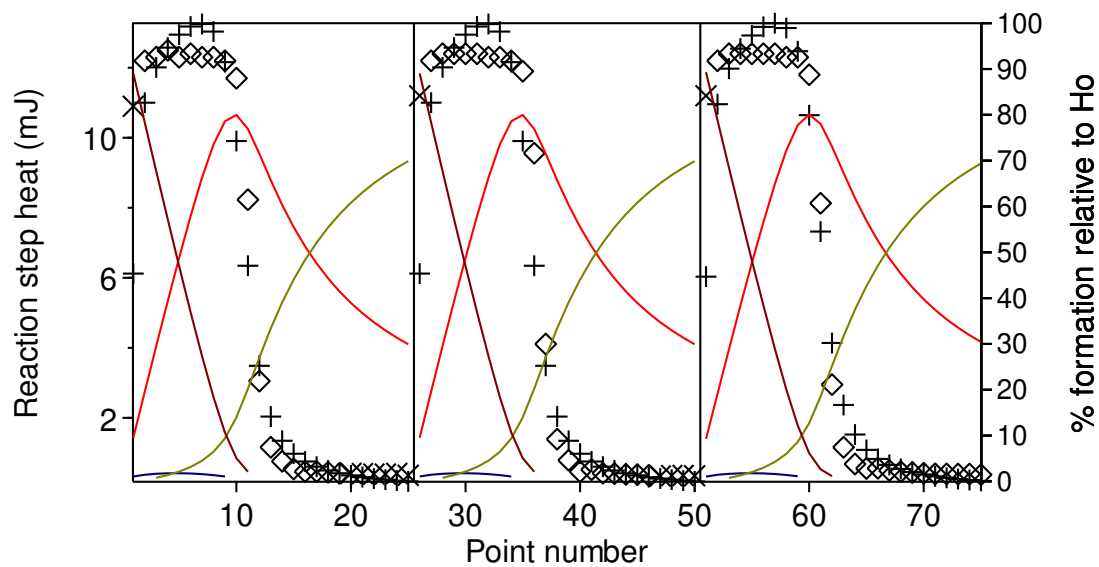


Figure D.4. Experimental fits for calorimetric titrations of 0.25 M TEDGA, 10 μL injections into 1 mL of 0.011 M $\text{Ho}(\text{NO}_3)_3$ at 1 M HNO_3 constant ionic strength and acidity in both solutions and 25°C reaction cell temperature. Speciation of free Ho^{3+} is shown in brown, $[\text{Ho}(\text{TEDGA})]^{3+}$ in blue, $[\text{Ho}(\text{TEDGA})_2]^{3+}$ in red, and $[\text{Ho}(\text{TEDGA})_3]^{3+}$ in yellow. Experimental data is shown as diamonds; calculated values are shown as crosses.

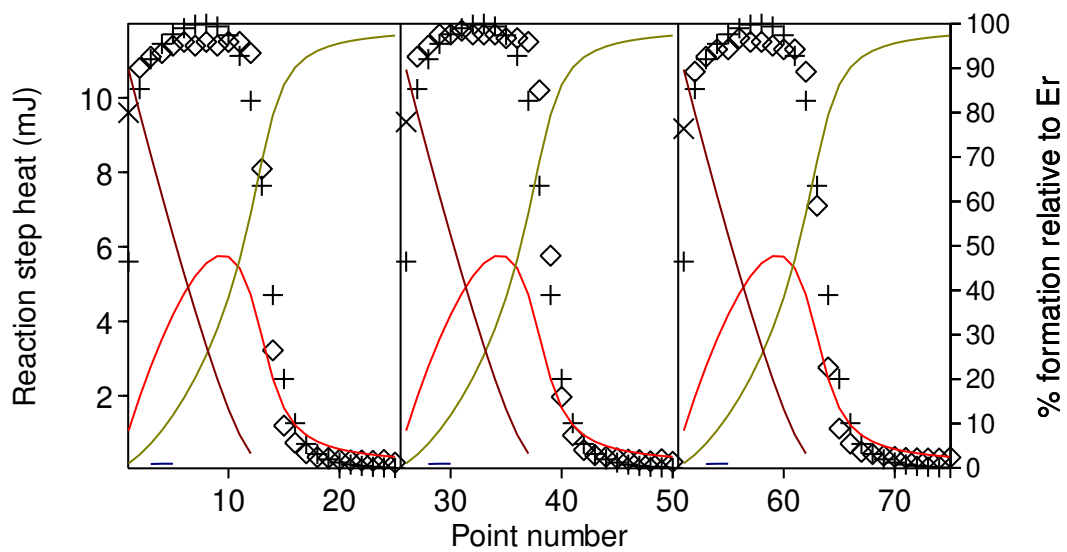


Figure D.5. Experimental fits for calorimetric titrations of 0.25 M TEDGA, 10 μL injections into 1 mL of 0.012 M $\text{Er}(\text{NO}_3)_3$ at 1 M HNO_3 constant ionic strength and acidity in both solutions and 25°C reaction cell temperature. Speciation of free Er^{3+} is shown in brown, $[\text{Er}(\text{TEDGA})]^{3+}$ in blue, $[\text{Er}(\text{TEDGA})_2]^{3+}$ in red, and $[\text{Er}(\text{TEDGA})_3]^{3+}$ in yellow. Experimental data is shown as diamonds; calculated values are shown as crosses.

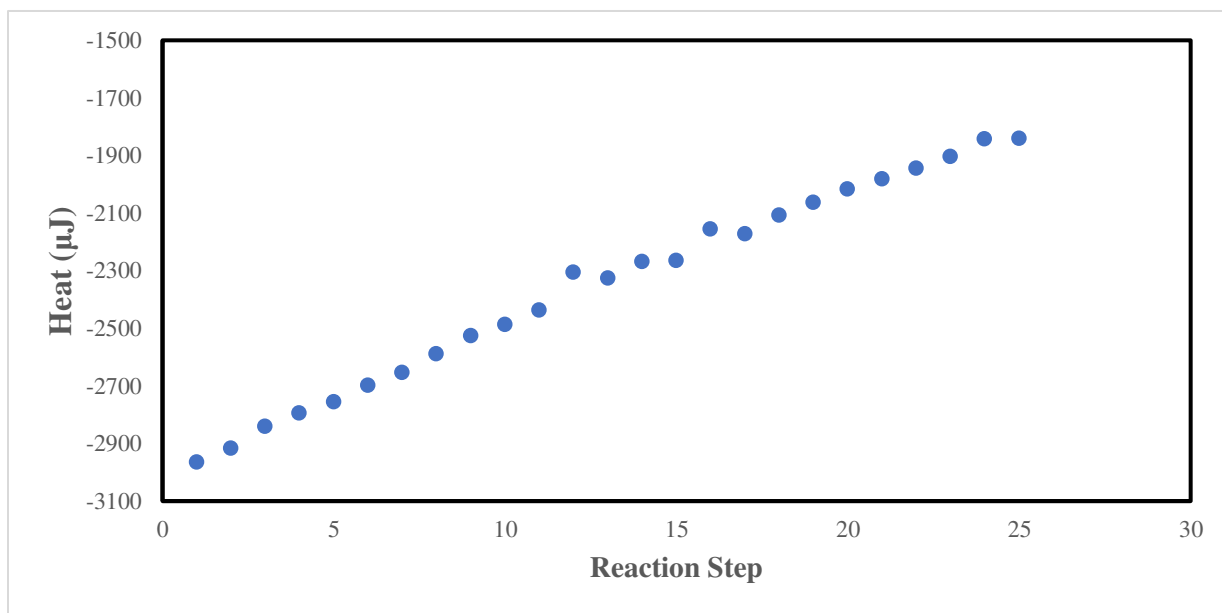


Figure D.6. Dilution correction of 0.25 M TEDGA, 10 μL injections into 1 mL of H_2O at 1 M HNO_3 constant ionic strength, 25°C.